Analysis of Dredge Material and Crushed Glass Blends with Uniaxial Geogrids in Pullout Tests

by

Kemp Sloan Lewis III, B.S.C.E.

Thesis

Presented to the Faculty of the Graduate School of

The University of Texas at Austin

in Partial Fulfillment

of the Requirements

for the Degree of

Master of Science in Engineering

The University of Texas at Austin

December, 2013

Acknowledgements

I would first off like to thank Dr. Jorge Zornberg for giving me the opportunity to conduct research during my undergraduate and graduate level studies at the University of Texas at Austin. His guidance and the experience I have gained working in the lab has been invaluable. I am thankful to have been a member of such a great team and would like to thank Jacob Robert Condo, Fabrizio Marcotulli, and Sangameshwar (Sangy) Hanumasagar for their dedication and many hours of effort given to this research over the entire project span; additional thanks go to Sean Hutcherson for his involvement early on in the project. Furthermore, thanks to Federico Castro for his deep involvement in addressing problems related to the testing equipment and in transporting and storing the various materials and samples. I also greatly appreciate the support of CETCO and Dr. Dennis Grubb in this research.

Special thanks to the Geotechnical Engineering faculty and staff at The University of Texas. The classes taken were very well organized, and their dedication to teach and help us to understand geotechnical concepts is greatly appreciated. Every one of the professors were fantastic teachers and mentors and are an inspiration.

I am eternally grateful for the support my parents and sisters have given and can't express the impact that their love, guidance, and prayers has had on my life. Lastly I would like to thank my friends for all the memories that have made this part of my journey unforgettably great.

Abstract

Analysis of Dredge Material and Crushed Glass Blends with Uniaxial Geogrids in Pullout Tests

Kemp Sloan Lewis III, MSE

The University of Texas at Austin 2013

Supervisor: Jorge Zornberg

Being able to identify blended dredged material and crushed glass of different proportions as materials suitable for Mechanically Stabilized Earth walls could help the adoption of these materials in civil engineering thereby reducing the environmental impact of these waste materials.

The objectives of this thesis include the following: Collect and organize data to facilitate material selection based on interaction properties with uniaxial geogrids; analyze the data for trends for varying percentages of crushed glass vs. dredged materials; compare the properties of different blends with those of a well-documented uniform sand; compare the pullout data with that of previous studies related to the presence of fines in the fill material; and compare the pullout data to that of previous studies on the effect of geogrid rib thickness.

The main findings of this thesis study include the following: A blend of 80% crushed glass and 20% dredged material is a legitimate alternative backfill material for reinforced soil slopes. The use of 100% crushed glass as a fill material is not recommended due to glass particles embedding into the geogrid thereby reducing the tensile capacity of the geogrid. Blends with lower percentages of crushed glass and higher percentages of dredged material may be appropriate based on the requirements of individual designs. The increased thickness of the UX1700 geogrid over the UX1400 geogrid contributed to higher a pullout resistance for each combination of fill material and normal stress.

Table of Contents

List of Figures

List of Tables

Chapter 1: Introduction

1.1 Motivation of This Study

The motivation of this study is to contribute towards reuse of recycled glass and dredged materials in the construction of reinforced, soil structures.

Many civil engineering projects require or benefit from changing the existing ground line. Limits of construction (LOC) are necessary to prevent physical damage to surrounding properties during construction and often require steep soil slopes or vertical walls to allow for increased changes in the grade line. For unreinforced soil slopes, the shear strength of the in-situ soil dictates the maximum angle that the slope can safely tolerate. A factor of safety (FS) against slope failure can be obtained by conducting stability analyses. If the FS from the stability analysis is not satisfactory, the slope will need to be decreased, constructed with a stronger material, or reinforced. There are many available options for reinforcing a soil slope, including Mechanically Stabilized Earth (MSE) walls and Reinforced Soil Slopes (RSS). Figure 1.1 illustrates a typical MSE wall.

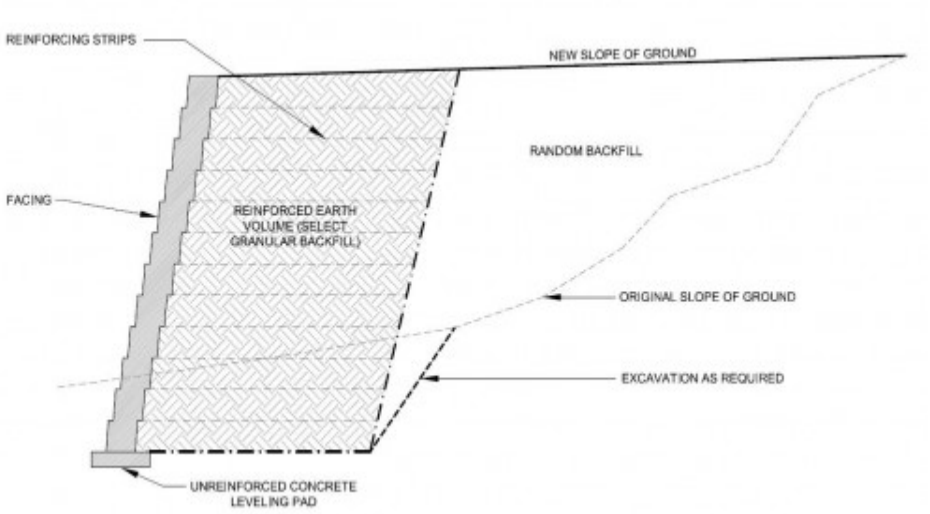

Figure 1.1: Mechanically Stabilized Earth (MSE) Wall.

An MSE wall includes the use of reinforcements within the soil mass and is built from the ground up, classifying the wall as an internally stabilized fill wall. The wall is constructed in layers alternating between soil and reinforcement. Strength properties of the fill and reinforcement, along with interaction properties between them, are necessary to design a stable wall that meets construction restraints.

This study also aims to determine whether a blend of crushed glass (CG) and dredged material (DM) would be a suitable fill material in order to offer a favorable disposal of the DM and provide a practical use option for curbside collected glass. Currently, confined disposal facilities (CDFs) are employed to store dredged material. CDFs operated by the U.S. Army Corps of Engineers (USACE) are nearing full capacity and it is costly and difficult to obtain permits for inland CDFs. Additionally, the rate at

which recycled crushed glass is produced has not been matched by the growth in demand for recycled glass particularly due to a lack of markets. The lack of new markets has led to a surplus of crushed glass that ends up being disposed as waste.

1.2 Background Information

DM characteristics may vary significantly depending on where the dredging takes place. Sand and gravel DM is usually found in streams and rivers where the current is still strong and able to carry finer sediments further downstream. Where the flow becomes very slow is usually where silts and clays are found. The composition and grain size distribution of dredged material is important in determining a suitable application. For simplicity, dredged material is characterized as one of five sediment types: rock; gravel and sand; consolidated clay; silt/soft clay; and mixture (rock/sand/silt/soft clay). Depending on their engineering properties, these categories have different lists of possible uses. For example, the recommended sediment types for use as a replacement fill are rock, gravel and sand, or mixture. This is because they are usually not very contaminated and require lesser treatment prior to usage. The majority of DM located in containment facilities in the United States are classified by the Unified Soil Classification System (USCS) as ML, MH, OH, and CH soils, which are commonly recognized as being among the poorest earthwork construction materials (USBR 1963). This classification is a major reason why the construction industry has neglected to adopt fine-grained DM as a construction material.

The opportunities for reuse of recycled glass are limited; about 28 percent of 11.5 million tons of glass generated in America in 2011 was recovered for recycling (USEPA, 2011). The main source for recycled glass is food and beverage containers that are collected from businesses, residencies, deposit stations, or recycling facilities. Glass from these sources is typically intermixed with other recycling products such as paper, cardboard, aluminum, and plastics (Landress, 2007). The quality of crushed glass is typically determined by the amount of debris in the material, which in turn depends on the waste recycling facilities. Ninety percent of the glass recycled is used to make containers; this glass is typically sorted by color and must be cleaned of debris and other materials commonly present in recycled glass. The difficulty and cost associated with processing glass into high quality cullet free of contaminants limits the number of recycling facilities that are able to recycle this material. Glass that cannot be reused must be disposed in landfills at costs of up to $50 per ton.

The geotechnical parameters of CG as an aggregate substitute depend on the glass percentage, glass gradation, compaction effort, and to a lesser degree on the glass source, water content, and debris content (Clean Washington Center, 1996). The water content has little impact due to the smooth, non-porous nature of the glass. The weight of the debris is insubstantial compared to the heavy glass thus rejections for quality control due to visual debris will most likely occur before engineering properties are affected by the debris. Local, State, and Federal regulations are perhaps the largest obstacle to the acceptance of CG as a building material; building codes and specifications either ignore

the beneficial uses for these recycled materials or they specifically prohibit them (Wartman et al. 2004).

Blending CG and DM offers a solution to recycling challenges of both materials. Recycled glass that is blended with dredged material does not require color sorting nor thorough removal of contaminants thereby facilitating the recycling process. Additionally, by blending the two materials, the geotechnical and workability characteristics are improved for fill applications. Investigations on the geotechnical properties were conducted by Grubb et al. (2006) and are discussed in the subsequent sections of this document.

1.2.1 Previous Studies

The material reports for the CG, DM, and CG-DM blends are from a "Laboratory Evaluation of CG-DM Blends" by Grubb et al. (2006a). The materials tested in this pullout evaluation are from the same source as those used by Grubb et al. In this evaluation, the tests were initially conducted on 100% CG and 100% DM specimens to define the endpoints of the material properties spectrum. Once these properties were determined, CG-DM blends were evaluated at the ratios of percentage of CG/DM of: 20/80, 40/60, 50/50, 60/40, and 80/20 based on the dry weight of both materials.

The crushed glass in this study was collected by the City of Philadelphia through their curbside collection program. The recycled class was crushed and passed through a 9.5 mm (3/8 in.) sieve. This size was chosen as it typically does not present a hazard for

physical handling of the glass as stated in the report. The dredged material used for the blends with CG in this study was collected from Basin A at the USACE Fort Mifflin CDF in Philadelphia. Two other Philadelphia CDFs, Pedricktown and Wilmington Harbor North, sourced additional DM to illustrate the similarities between these CDFs and to demonstrate the possibility of sourcing dredged material from various CDFs. The physical properties, compaction characteristics, strength characteristics of CG, DM, and the CG/DM blends determined by the program are found in Table 1.1 and Table 1.2.

Table 1.1: Physical properties and classification of CG, DM, and CG/DM blends (Grubb, 2006a).

				Partice Size D422			Plasticity Indices D4318				
Media tested	Water content *D2974* (%)	Specific gravity *D854*	LOI *D2974 (%)*	Gravel (%)	Sand (%)	Fines (%)	LL (%)	*PL (%)*	PI (%)	USCS *D2487*	AASHTO *D3282*
100% crushed glass (CG)											
Blends	1.7	2.48	3.1	29.2	70.4	0.4	NP	NP	NP	SP	A-1-a
80 / 20 CG–DM	11.9	—	2.9	26.6	59	14.4	71	48	23	SM	A-2-7
60 / 40 CG–DM	18.5	—	4.0	20	43.6	36.4	74	49	25	SM	A-7-5
50 / 50 CG–DM	24.5	—	5.7	6.8	44.8	48.4	73	46	27	SM	A-7-5
40 / 60 CG–DM	27.0	—	5.6	14.3	34.1	51.6	75	44	31	OH	A-7-5
20 / 80 CG–DM	32.9	—	8.7	6.4	18.3	75.3	80	51	29	OH	A-7-5
100% dredged material (DM)	45.8	2.40	11.0	0	3.4	96.6	81	53	28	OH	A-7-5
Pedricktown/Oldmans CDF material	50.8	2.50	6.6	0	9.7	90.3	83	47	36	OH	A-7-5
Wilmington Harbor North CDF material	39.6	2.43	7.2	0	1	99	83	38	45	CH	A-7-5

Note: All blends were made using Fort Mifflin DM. ASTM test designations shown where applicable.

The as received water content of the 100% DM and 100% CG were 45.8% and 1.7%, respectively. The water content increased from 11.9% to 32.9% as the percentage of crushed glass increased from 20% to 80%, respectively. The specific gravities of the

materials were 2.40 and 2.48 for the 100% DM and 100% CG, respectively. The loss on ignition (LOI) tests measures the amount of organic content of the materials and material blends; after drying in an oven for the water content tests, samples were placed in a furnace at 440°C for 12 hours. The LOIs of the 100% DM and the 100% CG were 11.0% and 3.1%, respectively. The LOIs of the blends increased with increasing proportion of DM. However, the amount of organic matter was less than would be expected through weight averaging. The organic matter of the crushed glass is attributed to debris such as paper labels, adhesives, and pieces of plastic caps. The organic matter of the dredged material consists primarily of decaying plant life such as roots and leaves. The grain size distributions were determined by mechanical sieving only, hydrometer tests were not conducted to determine the complete size distribution of the fine-grained soils; still, as expected the blends increased in coarseness with increasing percentage of crushed glass. The dredged material has a liquid limit (LL) of 81%, a plastic limit (PL) of 53%, and a plasticity index (PI) of 28%. These Atterberg limits (LL, PL, and PI) are not greatly affected by the addition of CG as the percentage of CG that passes the 0.425 sieve used for the test is typically 5% or less (Wartman et al. 2004). Under the Unified Soil Classification System (USCS), the 100% CG classifies as a poorly graded sand (SP), the blends with 80% to 50% of CG classify as silty sands (SM), and the blends with greater than 50% DM classify as highly plastic organic silts (OH).

Table 1.2: Compaction properties and select strength parameters of CG, DM, and CG/DM blends (Grubb, 2006a).

	Standard compaction *D 698*		Modified compaction *D 1557*		Direct shear *D 3080*		UU Triaxial *D 2850*		CIU Triaxial *D 4767*	
Media tested	$\gamma_{d,max}$ [kN/m^3 (lb/ft^3)]	*w* opt (%)	$\gamma_{d,max}$ [kN/m^3 (lb/ft^3)]	*w* opt (%)	*c* [kPa (lb/ft^2)]	ϕ (°)	*c* [kPa (lb/ft^2)]	ϕ (°)	*c* [kPa (lb/ft^2)]	ϕ (°)
100% CG	17.1 (109)	8	18.7 (119)	8	0	42	11 (225)	40	0	37
Blends										
80 / 20 CG–DM	17.3 (110)	14	18.2 (116)	10	11 (230)	36	29 (610)	34	1 (15)	39
60 / 40 CG–DM	15.6 (100)	19	17.3 (110)	10.5	19 (400)	33	28 (590)	26	6 (115)	39
50 / 50 CG–DM	14.8 (94)	24	16.6 (106)	15	26 (540)	32	48 (1,010)	30	2 (45)	38
40 / 60 CG–DM	13.7 (88)	25	16.1 (102)	11.5	25 (520)	31	45 (940)	23	2 (45)	37
20 / 80 CG–DM	11.8 (75)	29	15.1 (96)	11	26 (540)	33	70 (1,470)	16	1 (30)	35
100% dredged material (DM)	10.8 (69)	39	12.2 (78)	29	20 (420)	33	66 (1,380)	20	12 (260)	34

Note: All blends were made using Fort Mifflin DM. ASTM test designations shown where applicable.

Grubb et al. (2006b) focused on a field evaluation of the blends in which embankments were constructed with the 20/80, 50/50, and 80/20 CG-DM blends. A minimum compaction effort of 90% modified Proctor was applied to the 20/80 CG-DM embankment and a minimum compaction of 95% modified Proctor for the 50/50 and 80/20 CG-DM blends. A blend tolerance of 5% was allowed to minimize the significant effects of 20% increments in materials on the maximum dry density and optimum water content. This information is presented in Table 1.3. The 90% compaction specification for the 20/80 CG-DM blend was chosen due to the difficulty associated with compacting this blend to 95% modified proctor.

Table 1.3: Field compaction specifications for CG/DM blend embankments (adapted from Grubb et al 2006b)

	Standard compaction *D 698*		Modified compaction *D 1557*		Field Evaluation Study	
					90% mod.	95% mod
Media tested	$\gamma_{d,max}$ [kN/m^3 (lb/ft^3)]	*w* opt (%)	$\gamma_{d,max}$ [kN/m^3 (lb/ft^3)]	*w* opt (%)	$\gamma_{d,max}$ [kN/m^3 (lb/ft^3)]	$\gamma_{d,max}$ [kN/m^3 (lb/ft^3)]
100% CG	17.1 (109)	8	18.7 (119)	8	-	-
Blends						
80 / 20 CG–DM	17.3 (110)	14	18.2 (116)	10	16.4 (104.4)	17.3 (110.2)
50 / 50 CG–DM	14.8 (94)	24	16.6 (106)	15	14.9 (95.4)	15.8 (100.7)
20 / 80 CG–DM	11.8 (75)	29	15.1 (96)	11	13.6 (86.4)	14.3 (91.2)
100% DM	10.8 (69)	39	12.2 (78)	29	-	-

In compaction of the blended materials, the report details the improvements in workability of the materials with increasing percentages of crushed glass. Blends with higher proportions of crushed glass compacted with less difficulty and the control of moisture content is facilitated with the addition of crushed glass. Additionally the 80/20 CG-DM blend was compacted to the desired specification of 95% modified Proctor even under intense rainfall illustrating that this blend is not largely influenced by moisture content.

To measure the strength of the embankments, CPT tests were conducted at two outer locations 2 m from the top edge of the embankment and at one location in the

center of the embankment. The average tip resistances for the 20/80, 50/50, and 80/20 CG-DM embankments were about 1.0, 1.5, and 2.0 MPa respectively. While the CPT tests are not directly appropriate for silty soils (Robertson and Campanella, 1983), these tip resistances correlate to friction angles of 37° to 39°, which are consistent with friction angles obtained in the laboratory investigation by Grubb et al. (2006b).

CG-DM blend embankments exhibited double to triple values of cone tip resistances from cone penetrometer tests (CPT) after aging for 360 days. Additionally, the effective friction angles of the aged blends were up to 8° higher than freshly prepared samples in isotropically consolidated, undrained triaxial tests. Increased cementation was proportional to increased crushed glass percentage suggesting silica cementation as the cause of increased strength rather than carbonate formation. The increase in strength was lost upon demolition and reconstruction of the embankments (Grubb et al., 2008).

Cyclic triaxial testing on CG-DM blends showed that the materials performed well under cyclic triaxial loading conditions due to the compaction of the material and the reduction of water content in the DM by the addition of crushed glass (Gallagher et al., 2009).

A study by Grubb et al. (2007) assembled the investigations of Wartman (2001), Wartman et at. (2004 a,b), and Malsavage et al. (2006) on crushed glass from three different sources in order to compare the physical and chemical properties of crushed glass and to measure how different sources might affect these properties. A summary

table of this information is presented in Table 1.4. It was concluded that the three suppliers could provide consistent materials and the variability between suppliers was more linked to grain size distribution than processing factors such as debris content and characteristics of the parent glass. Furthermore, the study concluded that crushed glass, as a construction material, is comparable to or in may exceed the strength and hydraulic conductivity behavior of natural aggregates of the same gradation.

Table 1.4: Summary table of CG parameters from 3 PA sources (Grubb et al., 2007)

Test/Index	Units	ASTM standard	Supplier I	Supplier II	Supplier III
Water content	%	D2216-98	2.36	4.22	1.7
			[2.03-2.60]	[3.49-5.32]	
Debris content	%	Gravimetric	0.034	1.82	
			[0.0-0.75]	[0.62-3.41]	
Loss on Ignition	—	D2974			3.1
Specific gravity (G_s)	—	C127-88	2.48	2.49	2.48
Minimum density	g/cm^3	D4254-00	1.15	1.27	
			[1.14-1.16]	[1.23-1.30]	
Maximum density	g/cm^3	D4253-00	1.79	1.74	
			[1.77-1.80]	[1.72-1.75]	
Median grain size (D_{50})	mm		2.24	3	3.1
			[1.85-2.62]	[2.70-3.30]	
Coefficient of uniformity (C_u)	—		6.2	7.2	4.1
			[4.3-10.0]	[5.4-7.0]	
Sand content (.075-4.75 mm)	%		91.3	70	70.4
			[89.5-93.0]	[66.5-74]	
Fines content (<0.075 mm)	%		3.2	1.2	0.4
			[0.5-5.0]	[0.2-2.0]	
USCS classification	—	D2487-98	SW	SW	SP
LA abrasion	wt.%	C131-96	24	25	
Sodium sulfate soundness	wt.%	C 88-05	6.38	7.1	
Magnesium sulfate soundness	wt.%	C 88-05			1
Hydraulic conductivity	cm/s	D2434-68	1.61 x 10^{-4}[a]	6.45 x 10^{-4}[a]	6.2 x 10^{-2}[b]
			[1.36 x 10^{-4}–1.85 x 10^{-4}]	[6.42 x 10^{-4}–6.64 x 10^{-4}]	
Modified Proctor		D1557-00			
$\gamma_{d, max}$	kN/m^3		18.3	17.5	18.7
	(lb/ft^3)		(116)	(111)	(119)
w_{opt}	%		9.7	11.2	8
Standard Proctor		D698-00			
$\gamma_{d, max}$	kN/m^3		16.8	16.6	17.1
	(lb/ft^3)		(107)	(106)	(109)
w_{opt}	%		12.8	13.6	8
Direct shear (ϕ'_{DS})		D3080-98			
σ_n					
0-60 kPa			61-63°	59-62°	
60-120 kPa			58-61°	55-59°	42°
120-200 kPa			63-68°	47-55°	
Triaxial shear, Effective (ϕ'_{CID})		D4767-04			
10% axial strain			48°	47°	37°
max stress obliquity			41°	42°	37°

Most Supplier I and II data from Wartman et al. (2004b). Bracketed values show ranges.

Most Supplier III data from Grubb et al. (2006a).

[a] compacted to a min 90% (±1%) RC of $\gamma_{d, max}$ per ASTM D1557.

[b] compacted to 95% (±2%) RC of $\gamma_{d, max}$ per ASTM D1557.

1.2.2 Geogrids

Geogrids are polymeric reinforcement products meant to reinforce soil by intersecting potential failure places, and distributing load over a larger area than would naturally occur. Geogrids are made from one of various polymer types including polyester (PET), high density polyethylene (HDPE), and polypropylene (PP). Geogrids are also designed to carry loads in a specific way which falls into the categories of uniaxial, biaxial, and triaxial which are pictured in Figure 1.2, Figure 1.3, and Figure 1.4, respectively.

Figure 1.2: Uniaxial geogrids

Uniaxial geogrids carry tension along the longitudinal direction of the ribs. The geogrid in Figure 1.2 has longitudinal ribs running across the page and transverse ribs running up and down the page. Uniaxial grids are primarily used as reinforcement in soil structures such as reinforced soil slopes.

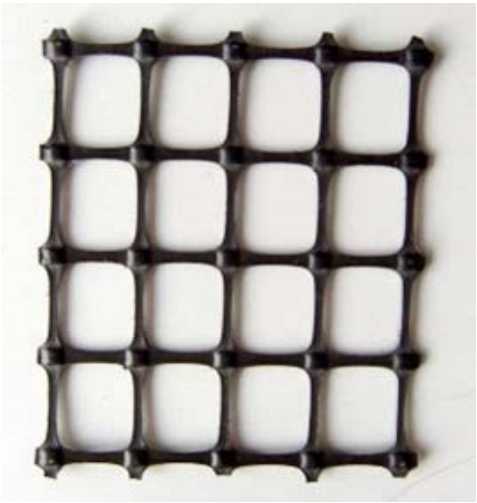

Figure 1.3: Biaxial Geogrids

Biaxial geogrids (Figure 1.3) carry tension in two directions and provide planar resistance though both directions. They are normally used in the base layer of pavement structures to improve resistance to low temperature cracking, rutting effects, and long term fatigue.

Triaxial geogrids (Figure 1.4) carry tension in multiple directions and have been developed for their potential as reinforcement material in pavement structures.

Figure 1.4: Triaxial Geogrids

HDPE geogrids are typically manufactured by punching a regular grid of holes into a sheet which is then stretched to the desired size. The sheet is only stretched in one direction for uniaxial geogrids, which creates apertures longer in the longitudinal (machine) direction than the transverse (cross machine) direction. This stretching also results in the longitudinal ribs being thinner and narrower than the transverse rib. HDPE geogrids are advantageous for their high tensile capacity and chemical inertness.

Geogrids characteristics include their polymer, strength, geometric characteristics and resistance to various forms of degradation. The tensile strength is largely affected by the polymer type and by the thickness of the grid. Resistance of the grid to degradation from chemicals and ultraviolet light is dependent on the polymer type and any coatings applied to the geogrid.

1.3 Objectives

This study aims at quantitatively comparing the performance of crushed glass and dredged material blended to various proportions in pullout tests with uniaxial geogrids. Monterey sand is set as a baseline for comparison. Additional data organized by Hutcherson (2012) from a database provided by SGI Testing Services, formerly GeoSyntec Consultants, is also used to encompass a wider variety of fill materials tested under similar conditions.

The objectives of this thesis include the following:

- Quantify pullout capacities of CG-DM blends with two different uniaxial geogrids.
- Analyze the data for trends related to percentage of crushed glass
- Quantify the geogrid-fill material interaction using the coefficient of interaction
- Compare the collected data to existing data on a uniform granular fill material
- Compare the collected data to previous studies on the effect of geogrid rib thickness to mean particle size ratio on normalized bearing stress and calculated CI values

1.4 Methodology

The scope of the experimental component of this project includes conducting pullout tests on 100% CG, 100% DM, and 80/20, 50/50, and 20/80 CG-DM blends. The mixtures were prepared by blending the materials on a dry weight basis. As reinforcement, two uniaxial Tensar geogrids, UX1400 and UX1700, were used. Monterey Sand was used to establish repeatability of the system and as a baseline material for comparison. Confining pressures of 4, 6, and 8 psi were applied to simulate field conditions anticipated in MSE walls; these pressures were chosen to avoid tensile failure of the geogrid. To minimize variability between tests for ease of comparing the data, the following constants were used: rate of pullout, geogrid sample size, and water content relative to the optimum water content of each blend. The results of the pullout tests were used to compare the materials and blends to one another and to compare the geogrids. Using crushed glass and dredged material blends in a pullout box is the first study of its kind to available knowledge from literature.

1.5 Thesis Organization

This thesis is divided into five main chapters. Chapter 1 includes the motivation and background information pertinent to this study. Chapter 2 describes the mechanisms of pullout testing and how different factors affect pullout results. Chapter 3 details the geogrids and materials used in the pullout testing program and the testing apparatus and

procedures used in each test. Chapter 4 presents an evaluation of the data collected and records trends observed in the data. Chapter 5 presents conclusions from this testing program and suggests future investigations that might compliment this research.

Chapter 2: Geogrid Pullout Testing

2.1 Overview of Geogrid Pullout Resistance Testing

There are a few different means by which geogrid reinforcements may fail. The modes of failure can be investigated through different testing devices and techniques. Figure 2.1 (Palmeira, 2008) displays four different modes of interaction between a fill material in a reinforced soil wall. Region A depicts soil sliding over the top of the geogrid. Direct shear interface tests would be appropriate in this case to determine the level of interaction between the materials. Region B shows lateral deformation of the soil and geogrid as a unit, in which case plane strain tests would be appropriate. Region C depicts shearing of the soil and reinforcement so direct shear tests with an inclined reinforcement would be appropriate. Region D shows the reinforcement being pulled out so pullout tests would be appropriate; this is the method of failure being investigated in this document. It should be noted that each of these tests are limited in precisely simulating the in situ conditions.

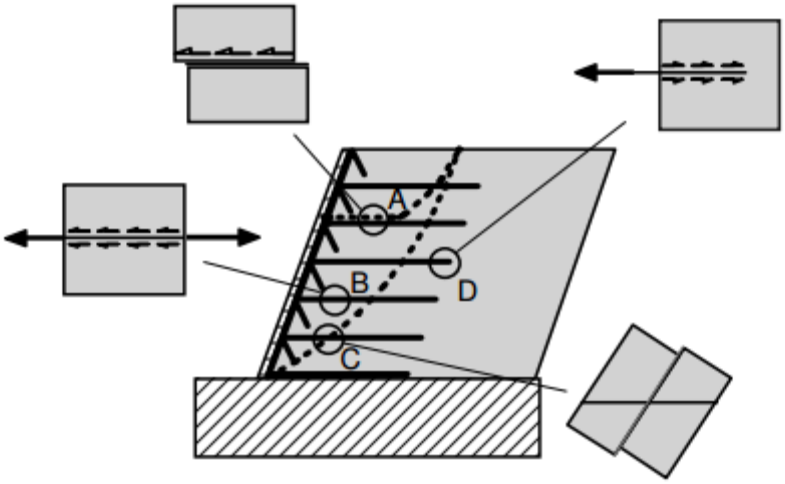

Figure 2.1: Soil-geogrid interactions for different failure surfaces (modified from Palmeira and Milligan 1989a).

Given the various methods by which a geosynthetic may fail in an earthen slope it is important to accurately test the pullout condition. ASTM D6706 is the Standard Test Method for Measuring Geosynthetic Pullout Resistance in Soil. The test is commonly used as a research and developmental procedure to "compare different geosynthetics, soil types, and etc." It is important to replicate the field conditions in the laboratory to obtain appropriate results. However, testing equipment varies significantly between labs and the differences can significantly affect the results.

In a pullout test the geosynthetic specimen is embedded between two layers of soil, subjected to normal compressive stresses applied to the top soil layer, then subjected to a horizontal force which is recorded during a constant rate of frontal displacement.

Failure in pullout is obtained when the load reaches a peak value and either remains constant for an extended period of time or drops. Failure will also be confirmed by the entire length of the geosynthetic specimen displacing at the same rate. Failure can be defined as a reaching a predetermined displacement without failing through either of the mechanisms discussed above. Variables recorded during a standard pullout test are time, displacement at multiple points along the length and width of the specimen, and the load. The maximum horizontal force applied is recorded. The Pullout Resistance is obtained by dividing the maximum pullout load by the width of the test geosynthetic specimen. A typical pullout setup is shown in Figure 2.2.

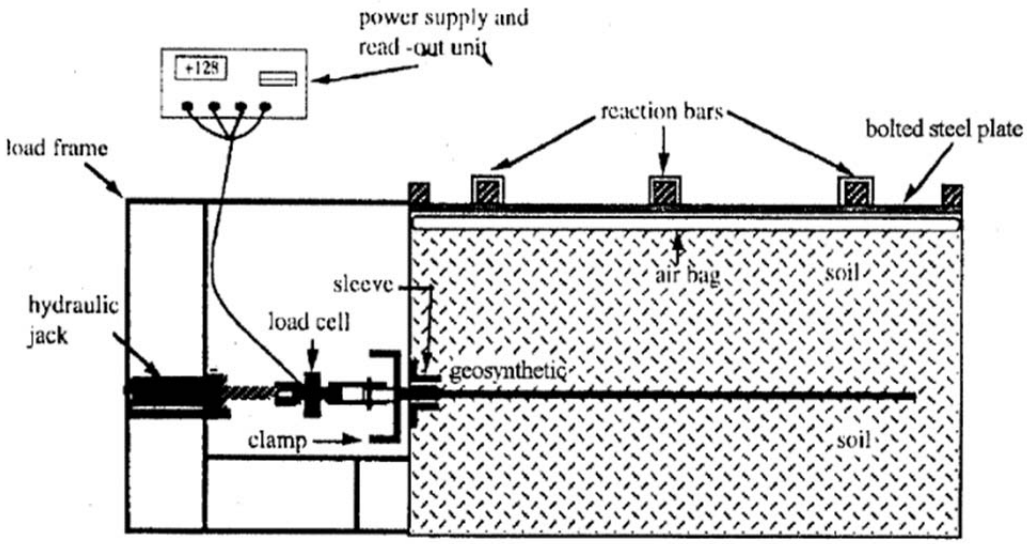

Figure 2.2: Experimental setup for a geosynthetic pullout testing program.

Tension failure occurs when the pullout force exceeds the tensile strength of the geosynthetic specimen, causing rupture of the specimen. For these reasons it is important

to study the geosynthetic specimen after each test and record the appropriate mode of failure.

Upon completion of a pullout test the data is analyzed to obtain relevant parameters to quantify the performance of the geosynthetics in the fill material. The Pullout Resistance is a primary metric to compare various materials and test conditions. Additionally, force-displacement plots aid in visualizing the displacements along the geogrid as the test progresses as well as identifying the peak pullout force. Plots of the Pullout Resistance with varying normal stress allow comparison of results in various conditions. Another commonly used parameter in comparing results from pullout tests is the coefficient of interaction (CI).

A laboratory pullout test is typically conducted to obtain a coefficient of interaction (CI) between a geogrid and the fill material the grid is placed within. The CI helps determine the required embedment length and vertical reinforcement spacing for a particular design.

There are several aspects of pullout tests that have an effect on the measured pullout load. These aspects include length and width of the specimen. These aspects will not be analyzed in depth for this pullout program but are discussed here for more thorough knowledge of this testing method.

The testing apparatus and procedures were conducted in general accordance with ASTM D 6706 "Standard Test Method for Measuring Geosynthetic Pullout Resistance in Soil."

2.2 Coefficient of Interaction

The coefficient of interaction (CI) is a measure of the interaction between the soil and the geosynthetic. The CI is defined as the ratio of the shear strength of the geosynthetic-soil interface to the shear strength of the soil. The interfacial shear strength in a pullout test is represented as the pullout force per unit contact area ($P_r/2L_e$). The CI is effectively a measure of the efficiency of the interaction between the soil and the geosynthetic. For design purposes, an upper bound for the CI is 1.0 which represents perfect contact between the soil and the geosynthetic. A CI greater than 1.0 would indicate greater interaction at a soil-geosynthetic interface than at a soil-soil interface. Typical soils used as backfill material are granular, cohesionless soils and thus their shear strength is a function of the normal stress and the friction angle.

There are various expressions used to define the CI. One such is in terms of the interface friction angle (δ) at the soil-geosynthetic interface. This gives the interfacial shear strength at the soil-geosynthetic interface (τ_{s-g}) the following expression:

$$\tau_{s-g} = \frac{P_r}{2 \times L_e} = \sigma_y \times \tan(\delta) \qquad (2.1)$$

where σ_y is the normal stress on the system.

If the soil shear strength from a direct shear test is expressed as τ_s and ϕ is the soil friction angle then the CI can be expressed as:

$$ci = \frac{\tau_{s-g}}{\tau_s} = \frac{\tan(\delta)}{\tan(\phi)} \qquad (2.2)$$

Combining equations (2.1) and (2.2) allows the CI to be expressed in terms of the Pullout Resistance (Pr), the embedded length of the geogrid (L_e), the normal stress on the system (σ_y), and the friction angle of the soil (ϕ):

$$ci = \frac{\tau_{s-g}}{\tau_s} = \frac{P_r}{2 \times L_e \times \sigma_y \times \tan(\phi)} \qquad (2.3)$$

2.3 Factors Affecting Pullout Interaction

ASTM D6706 states that the factors affecting Pullout Resistance include "soil gradation, plasticity, as-placed dry unit weight, moisture content, the length of the geogrid, and the surface characteristics of the geogrid." There are other aspects that influence the Pullout Resistance of a specimen; these parameters are classified into one of three categories: test setup and procedural factors, soil factors, and geogrid factors.

Additionally, since these tests can be performed on all types of geosynthetics, this review will focus on the pullout mechanism of geogrids.

2.3.1 Test Setup and Procedural Factors

ASTM D6707 includes specifications on box height, width and length, relative opening size, sleeve length, normal stress, clamping system, horizontal load application and displacement rate.

The height of the box, and thereby the height of the soil, has an impact on the Pullout Resistance as concluded through extensive research previously conducted (Palmeira and Milligan 1989a, Farrag et al. 1993, Lopes and Ladiera 1996, and Dias 2003). ASTM D6707 recommends a minimum depth of 150 mm (6 in.) of soil above and below the geogrid for a total minimum depth of 300 mm. The results showed that stiffer pullout responses and higher maximum pullout loads occurred for decreasing soil thickness; as the thickness increased the pullout load decreased. However, this influence was minimal when the box height was greater than the length of the reinforcement. The results of the finite element analysis by Dias (2003) can be seen in Figure 2.3.

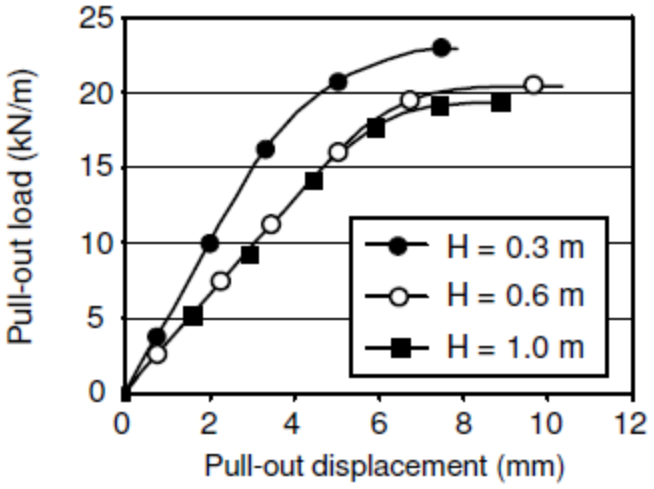

Figure 2.3: Numerical analyses of influence of box height on Pullout Resistance (Dias 2003).

The Pullout Resistance can also be affected by the width of the box; to minimize side friction ASTM D6707 recommends a minimum width of 460 mm (18 in.) and bonding of a HDPE geomembrane to the inside surfaces of the pullout box. The length of the box is also specified by ASTM D6707 to allow for a minimum of 610 mm (24 in.) beyond the sleeve. The specification also notes that larger boxes should be used when testing geogrids with larger apertures.

Extensive research has shown that the frontal face of the pullout box can significantly affect the results of a pullout test (Palmeira 1987, Palmeira and Milligan 1989a, Johnston and Romstad, 1989, Farrag et al. 1993, Lopes and Ladeira 1996, Raju 1995, Moraci and Montanelly 2000 and Sugimoto et al. 2001). The literatures from these results however do not agree on a definite trend regarding the presence and size of a

sleeve. For example: a finite element analysis by Dias (2003) concluded that sleeves measuring 15 cm and 30 cm did not show a significant impact on the maximum pullout load whereas Farrag et al. (1993) recorded a 20% greater Pullout Resistance for a 20 cm long sleeve over a 30 cm long sleeve. The finite element analysis by Dias did conclude that the presence of a sleeve resulted in a higher maximum pullout load compared to a test conducted with a lubricated frontal face and no sleeve. The recommendation by ASTM D6707 is for a sleeve consisting of two thin plates that extend across the entire width of the box and extend into the box a minimum of 150 mm (6 in.).

The normal stress is applied to the top layer of soil and must be uniform and constant throughout the test. ASTM D6707 recommends a flexible pneumatic or hydraulic diaphragm-loading device that is continuous over the entire pullout box area and that can maintain the required normal stress to within ± 2%. Numerous studies have shown that the Pullout Resistance increases continually with increasing confining stress for pullout loads less than the tensile strength of the specimen (Lopes & Ladeira, 1997).

ASTM D67078 states that the clamping system must connect the specimen to the pullout force system without slipping or weakening the material. To keep the pullout load evenly distributed along the width of the specimen, the clamping system should be allowed to rotate. The system should also keep the specimen horizontal and at a height such that the specimen does not encounter interference with the sleeve of the pullout box.

The specification allows for gluing, bonding, or otherwise molding the specimen to the clamping system when necessary.

ASTM D67078 states that the pullout force loading device must be able to apply a horizontal force on the specimen and at the same level of the specimen. The device must be capable of applying the pullout force at a constant rate of displacement; the specification is for a rate of 1 mm/min when excess pore pressures are not anticipated. Lopes & Ladeira (1997) showed that increased displacement rates result in increased Pullout Resistance; this research suggested this increase in Pullout Resistance was due to the increased stiffness of the geogrid and a "reduction of the soil's capacity to rearrange." A load cell capable of accurately measuring the pullout load must be attached to point of pullout load application.

2.3.2 Geogrid and Soil Factors

Geogrid factors include the geometry of the grid (uniaxial, biaxial, or triaxial); dimensions (length, width, thickness, size and spacing of apertures and ribs); tensile strength; stiffness; and texture. Soil factors can include, but are not limited to, particle size distribution, moisture content, density, plasticity, and shear strength.

A study conducted by Moraci and Gioffrè (2006) determined that the apparent friction coefficient decreases as the embedded length of the geogrid is increased as seen in Figure 2.4. ASTM D6706 suggests a length to width ratio greater than 2 and a minimum width of 305 mm (12 in.).

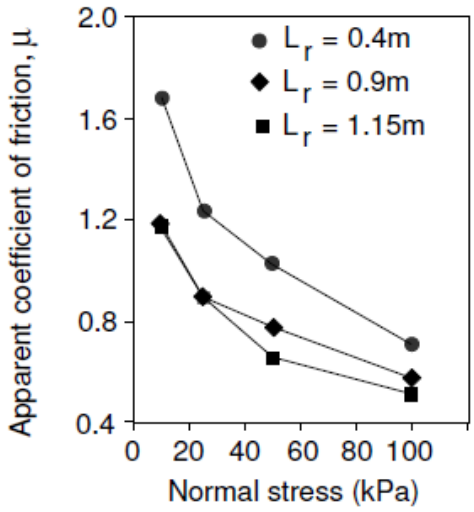

Figure 2.4: Variation of the coefficient of friction with different geogrid lengths at various confining pressures (Moraci and Gioffrè 2006).

Photo elastic tests conducted by Dyer (1985) have shown that for steel geogrids, the load distribution between different transverse members is dependent on the spacing of the transverse members. The distribution of bearing stresses is even only when the transverse members are sufficiently far apart (Figure 2.5 (a)) and as the distance is reduced, the bearing stress distribution among transverse ribs can become non-uniform (Figure 2.5 (b)).

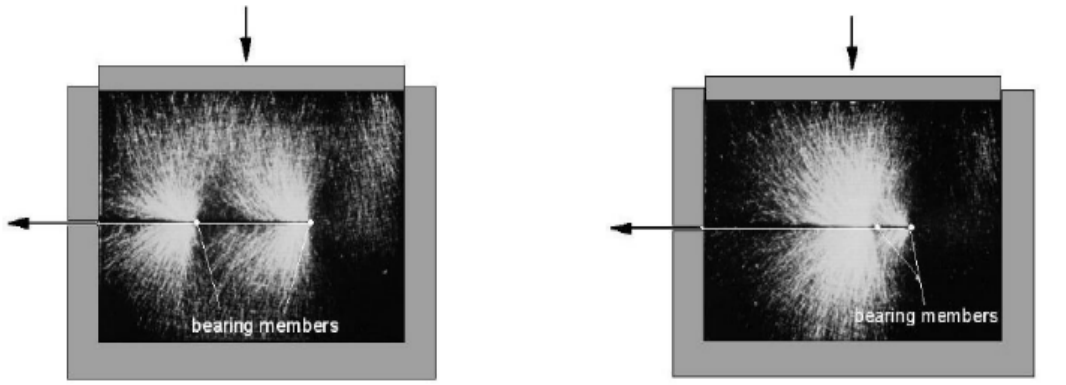

(a) Large spacing between transverse members. (b) Short spacing between bearing members.

Figure 2.5: Photo elastic results of interference between transverse members (Dyer,

The movement of the geogrid leaves loose sections of soil behind the transverse members and the magnitude of the area affected by the failure mechanism can depend on the size of soil particles and on the thickness of the transverse ribs. Results from Palmeira (1987) and Palmeira and Milligan (1989a) suggest that interference between transverse members is negligible for S/B ratios greater than 40; where S was the spacing of the transverse ribs and B was the diameter of steel grids with round transverse ribs.

Similar tests conducted on polymer grids resulted in greater non-uniformity of bearing stress distribution (Milligan et al., 1990). Palmeira (2008) suggests that the stiffer geogrids of today may more closely match the results obtained from the tests on steel grids and that the results seen in Figure 2.6 may be extrapolated for very stiff polymeric grids.

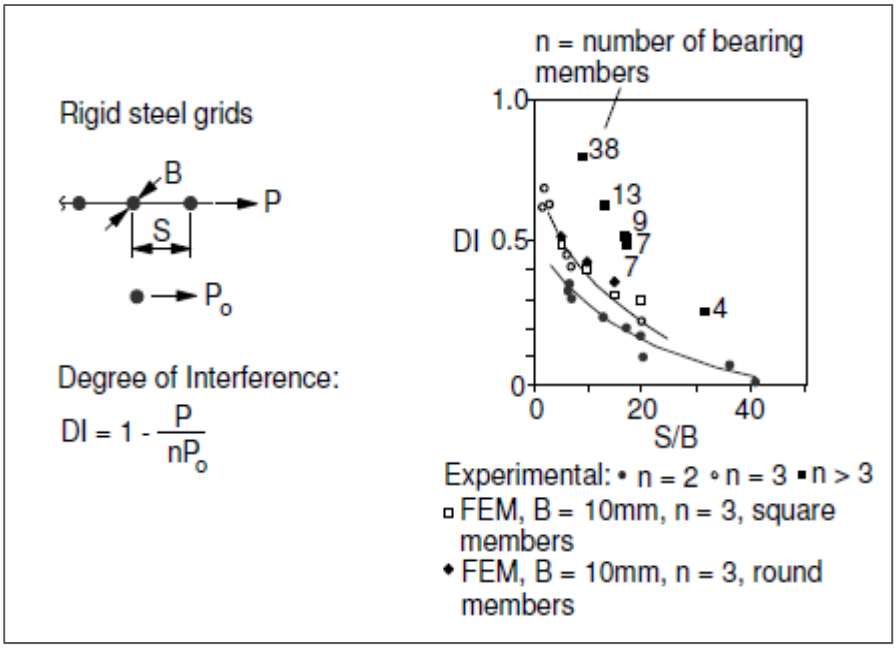

Figure 2.6: The degree of interference versus the ratio of transverse member spacing and member thickness.

2.4 Mechanism of Pullout Interaction

The Pullout Resistance mechanisms of a geogrid include frictional response and bearing resistance. Skin friction develops between the fill material and the geogrid primarily along the top and bottom surfaces of the geogrid. The bearing resistance develops at the leading face of each transverse rib. The proportion of resistance from either friction or bearing depends on the geometry of the geogrid and the fill material's characteristics. Figure 2.7 depicts these contributions of shear strength and bearing (anchorage strength) between a geogrid and soil under pullout conditions.

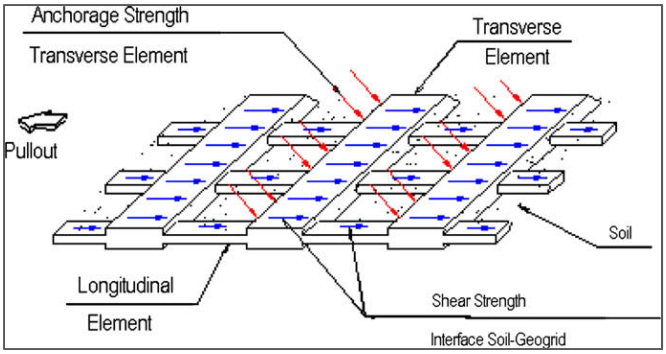

Figure 2.7: Soil geogrid interaction under pullout condition (Cristina et al., 2009).

The total Pullout Resistance corresponds to the sum of the bearing and friction components. The frictional resistance could be calculated using the total contact area between the grid and the soil. Various sources have proposed multiple methods of development of the bearing resistance and then quantifying this parameter. Passive bearing resistance from the transverse ribs can fail by general shear mechanisms (Jewell, 1984), punching shear failure (Peterson and Anderson, 1980), or a modified punching shear mechanism (Chai, 1992).

General shear and punching shear failure of geogrids resemble bearing capacity failures of shallow footings as shown in Figure 2.8. General shear failure (Figure 2.8 (a)) is the most common type of bearing capacity failure and typically occurs in strong, granular soils. Punching shear failure (Figure 2.8 (b)) typically occurs is weak clays or loose sands.

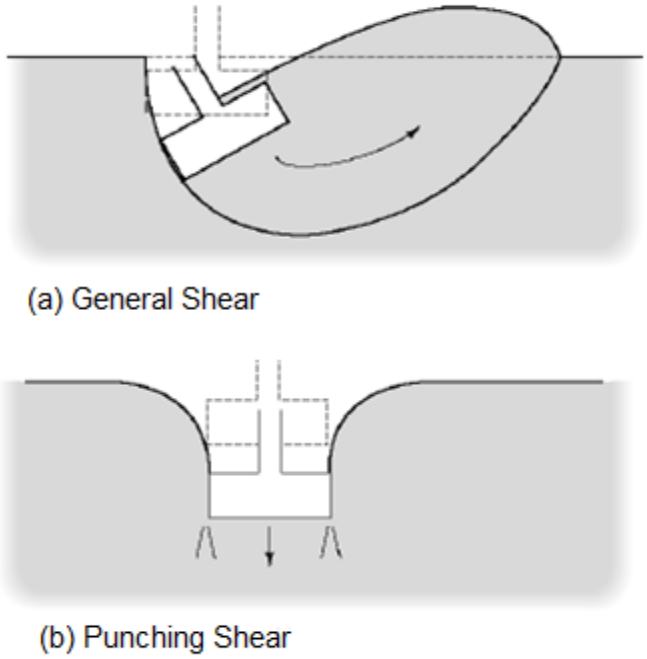

Figure 2.8: Bearing capacity failures of shallow footings: (a) General Shear Failure and (b) Punching Shear Failure. (Adapted from Coduto, 2001).

The mechanism of bearing failure in general shear and punching shear for a geogrid is presented in Figure 2.9. Under drained conditions, the effective vertical stress can be related to bearing resistance through the generalized bearing capacity equation. These equation is beyond the scope of this research however they can be found in Coduto (2001). Furthermore, the expressions for general and punching shear failure presented in Palmeira and Milligan (1989) represent an upper and lower bound respectively for the bearing resistance. The results and origin of this observation is presented in Figure 2.10.

Also in Figure 2.10 are the results from a series of pullout tests presented as the normalized bearing resistance versus the friction angle of the soil.

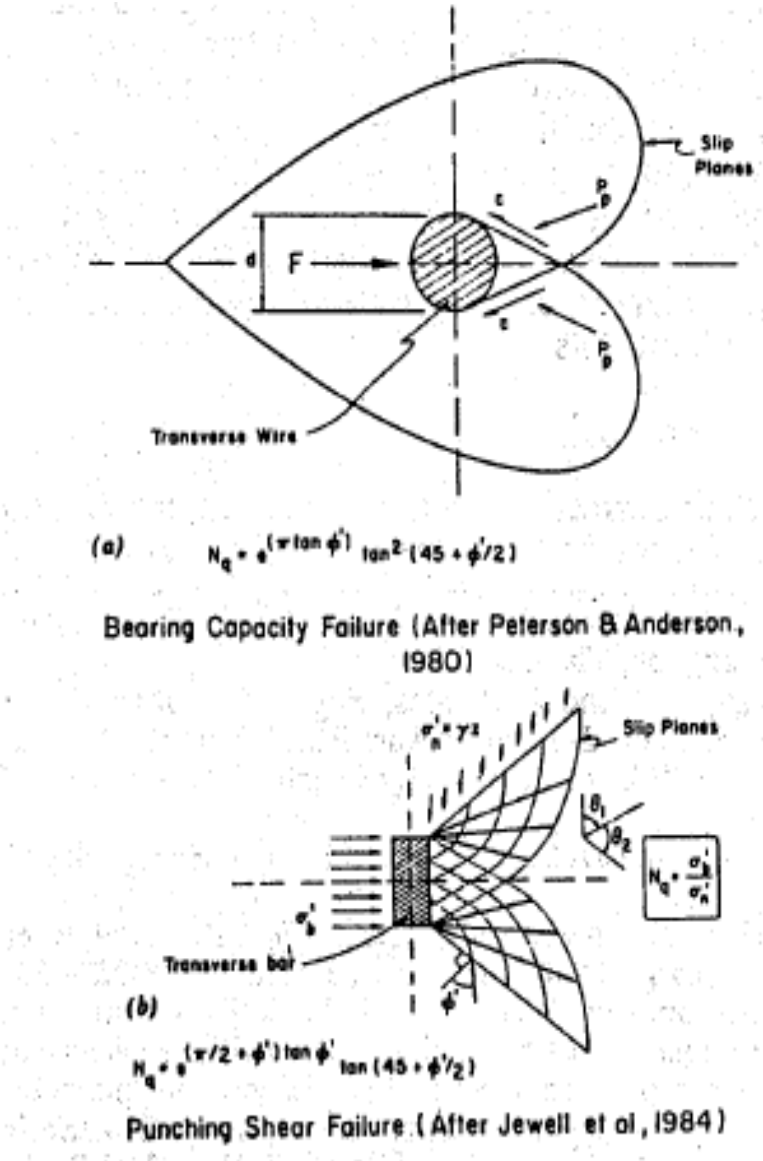

Figure 2.9: Bearing resistance mechanism in grid reinforcement (Bergado and Chai, 1991)

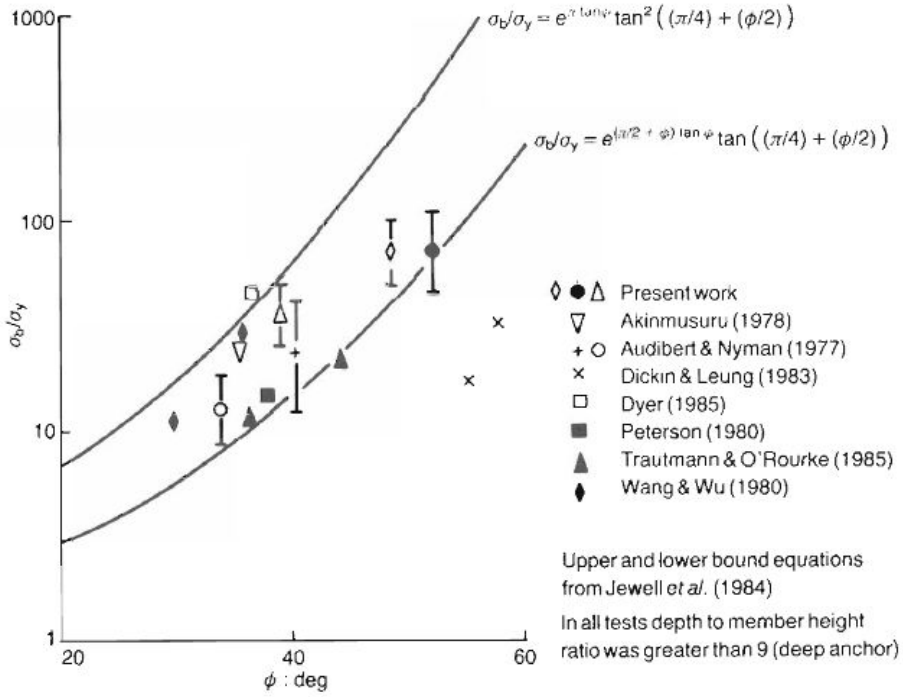

Figure 2.10: Normalized bearing resistance versus soil friction angle (Palmeira and Milligan, 1989).

The normalized bearing stress for a single transverse rib is calculated using the following equations:

$$\sigma_b = \frac{P_0}{B \times W_r} \tag{2.4}$$

$$Normalized\ Bearing\ Stress = \frac{\sigma_b}{\sigma_y \times \tan(\phi) + c} \tag{2.5}$$

Where "σ_b" is the bearing stress on the transverse rib, "P_0" is the maximum pullout force, "B" is the thickness, "W_r" is the width of the rib being tested, "σ_y" is the

normal stress on the geogrid, "φ" is the peak friction angle of the fill material, and "c" is the peak cohesion of the fill material.

Jewell (1984) explains the relation for pullout resistance of particle size to aperture size of the geogrid at failure. At failure, fine soils have greater "kinematic freedom" to displace in various directions at various orientation thus leasing to a smaller zone of rupture and lower all displacement. For smooth surfaces, the particles slide over the geogrid with relative ease. For coarse materials, the particles interlock against the face of the transverse ribs resulting in a larger rupture zone that extends back further into the fill material. For this to occur, the particles must still be small enough to fit inside the grid apertures, otherwise the only resistance would be from surficial friction. This qualitative explanation lends to the idea that pullout resistance increases with increasing particle size given that the particles can fit between apertures.

Palmeira and Milligan (1989) discussed the effect on pullout of the ratio of the thickness of the transverse rib (B) to the mean soil particle diameter (D_{50}) in order to understand the interaction between the soil and geogrid along the transverse rib. Palmeira went on to summarize pullout tests conducted on isolated transverse members with dense sand and crushed glass (2008) as presented in Figure 2.11. The normalized bearing resistance decreased with increasing B/D_{50} for values of B/D_{50} less than about 12 and showed little to no change for B/D_{50} ratios greater than 12. A simple way of looking

at the results is considering that the soil-geogrid interaction is better for smaller ratios of B/D_{50}.

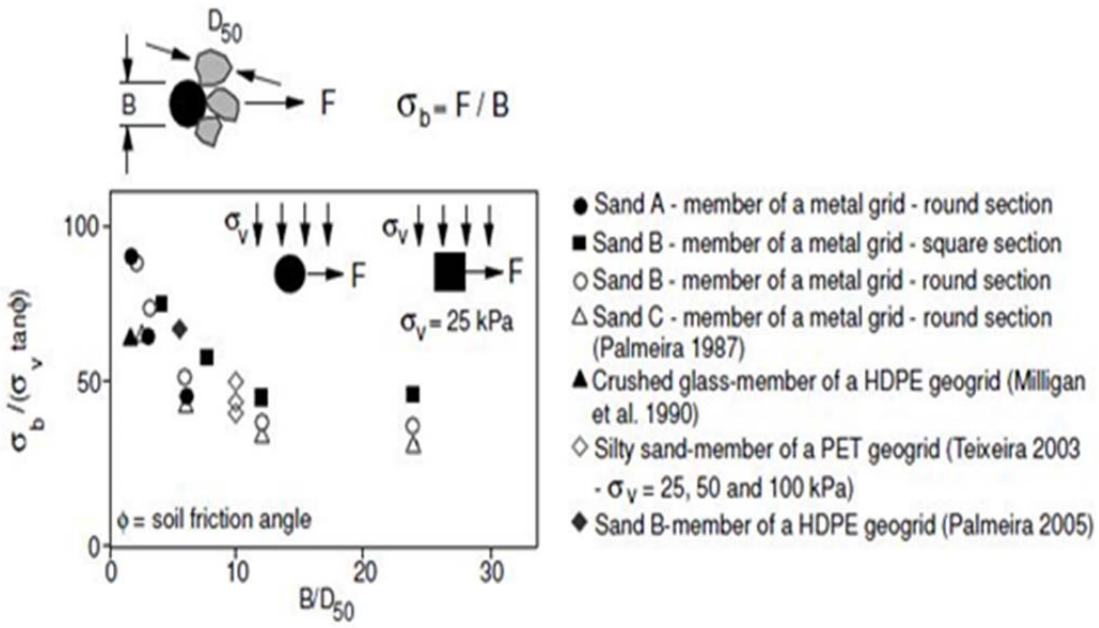

Figure 2.11: Normalized bearing stress versus transverse rib thickness to mean soil particle diameter (B/D50) for various grids and materials (Palmeira, 2008).

Teixeira et al. (2007) conducted a pullout test study on geogrids with and without transverse ribs. The geogrids were made of polyester and had apertures of 23 x 23 mm and were tested in a dense granular material. The transverse members proved to contribute to a significant portion of the pullout resistance at large strains. The geogrids with transverse ribs plateaued at the pullout resistance while the geogrids with only longitudinal ribs showed strain softening with additional displacement after a peak pullout resistance. The pullout force – displacement plot from this study is presented in Figure 2.12.

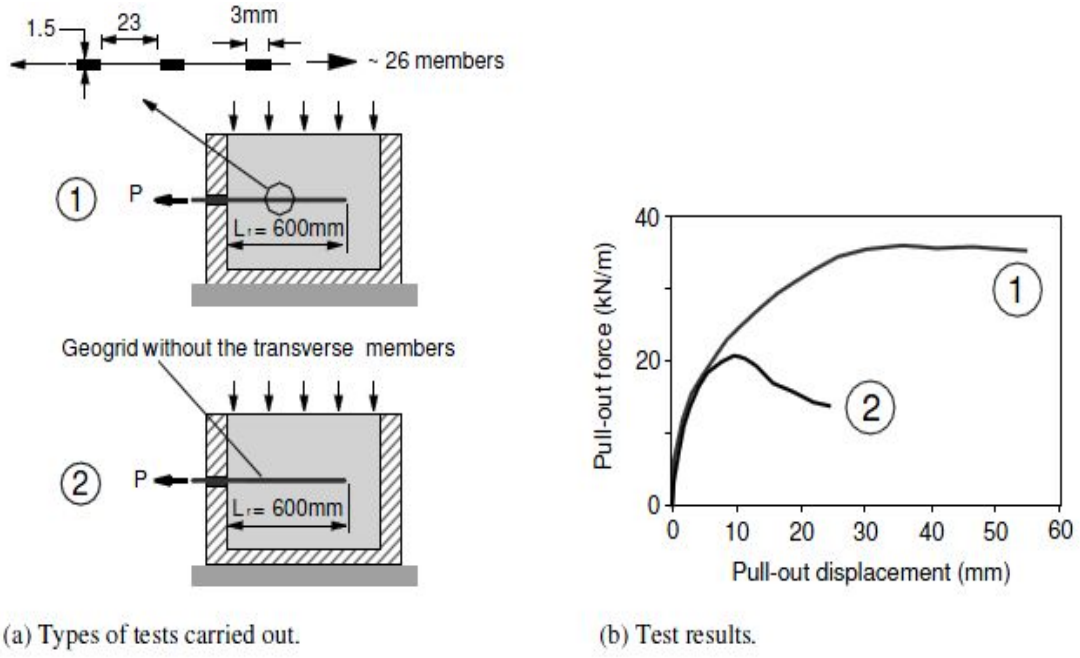

(a) Types of tests carried out. (b) Test results.

Figure 2.12: Bearing member influence on the load-displacement behavior of a geogrid (Teixeira et al., 2007).

An experimental study by Teixeira et al. (2007) further investigated the contribution of longitudinal and transverse ribs. Uniaxial, polyester geogrid samples were tested in a non-plastic sandy soil at two normal pressures of 25 kPa and 50 kPa. A specifically designed small scale pullout box was used to test longitudinal and transverse ribs individually while maintaining their spacing.

Force-displacement curves of the tests are presented in Figure 2.13. For both longitudinal and transverse ribs there was a well-defined peak which was followed with a drop in pullout resistance; the displacements at peak pullout resistance for the longitudinal ribs was about 1/4th less than the displacement for the transverse ribs at peak pullout resistance.

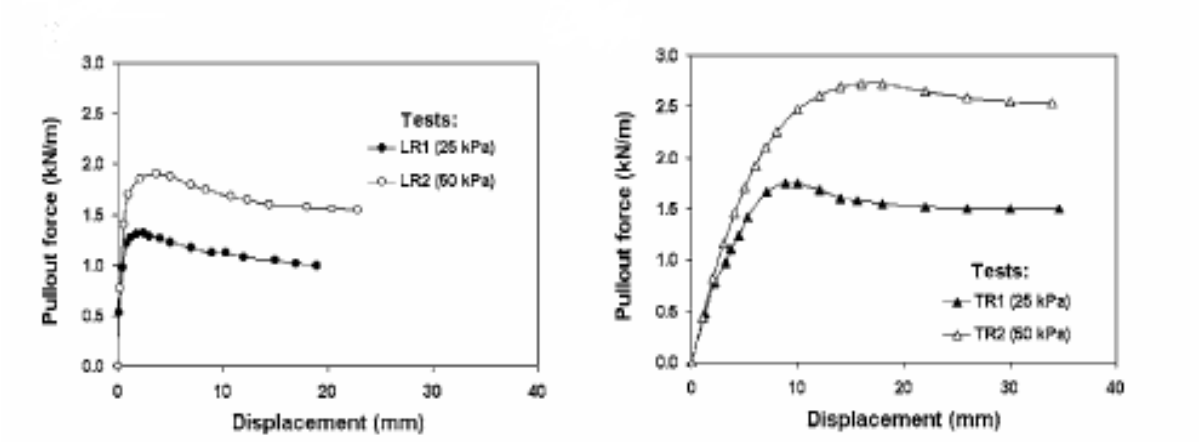

Figure 2.13: Results of pullout tests on (a) longitudinal ribs only and (b) transverse ribs only (Teixeira et al., 2007).

Further tests were conducted in a large pullout box on geogrids with and without transverse ribs; force-displacement curves are presented in Figure 2.14. The transverse ribs provided greater resistance to pullout.

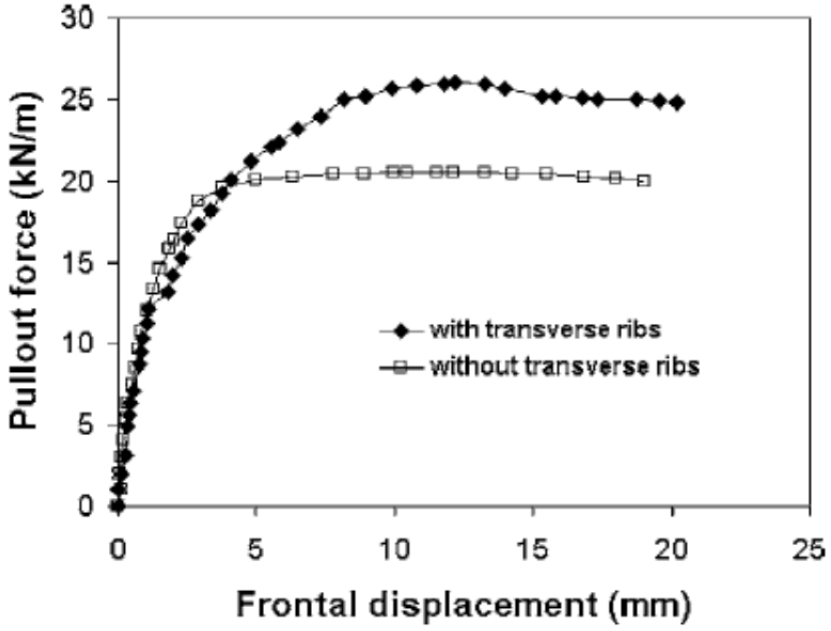

Figure 2.14: Pullout test results of geogrids with and without transverse ribs (Teixeira, 2007).

This test also measured the total normal stress using two earth pressure cells. In one setup both cells were placed between longitudinal ribs at different distances from the front of the box (Figure 2.15 (a)). For the other setup, the cells were located at the same distance from the front face of the pullout box however one cell was placed directly over a longitudinal rib while the second was placed in between two longitudinal ribs (Figure 2.15 (b)). For the cells measuring between the two longitudinal ribs (a) the normal pressure oscillated between 10 and 50 kPa. Teixeira notes that the distance between the

peaks in the localized normal pressure matches the spacing between the transverse ribs of the geogrid. “The soil in front of the transverse ribs is displaced over and under the transverse ribs during pullout testing, which causes a tendency toward dilation over the transverse ribs (Dyer, 1985).” In areas over the transverse ribs the dilation is restricted thus increasing the normal pressure; the areas between the transverse ribs showed a comparative decrease in normal pressure. For the pressure cell placed directly over a longitudinal rib (b), the normal stress oscillates around a stress of less than the applied 25 kPa. This indicates that under pullout, the bearing force on the transverse ribs creates a low stress zone over the longitudinal ribs thus negatively impacting the interface shear resistance along the longitudinal ribs. Thus adding to the evidence that pullout resistance is not merely a summation of the resistances due to bearing and shear but that the bearing resistance can result in a reduced contribution of shearing resistance along the longitudinal ribs. It does reason to follow that the shearing resistance at the transverse ribs would benefit from the increased localized normal pressure however the existing literature has not quantified this contribution.

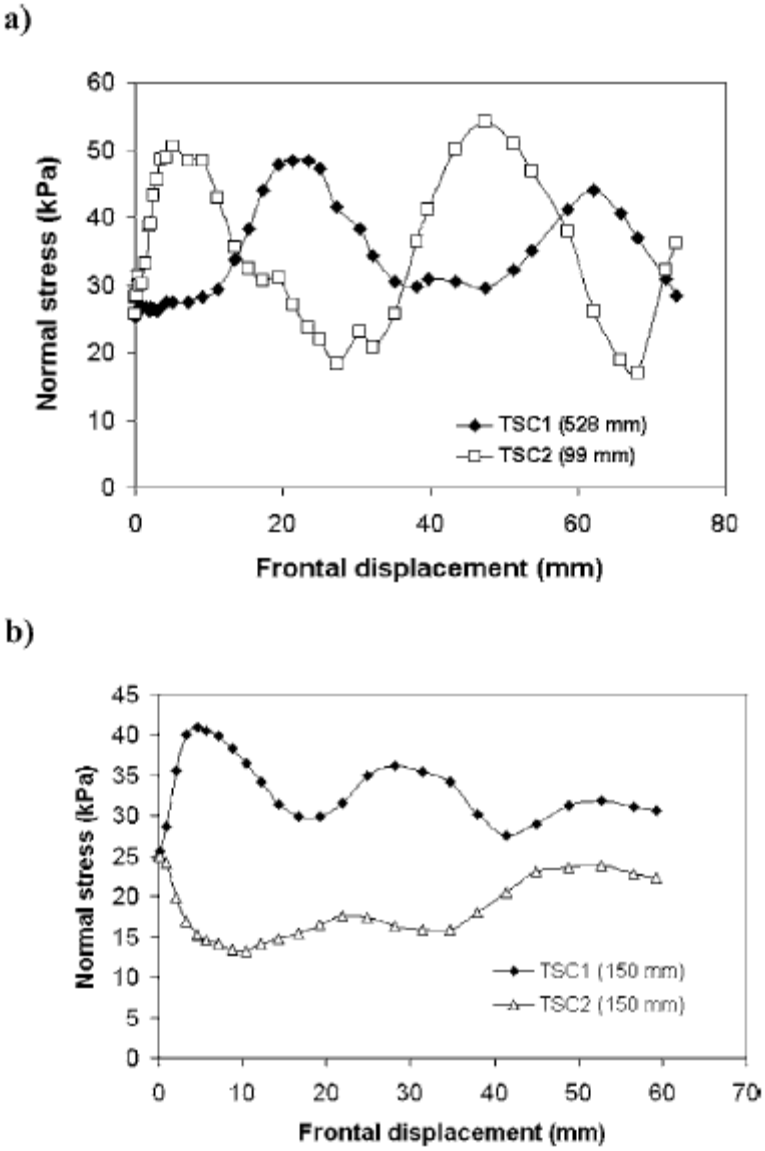

Figure 2.15: Localized normal stresses measured with stress cells located at (a) between longitudinal ribs and (b) between and directly over longitudinal ribs (Teixeira, 2007).

Teixeira et al. (2007) summarize the contributions from the longitudinal and transverse ribs as for small displacements, the pullout resistance is mostly provided by

the interface shear resistance and that as pullout progresses towards larger displacements the bearing resistance adds to the overall pullout resistance.

A study through finite element analysis (Koerner, 1993) showed that as the load increases to the ultimate pullout force, the proportion of bearing resistance to friction resistance begins to rise (Figure 2.16). For a flexible geogrid, the Pullout Resistance is almost entirely frictional until about 25% of the maximum pullout load is reached. At ninety percent of max pullout force, the bearing resistance provides anywhere from 48% to 60% of the total resistance. As Koerner expected, the displacements required to mobilize the frictional resistance are much lower that the displacements required to mobilize the bearing resistance of the transverse ribs.

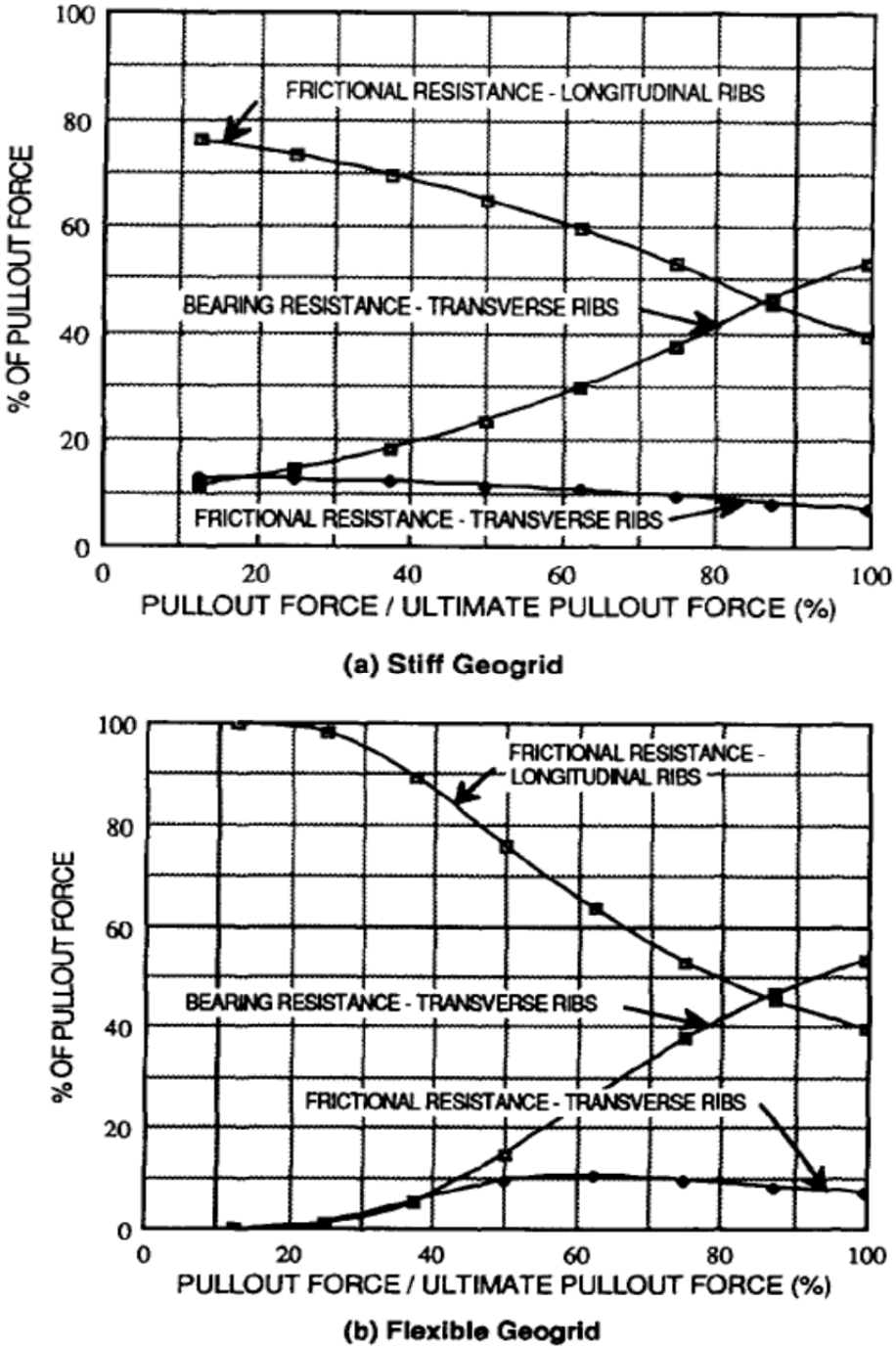

Figure 2.16: Contributions to the ultimate pullout force (Koerner, 1993).

Chapter 3: Materials and Methods

3.1 Geogrids

Two Uniaxial geogrids, the UX1400MSE and UX1700MSE manufactured by Tensar International, were used as reinforcement in this testing program. Information on the geogrids' geometric and strength properties can be found in 'Final Product Qualification Report for Tensar UX-MSE/UX-HS Geogrid Product Line (AASHTO, 2010).

Pictures of the UX1400 and UX1700 are displayed Figure 3.1 with the transverse ribs running across the page and longitudinal ribs running up and down the page. The primary difference between the two grids is the thickness of the ribs.

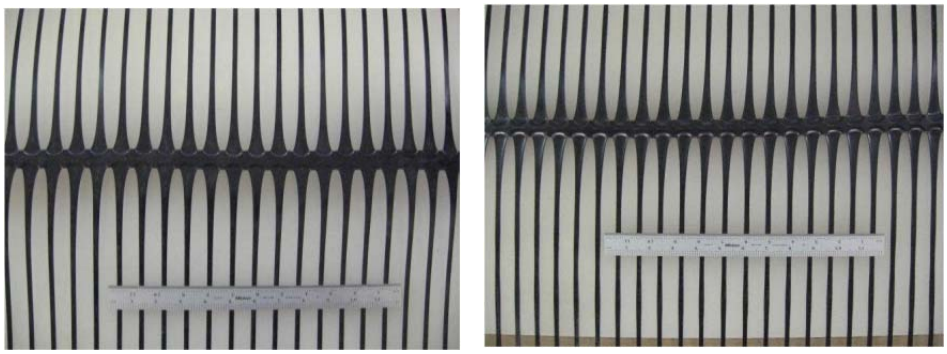

Figure 3.1: UX1400MSE (left) and UX1700MSE (right)

The relevant geometric properties and index properties are presented in Table 3.1 and Table 3.2.

An average of 5 readings were taken to confirm the geometric characteristics of the geogrids (width, spacing, aperture size, and rib thickness). Figure 3.2 illustrates the geometric measurement locations of a uniaxial geogrid. The ultimate tensile strength of the geogrids was obtained though wide width tensile tests conducted in accordance to ASTM D6637 and is reported as the minimum average roll value (MARV) for the geogrids. The primary difference between the two geogrids is the thickness of the ribs in both machine and cross machine direction with the UX1700 measuring 2 to 2.5 times thicker than the UX 1400. The corresponding ultimate tensile strengths are 11,990 lbs/ft and 4,800 lbs/ft for the UX1700 and UX1400 geogrids respectively.

Table 3.1: Geometric properties of the geogrids (AASHTO, 2010).

Machine Direction (Longitudinal) Ribs				
Geogrid	Width (in)	Spacing (in)	Aperture Size (in)	Rib Thickness (in)
UX1400	0.202	0.91	16.8	0.059
UX1700	0.221	0.87	17.1	0.12
Cross Machine Direction (Transverse) Ribs				
Geogrid	Width (in)	Spacing (in)	Aperture Size (in)	Rib Thickness (in)
UX1400	0.762	17.6	0.71	0.137
UX1700	0.83	17.9	0.65	0.325

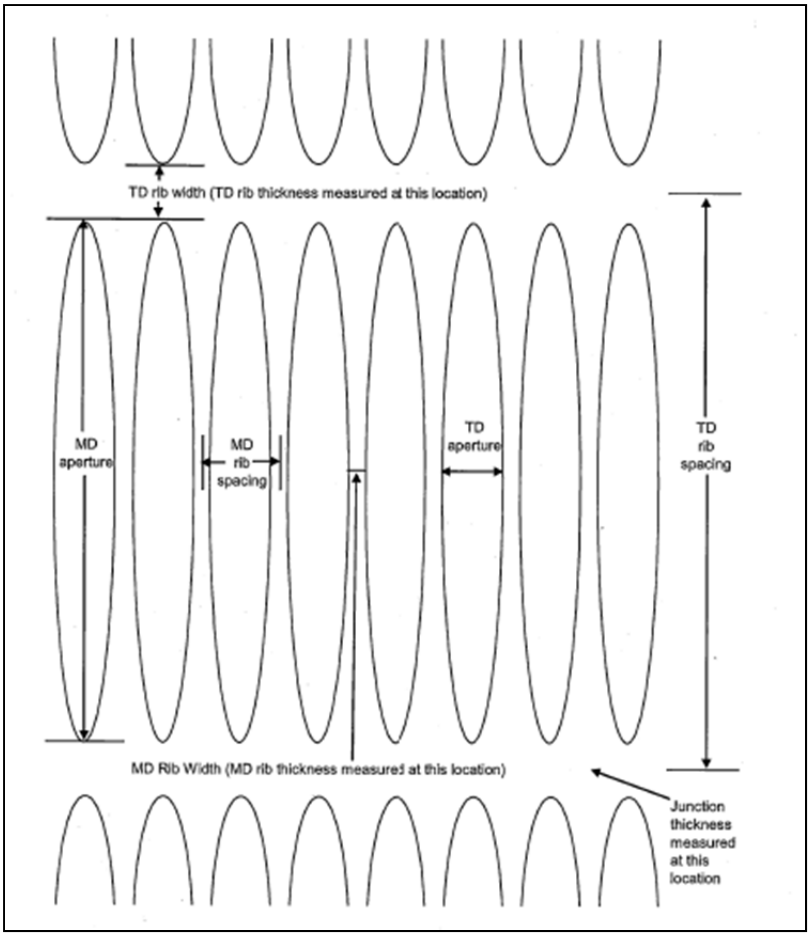

Figure 3.2: Diagram of geometric properties and locations of measurement (AASHTO, 2010).

Table 3.2: Index properties of the geogrids (AASHTO, 2010).

Index Properties	Units	Geogrid	
		UX 1400	UX1700
Tensile Strength @ 5% Strain	kN/m (lb/ft)	31 (2,130)	75 (5,140)
Ultimate Tensile Strength	kN/m (lb/ft)	70 (4,800)	175 (11,990)
Junction Strength	kN/m (lb/ft)	66 (4,520)	160 (10,970)
Flexural Stiffness	(mg-cm)	730,000	9,075,000

3.2 Monterey Sand

Monterey No.30 sand was chosen as the control fill material in the testing program in order to establish repeatability between tests and to compare the system with the existing literature on sand. The sand was verified to be representative though sieve analysis and direct shear tests conducted at the University of Texas at Austin.

Monterey No. 30 sand is clean uniformly graded sand classified as SP in the unified system. The particles are rounded to sub rounded consisting predominantly of quartz with a smaller amount of feldspar and other minerals (Zornberg, 1994). The largest particle size (D_{max}) was controlled through prior sieving though the no. 20 sieve which corresponds to a D_{max} of 0.333 in (0.841 mm). The grain size distribution is presented in Figure 3.3 and the particle sizes, particle size coefficients, specific gravity (Gs) and maximum and minimum void rations (e_{max} and e_{min}) are presented in Table 3.3.

The relative density for all pullout tests with Monterey Sand was 70% with a water content of 1.5%. Direct shear tests were also conducted in the lab at 70% relative density of Standard Proctor and for a water content values of 1.5% and oven-dry. The friction angle from direct shear tests for these two moisture contents was 39°. The Mohr Coulomb friction envelope is presented in Figure 3.4.

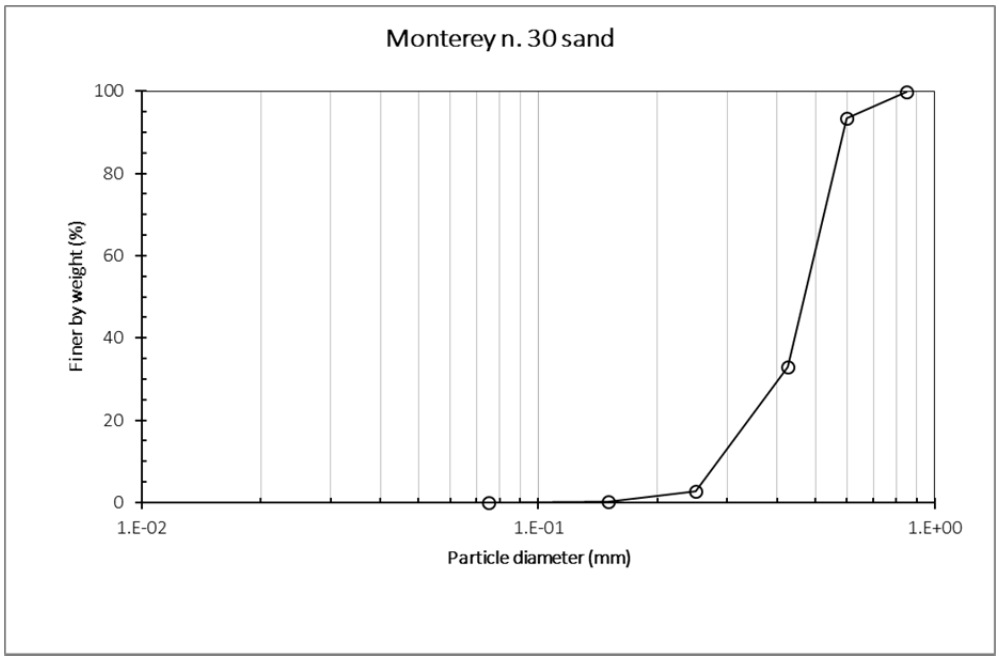

Figure 3.3: Grain size gradation curve for Monterey No. 30 sand.

Table 3.3: Particle sizes and size coefficients and void ratios of Monterey No. 30 sand.

D_{max}	0.850 mm (0.033 in)
D_{50}	0.48 mm (0.019 in)
D_{60}	0.50 mm (0.020 in)
D_{30}	0.41 mm (0.016 in)
D_{10}	0.28 mm (0.011 in)
Uniformity coefficient, C_u	1.8
Coefficient of gradation, C_c	1.20
G_s	2.655
e_{max}	0.76
e_{min}	0.56

$$C_u = \frac{D_{60}}{D_{10}} \qquad C_c = \frac{D_{30}^2}{D_{60} \cdot D_{10}}$$

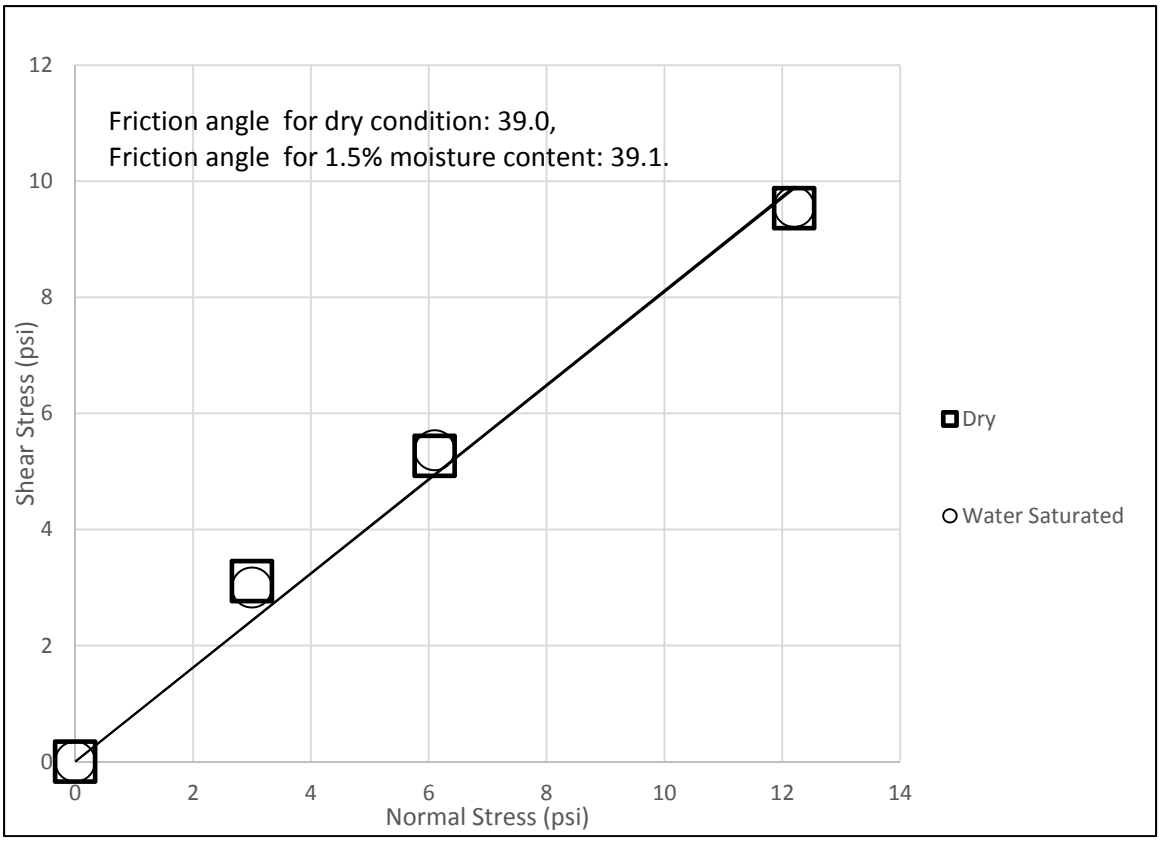

Figure 3.4: Mohr Coulomb failure envelope for Monterey No. 30 sand from direct shear tests.

3.3 Crushed Glass, Dredged Material, and CG-DM Blends

It has been reported (Grubb, 2006) that the granular nature, mineralogy, and reactivity of the CG media are well suited for blending with high plasticity organic soils. Table 1.1 and Table 1.2 from Chapter 1 list the geotechnical properties of CG, DM, and their blends. The properties that will have the greatest influence on the pullout tests are the optimum water content, maximum dry unit weight, grain size distribution, Atterberg limits, and shear strength. These important properties are detailed in this section. The

grain size distributions from Grub et al. for these materials are presented in Figure 3.5 (2006a).

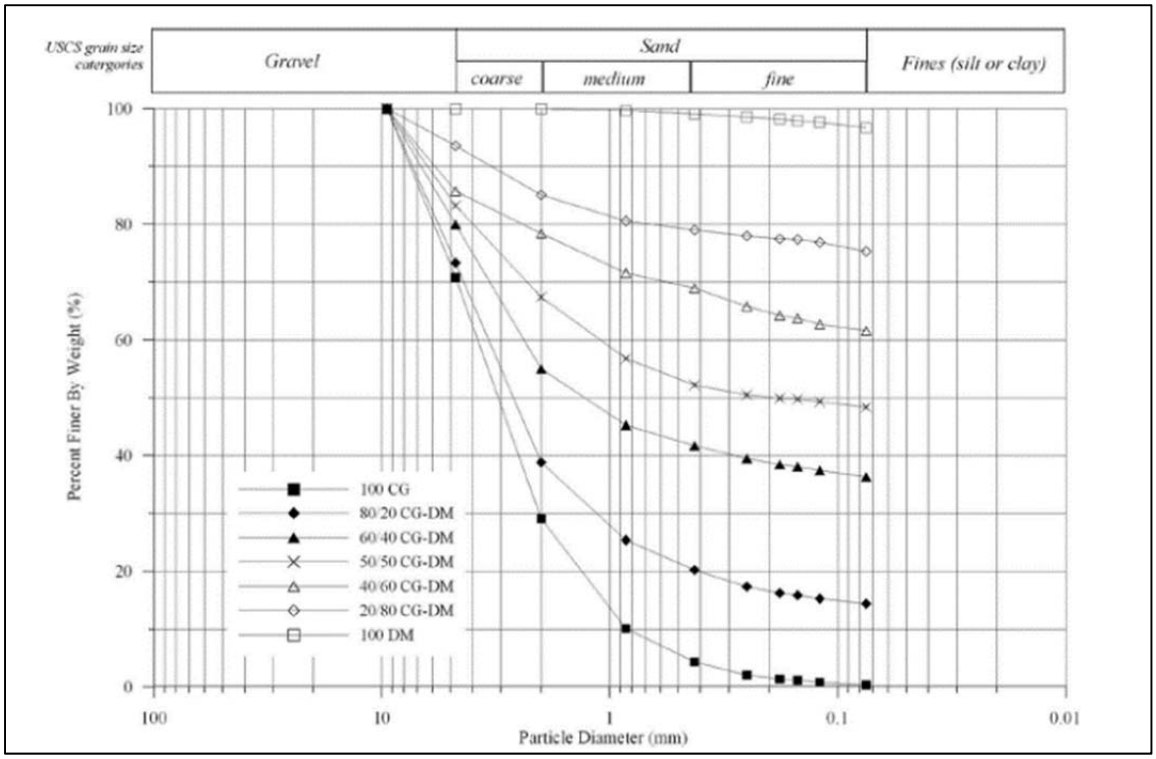

Figure 3.5: Grain size distributions for CG and DM blends (Grubb, 2006a).

The grain size distribution shows that about 99% of the DM passes the No. 200 sieve (0.075 mm) which signifies that this material is almost completely composed of fine particles. The CG has about 4% passing the No. 200 sieve. The percentage of fines for the blends are intermediary between the two 100% materials as seen in Table 3.4.

Table 3.4: Particle size proportions of CG, DM, and CG-DM blends (modified from Grubb, 2006a).

Media	Gravel (%)	Sand (%)	Fines (%)
100% CG	29.2	70.4	0.4
80/20 CG-DM	26.2	59	14.4
50/50 CG-DM	6.8	44.8	48.4
20/80 CG-DM	6.4	18.3	75.3
100% DM	0	3.4	96.6

Standard Proctor curves are presented in Figure 3.6 (Grubb, 2006a). The 100% CG has a higher dry unit weight than the 100% DM; additionally, the optimum moisture content for each material increases with increasing DM content from about 8% for 100% CG to about 40% for 100% DM. It also should be noted that a clear peak in the compaction curve is observed for the CG while the DM compaction curve is relatively flat with little change with water content. The low hydraulic conductivity of the DM would require significant work to alter the water content to achieve a desired value thus the pullout tests were conducted on the materials in the condition that they were received.

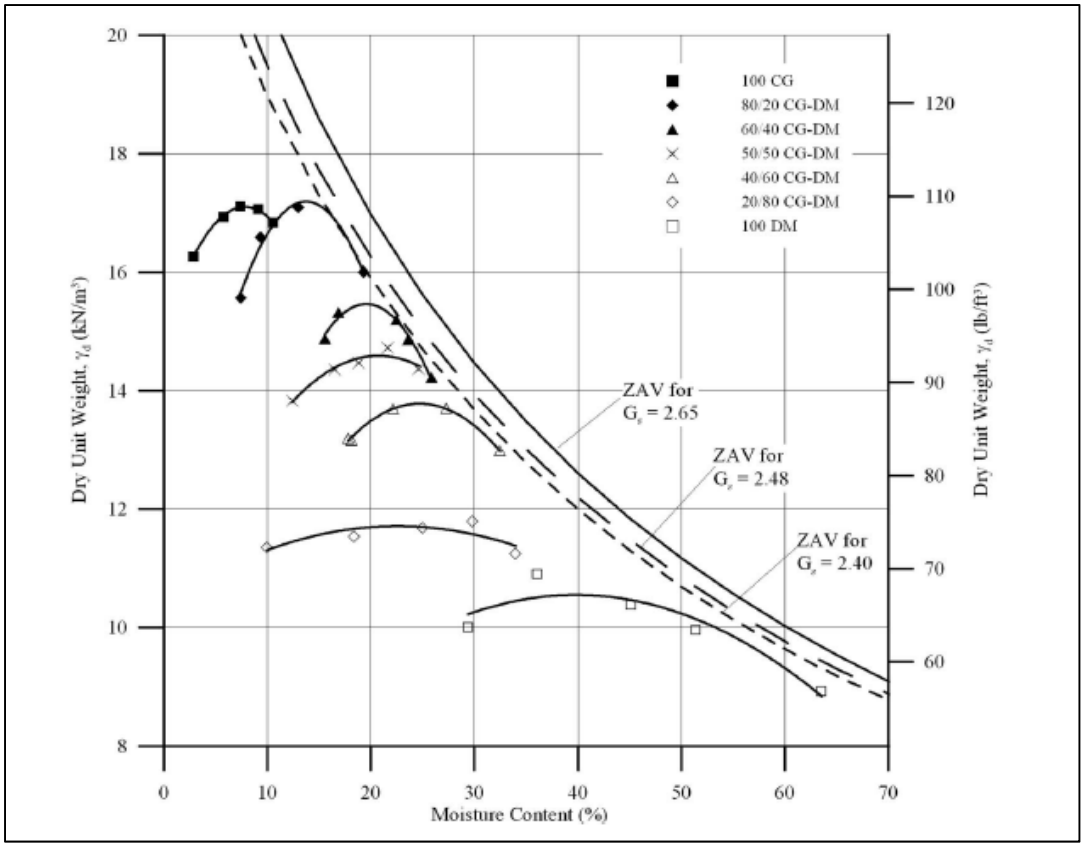

Figure 3.6: Standard Proctor curve for CG, DM, and CG-DM blends from laboratory (dashed lines) and field samples (solid lines) (Grubb, 2006a)

3.3.1 Moisture Content and Relative Density

The moisture conditions of a soil are relevant for proper interpretation of the results of pullout tests. The moisture contents were kept constant at the materials' as received conditions for the pullout tests. In order to control moisture conditions the materials were stored in sealed plastic bins between tests and samples were taken to measure the moisture content after each test. If the moisture content had dropped, an

appropriate amount of water was added during the compaction stages. The moisture contents of the blends, as tested, are presented in Table 3.5

Table 3.5: As tested moisture content and dry unit weight of the CG, DM, and CG-DM blends.

Media Tested	γ_d (lb/ft^3)	ω (%)
100% CG	98	8
80/20 CG-DM	88	14
50/50 CG-DM	75	20
20/80 CG-DM	75	33
100% DM	60	50
Monterey Sand	99.3	1.6

3.4 Apparatus

A large pullout box was used to measure the Pullout Resistance geogrids and fill material combinations. The pullout box measures 24 inches wide, 60 inches long, and 12 inches deep (0.6 x 1.5 x 0.3 m). There is a 2 inch (75 mm) sleeve at the front of the box approximately midway between the top and the bottom through which the geogrid passes. Normal stress was applied to the soil/geogrid system by a six-air-cylinder system, and discussed below. A steel reaction frame was secured atop the pistons using threaded iron bars. A 10,000 lb load cell was attached to the pullout loading harness to measure the Pullout Resistance. Linear variable transformers (LVDTs) were used to measure the displacement of the pistons and the geogrid. Needle valves controlled the rate of displacement of the hydraulic pistons on both sides of the box. LVDTs in the back of the

pullout box were attached to the geogrid by inextensible wires which were threaded through high strength tubing in order to record the geogrid displacements. Smooth geomembrane liners were glued to the inside walls of the box to minimize side friction. The geogrids were secured to a roller grip at the front of the box. A completed setup of this pullout box is presented in Figure 3.7.

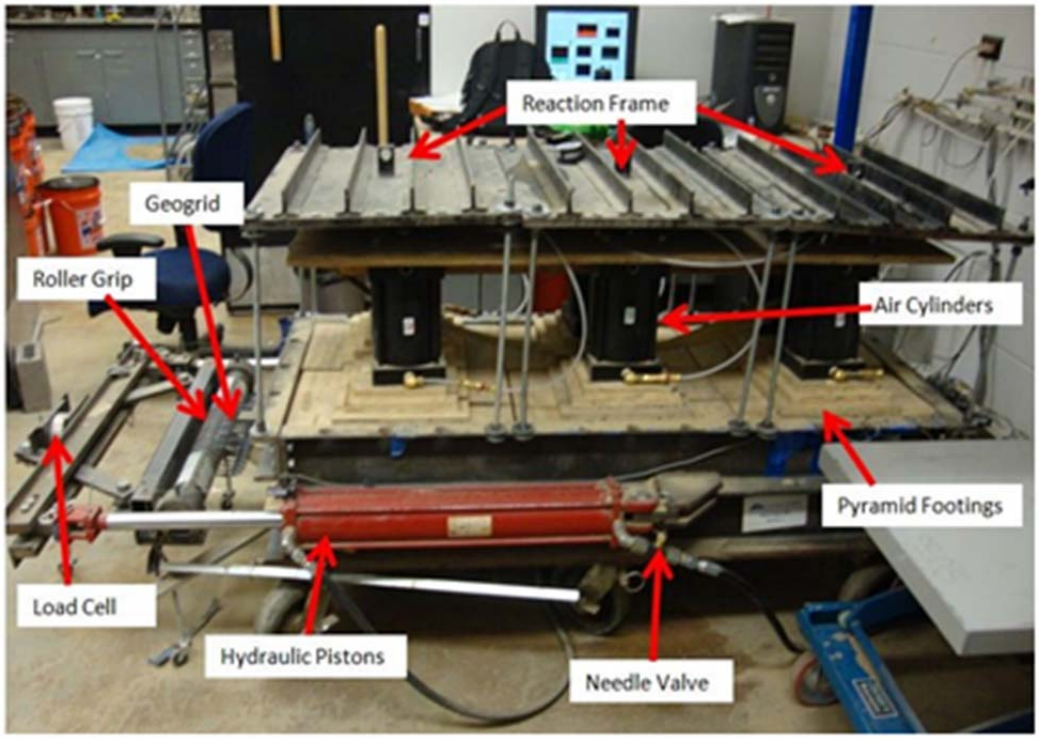

Figure 3.7: Pullout box set up and ready for testing

In order to accomplish a uniform and accurate normal stress, the setup, from bottom to top, included a neoprene mat covering the soil, followed by the plywood pyramids, air cylinders, and metallic plates which were secured by threaded steel bars to

the pullout box. This system was determined to be the most efficient method of applying the desired normal stress to the soil/geogrid system after a series of investigations which included use of an air bladder that is widely used in pullout testing. The six air cylinders were affixed to a plywood sheet which was hoisted by a crane in order to place the cylinders atop their respective plywood pyramid. The plywood pyramids were constructed by affixing four consecutively smaller pieces of plywood (from bottom up). The plywood pyramids measured 20" x 12" at the base. The plywood pyramids acted as footings beneath the air cylinders which facilitated even distribution of the load over the entire area. The neoprene pad was placed between the soil and the plywood pyramids to facilitate good contact. A small gap was left between the pyramids and the side walls of the pullout box to transfer 100% of the normal load was applied to the soil. The metallic plates provided a reaction surface for the hydraulic pistons to act against. The plates secured to the pullout box through threaded iron rods that used washers and nuts to secure the position of the plates relative to the pullout box. A system of high-pressure tubes connected the pistons to an air entry valve; the pressure in the cylinders was regulated by a digital pressure gauge. In order to convert the air pressure in the cylinders to the desired normal stress the following equation was used:

$$Desired\ Pressure = \frac{M_{system} + 6 \times P_{air} \times A_{cylinder}}{A_{box}} \qquad (3.1)$$

where *Desired Pressure* is the pressure at the soil surface; M_{system} is the combined mass of the soil above the geogrid, the neoprene sheet, the plywood pyramids, and the

hydraulic cylinders; P_{air} is the air pressure in the hydraulic cylinders; $A_{cylinder}$ is the area of one individual cylinder; and A_{box} is the area of the pullout box. These values are presented in Table 3.6.

Table 3.6: Mass and dimensions of normal stress components.

Component	Mass (lbs)	Area (in^2)
Soil above geogrid	$\gamma' * A_{box} * h$	1440
Neoprene Sheet	4.66	1440
One Plywood Pyramid	8.35	240
One Hydraulic Cylinder	60.6	28.3

The clamping system in the front section of the pullout box is built with hinge joints. This section is locked to the rigid pistons with the load cell acting as the point of contact. It is important for the load cell to be centered on the clamping system when the load starts increasing otherwise the clamping system will likely swivel, resulting in a pullout force that does not act equally across the width of the geogrid. Given a properly positioned clamping system and load cell, a uniform stress is applied across the full width of the geogrid during pullout. Additional pictures of the test setup are included in Figure 3.8, Figure 3.9, and Figure 3.10.

Figure 3.8: Clamping mechanism of the geogrid with a centered load cell.

Figure 3.9: Clamping mechanism with load cell detail; prior to the start of a test.

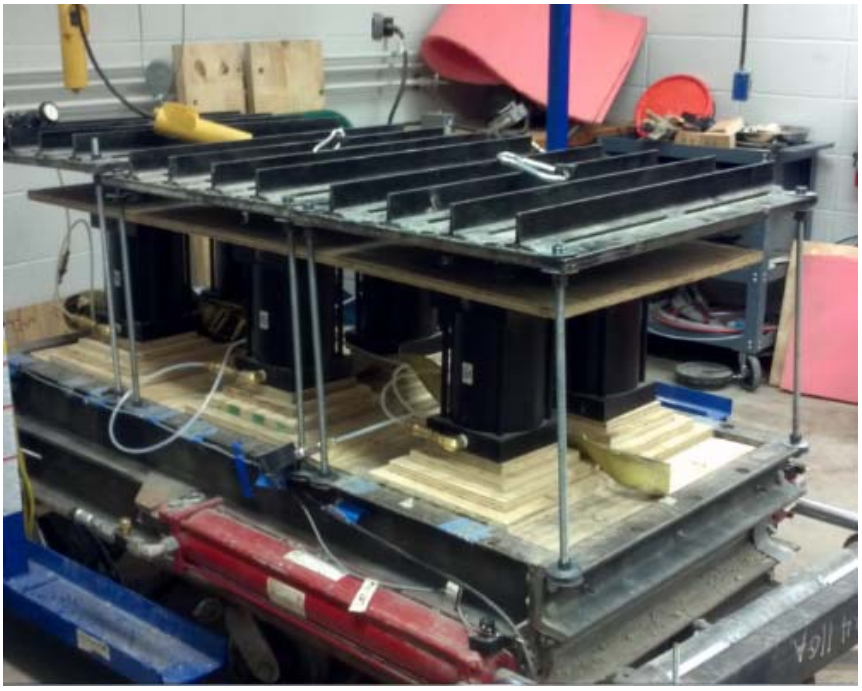

Figure 3.10: Additional view of the test setup.

3.5 Testing Procedures

The first step of the testing involved preparing a geogrid specimen in accordance with ASTM D6706-01; a prepared and ready for testing sample is presented in Figure 3.11. To ensure the same number of longitudinal and transverse ribs in each test, the dimensions were kept constant at roughly 2.97 in long and 12 in wide (0.9 m x 0.3 m). These dimensions provided for 13 longitudinal ribs and 4 transverse ribs total, two of which fit inside the box due to the setup process that is discussed later. Three inextensible tell-tales were tied to the grid in a diagonal pattern across the geogrid from front to back and connected to the LVDTs in the back of the box. Inextensible fishing wire was used as

the tell-tales after repeated tests which reproduced the results from steel wires. The fishing wire was found to be easy to handle in that it didn't crease easily and it was simple to spool off. The wires were threaded through high-strength polyethylene tubes to avoid any frictional effects from the fill material.

Figure 3.11: Geogrid specimen with attached tell-tales and high strength tubing.

The next step was to verify the moisture content of the sample. Prior to the first test of a given material and after each test, samples were weighed and oven dried overnight then reweighed to obtain the moisture content of the material. If the measured moisture content was under the optimum moisture content based on the Standard Proctor compaction curve then moisture was added to the soil during placement. For material moisture contents that exceeded the optimum value, the soil was tested at that condition. Between tests, the material was stored in sealed plastic containers to avoid moisture loss.

To place the soil layers the box was first cleaned. The dry density was pre-determined in relation to the maximum dry density, water content, and attainable compaction. The fill material was weighed out placed in the pullout box and hand tamped to a 3 inch layer of soil and then scarified. Another layer of soil was placed on top and hand tamped for a total depth of 6 inches. A virgin geogrid specimen was placed on top of the compacted soil layer. The specimen was slid through the front aperture and clamped to the pullout loading harness; the rotating clamp bar was then rotated 270° to minimize the effects of the clamping stresses placed onto the geogrid and to facilitate completely horizontal load application. Images of the clamping mechanism and setup are presented in Figure 3.12 and Figure 3.13. The tell-tales were then attached to the LVDTs at the back of the pullout box. See Figure 3.14 for images of the tell-tales connected to the LVDTs at the back of the pullout box and of the LVDTs mounted on the pistons. Figure 3.15 illustrates the location on the geogrid that the tell-tales were attached; LVDTs A, B, and C. The embedded length of the geogrid was measured from the inside edge of the aperture to the end of the geogrid.

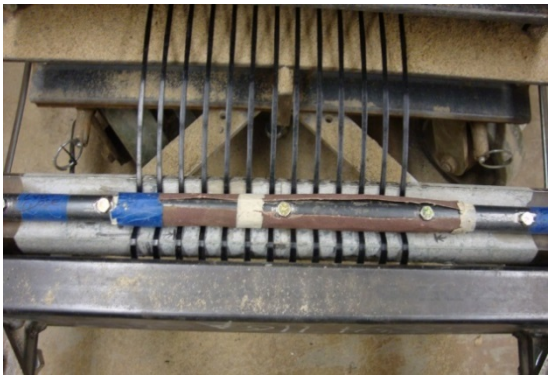

Figure 3.12: Geogrid specimen clamped to the rotating clamp bar via bolts.

Figure 3.13: Clamping mechanism in the rotated, as-tested state.

Figure 3.14: LVDTs mounted on a hydraulic piston and at the back of the pull-out box.

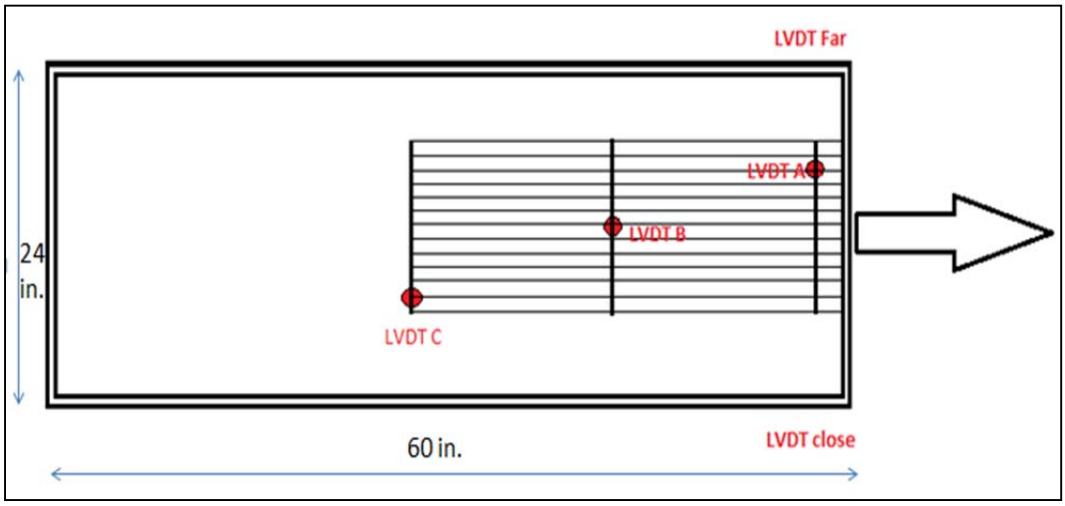

Figure 3.15: Illustration of geogrid in the pullout box with the locations of tell-tale attachment.

Two additional 3 inch soil layers were placed and compacted for a total of 4 lifts and a total depth of 12 inches. The top surface was smoothed out and measured for equal thickness. A thin neoprene cushion was placed on top of the soil and six plywood pyramids were placed on top of that as seen in Figure 3.16. Six air pistons were then placed on top of the plywood pyramids (Figure 3.17). A steel reaction frame was lifted on

top of the pistons using a small crane and secured by bolts and threaded steel bars to the pullout box (Figure 3.18). The pistons were then connected to an air supply valve, which was set to an appropriate air pressure for the desired normal stress on the soil. Testing was initiated by applying a load to the geogrid by extending the hydraulic cylinders on the sides of the box at a constant displacement rate of 0.04 inches per minute. A National Instruments data acquisition box and Labview program were used to monitor the displacement rate; the needle valves were opened to an approximate mark and the adjusted to obtain the specified rate. Space was left between the load cell and the contact point at the beginning of each test in order to facilitate obtaining the proper displacement rate at the beginning of load application. Continuous monitoring of the rate of displacement and adjustments of the valves was necessary to apply the correct rate of displacement. Testing continued until failure was observed or until the pistons reached their maximum length.

Figure 3.16: Plywood pyramid configuration.

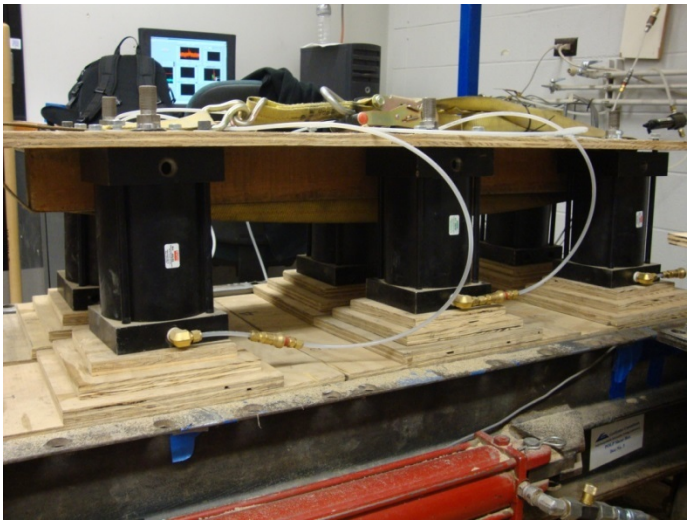

Figure 3.17: Air cylinders atop the plywood pyramids.

Figure 3.18: Test setup with reaction plates secured over the air cylinders.

Chapter 4: Test Results

4.1 Scope of Testing Program

A total of 36 pullout tests were conducted in this program; typically, six tests were conducted for each fill material: 100% DM, 100% CG, the three CG-DM blends, and the Monterey Sand. Of these six tests, three were conducted using the UX1400 geogrid at normal stresses of 4, 6, and 8 psi; and the other three tests were conducted using the UX1700 geogrid under the same normal stresses. There were a few instances where duplicate tests were ran to verify a previous test's results. Also there were instances where tests were not run for reasons specified in the following sections. The target testing program is presented in Table 4.1.

Table 4.1: Matrix of pullout testing program

Material	Geogrid	Normal Stress (psi)		
Monterey Sand	UX1400	4	6	8
	UX1700	4	6	8
100% CG	UX1400	4	6	8
	UX1700	4	6	8
20/80 - CG/DM	UX1400	4	6	8
	UX1700	4	6	8
50/50 - CG/DM	UX1400	4	6	8
	UX1700	4	6	8
80/20 - CG/DM	UX1400	4	6	8
	UX1700	4	6	8
100% DM	UX1400	4	6	8
	UX1700	4	6	8

4.2 Test Results

Pullout test reports were compiled for each test. The reports include a summary table detailing the results from each test and a plot of Pullout Resistance versus displacement. The details on the summary tables included the following: geogrid manufacturing details, geogrid length and width, applied normal stress, date, operators, box dimensions; fill material and its properties including the friction angle, moisture content, dry density, target compaction, weight of each lift, and number of lifts; the rate of pullout, maximum load and Pullout Resistance, maximum displacement of each LVDT, and the coefficient of interaction.

Some discrepancies were noticed in the target dry density of the tests. The 100% CG was compacted to 90% of the max dry density from Standard Proctor; the 80/20 and 50/50 CG/DM blends were compacted to 80%; the 20/80 – CG/DM was compacted to 100%; and the 100% DM was compacted to 87%; these values and the resulting dry densities as tested are summarized in Table 4.2. A material with a greater relative density is expected to have a greater shear strength and thus a larger Pullout Resistance than the same material compacted at 80% of $\gamma_{d,max}$ from Standard Proctor.

Table 4.2: As tested dry densities and relative compaction of CG, DM, and CG/DM blends

	$\gamma_{d,max}$ (pcf) standard proctor	γ_d as tested (pcf)	Relative Compaction to Standard Proctor	ω_{opt} (%)	ω as tested (%)
100% CG	109	98	90%	8	8
80/20 - CG/DM	110	88	80%	14	14
50/50 - CG/DM	94	75	80%	21	20
20/80 - CG/DM	75	75	100%	29	32
100% DM	69	60	87%	39	50

Table 4.3 lists the results of the pullout tests. Each test has its own serial number, which is part of a larger program involving other materials; the CG/DM tests start at number 58. Also listed in Table 4.3 is the date of which each test was conducted, the material, the geogrid, the normal stress is pounds per square foot (psf), the Pullout Resistance in pounds per foot (lbs/ft), and comments pertinent to interpreting the results of the test. Table 4.4 further summarizes the results for easier digestion.

Test Serial No's 1 and 2 were conducted to assess repeatability of the testing procedure. The test results were compared to existing pullout test data on the Tensar BX1100 geogrid in Monterey Sand. The results were sufficient to be confident in the system.

Plots of Pullout Resistance versus normal stress for all materials are presented in Figure 4.1 with specification of geogrid. Figure 4.2 compares the Pullout Resistance across the different blends for the UX1400 and the UX1700 geogrids, each graph is for a

specified normal pressure. The test that failed to tension is marked accordingly in these figures; any analysis that includes this result is treated accordingly.

Table 4.3: Results of pullout tests.

Serial No.	Date of Test	Material	Geogrid	Normal Stress (psi)	Pullout Resistance (lbs/ft)	Comments
1	27-Feb-12	Monterey Sand	BX1100	3	1011	Repeatability, Le-1.98 ft
2	4-Mar-12		BX1100	3	962	Repeatability, Le-1.98 ft
56	4-Jul-12	100% DM	UX1400	4	380	
57	5-Jul-12		UX1400	6	435	
58	6-Jul-12		UX1400	8	625	
59	6-Jul-12		UX1700	4	520	
60	7-Jul-12		UX1700	6	700	
61	8-Jul-12		UX1700	8	840	
62	10-Jul-12	20/80 CG/DM	UX1400	4	624	
63	12-Jul-12		UX1400	6	764	
64	12-Jul-12		UX1400	8	1068	
65	13-Jul-12		UX1700	4	1285	
66	13-Jul-12		UX1700	6	1495	
67	14-Jul-12		UX1700	8	1693	
76	23-Jul-12	80/20 CG/DM	UX1400	4	1150	
77	24-Jul-12		UX1400	6	1487	Clamp bar rotated but still appeared to fail in pullout
78	25-Jul-12		UX1400	8	1915	
79	26-Jul-12		UX1700	4	2531	Software disruption for 30 minutes in the middle of the test
81	31-Jul-12		UX1700	6	3000	Pistons maxed
82	2-Aug-12		UX1700	8	3345	Pistons maxed

Table 4.3 (continued): Results of pullout tests.

83	4-Aug-12	100% CG	UX1400	4	1175	Water leaked from the back of the box
84	4-Aug-12		UX1400	6	1808	Tensile failure. Middle LVDT moved first then the front LVDT and caught up/passed the middle LVDT
85	5-Aug-12		UX1700	4	3599	
86	5-Aug-12		UX1700	6	3977	Pistons maxed, LVDT ceased functioning at around 60 mm
87	9-Aug-12	50/50 CG/DM	UX1400	4	616	
88	10-Aug-12		UX1400	6	1265	
90	14-Aug-12		UX1400	8	1709	Pistons maxed
91	17-Aug-12		UX1700	4	1594	
92	17-Aug-12		UX1700	6	2325	Pistons maxed
93	18-Aug-12		UX1700	8	2550	Pistons maxed
94	17-Jul-12	Monterey Sand	UX1700	4	2005	
95	17-Jul-12		UX1700	6	2475	
96	18-Jul-12		UX1400	8	2500	
97	19-Jul-12		UX1400	4	950	
98	19-Jul-12		UX1400	6	1323	
99	20-Jul-12		UX1700	8	4025	

Table 4.4: Pullout Resistance (lbs/ft) of CG, DM, and CG-DM blends.

		Normal Stress (psi)		
Material	**Geogrid**	4	6	8
100% CG	UX1400	1175	1808	-
	UX1700	3599	3977	-
80/20 - CG/DM	UX1400	1150	1487	1915
	UX1700	2531	2564	3345
50/50 - CG/DM	UX1400	616	1265	1709
	UX1700	1594	2325	2550
20/80 - CG/DM	UX1400	624	764	1068
	UX1700	1285	1495	1693
100% DM	UX1400	380	435	625
	UX1700	520	700	840
Monterey Sand	UX1400	950	1323	2500
	UX1700	2005	2465	4025

*The field highlighted in orange indicated test failed though mechanisms other than pullout.

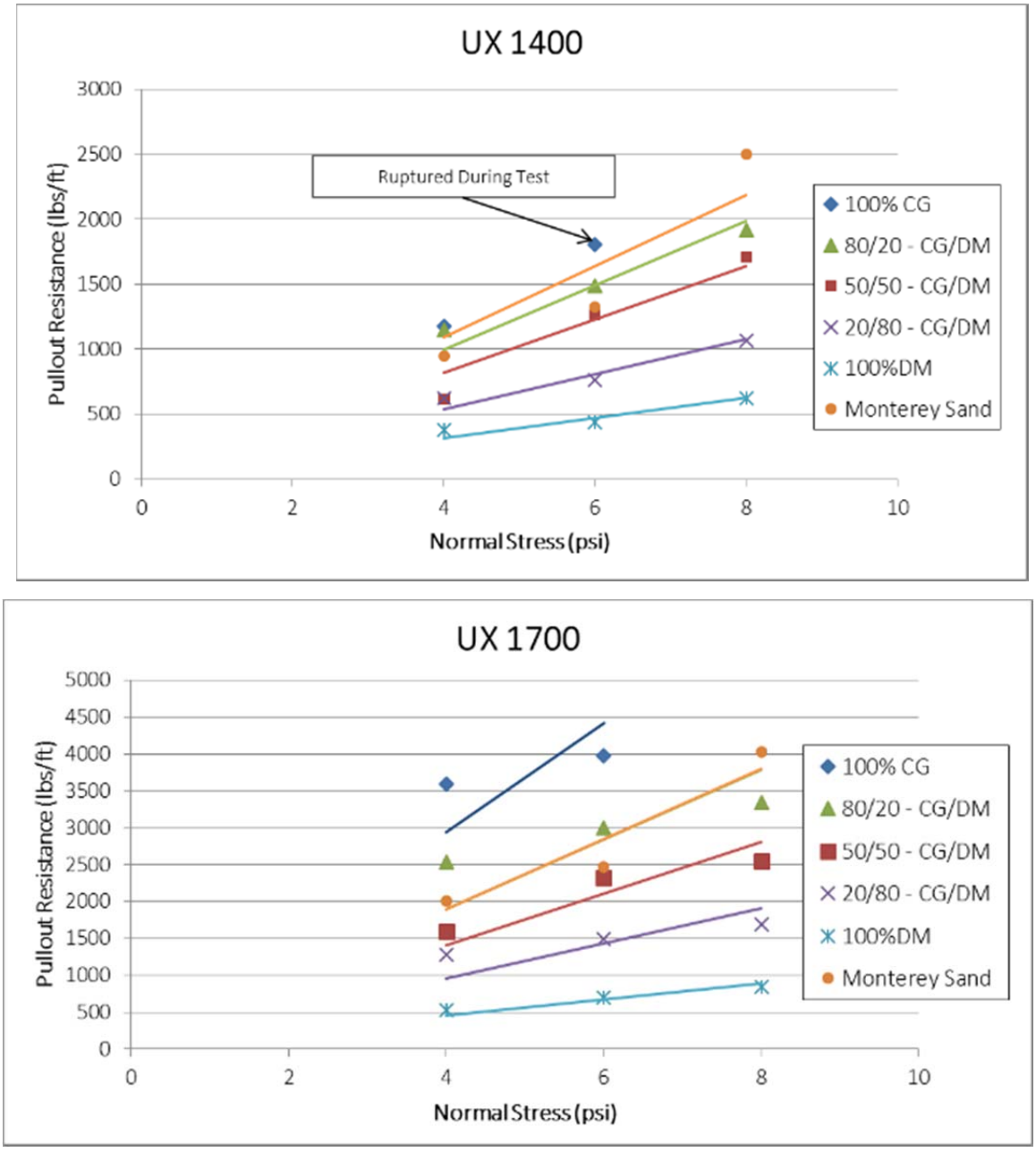

Figure 4.1: Pullout Resistance versus normal stress for all materials with UX1400 (top) and UX1700 (bottom). The trendlines pass through the origin (0,0).

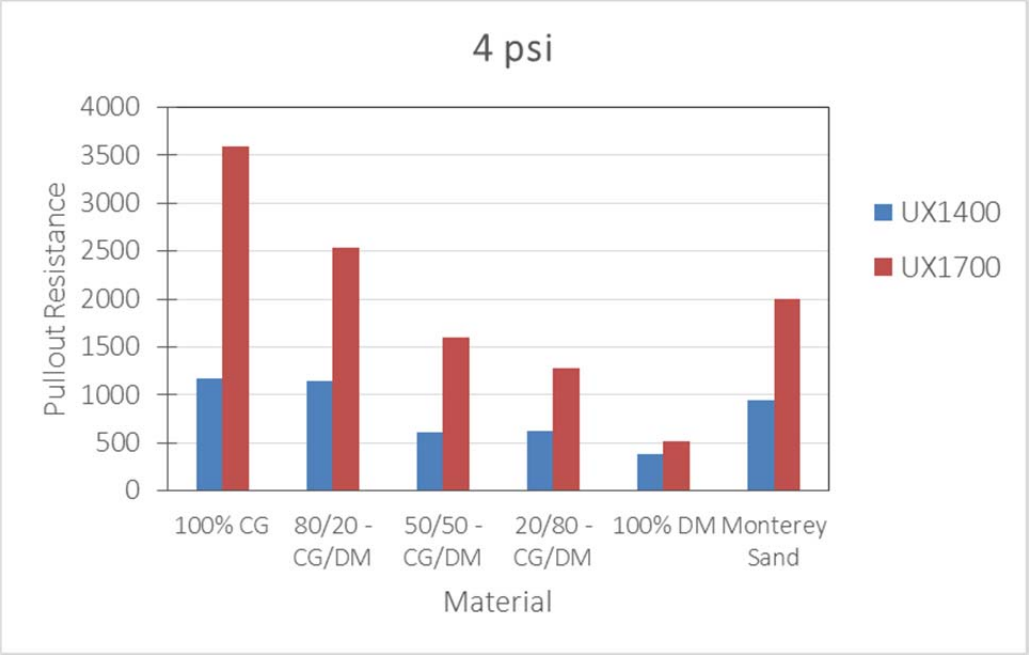

(a) Confining pressure of 4 psi.

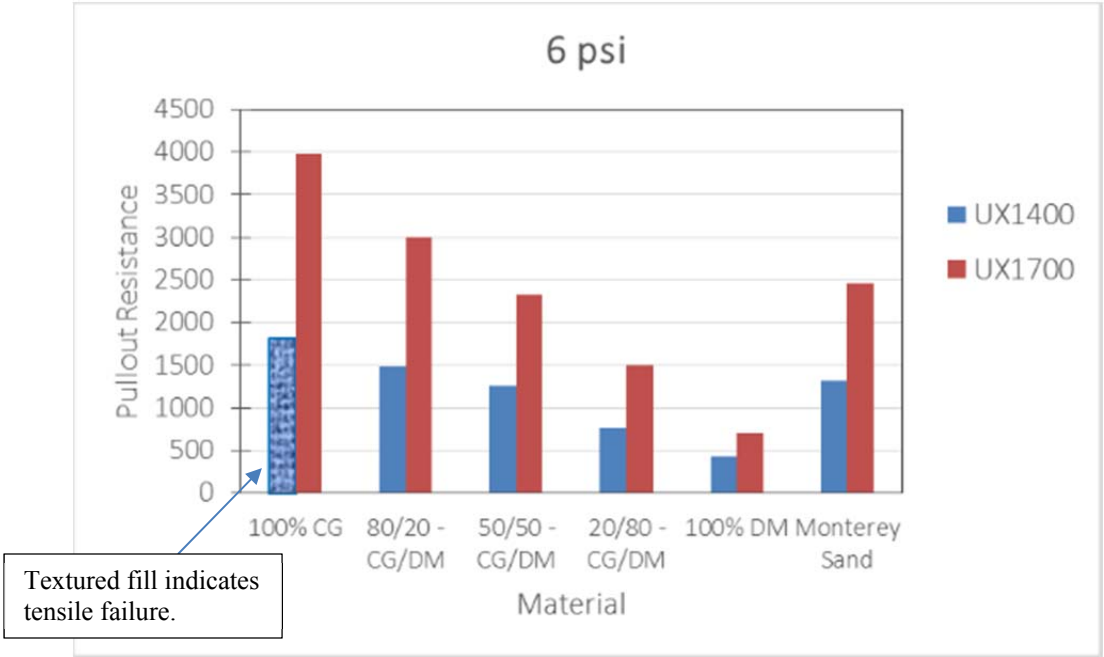

(b) Confining pressure of 6 psi.

Figure 4.2: Pullout Resistance versus percentage of crushed glass in a blend for confining pressures of 4 psi (a), 6 psi (b), and 8 psi (c).

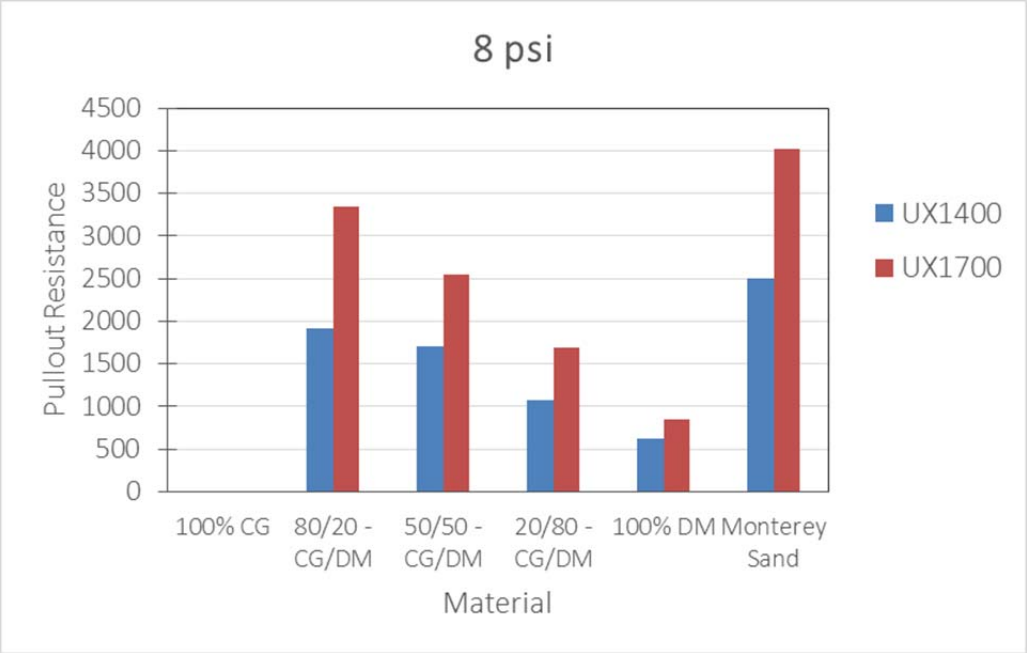

(c) Confining pressure of 8 psi.

The 100% crushed glass was the material with the highest Pullout Resistance of any material for a given geogrid and normal stress. Even the test that ruptured the UX1400 geogrid at 6 psi normal stress exceeded the pullout resistance of the other materials at that normal stress. The tensile rupture of the UX1400 was unexpected as the ultimate tensile strength was reported and confirmed in a wide-width tensile test as 4800 lbs/ft. Two factors may have led to this unexpected result; the first is that the wide-width tensile tests are conducted at a strain rate of about 30 mm/min while the pullout test is run much more slowly at 1 mm/min; the second factor is that after the test was run, glass pieces were found to be embedded into the geogrid thus reducing the effective area and thus reducing the tensile capacity. The Pullout Resistance for the UX1400 at 8 psi

normal stress for the 80/20 – CG/DM blend and the Monterey Sand (1,915 and 2,500 lbs/ft respectively) both exceeded the load at tensile failure of this test (1,808 lbs/ft). The 100% CG had a Pullout Resistance (Pr) of 1.2 times the Pullout Resistance of Monterey Sand for the UX1400 and at least 1.6 times for the UX1700 geogrid. The relative compaction of 90% of $\gamma_{d,max}$ from Standard Proctor may have contributed to some of the effects and results listed above. At 4 psi the UX1700 outperformed the UX1400 with Pr's of 3,599 and 1,175 lbs/ft, respectively, giving a factor of 1.8 for Pr with UX1400 to UX1700. Even with the rupture of the UX1400, at 6 psi the difference was less significant with a Pr of 3,977 lbs/ft for the UX1700 and a resistance at tensile failure of 1,808 lbs/ft for the UX1400.

The 80/20 – CG/DM blend outperformed the Monterey Sand for normal stresses of 4 and 6 psi with both geogrids however for the normal stress of 8 psi the Monterey Sand achieved a higher Pr. It should be noted that the Pr for the UX1700 at 6 and 8 psi (3000 and 3345 lbs/ft respectively) was determined by the max displacement of about 300 mm. No Pr peak was identified thus higher Pullout Resistance values are possible with additional displacement. Overall, considering all geogrids and normal stresses in the testing program, the 80/20 – CG/DM blend was between about 0.8 to 1.3 times the Pr of the Monterey Sand. No physical damage was observed on any of the specimens for this blend, this may a result of the lower relative compaction, 80% $\gamma_{d,max}$ of Standard Proctor, than the 100% CG or this may be the result of additional fines content from the DM. For

the 80/20 – CG/DM blend, the Pr with the UX1700 geogrid was about twice the Pr for the UX1400 geogrid. These Pullout Resistances for the UX1700 were 2531, 3000, and 3345 lbs/ft for 4, 6, and 8 psi, respectively and 1150, 1487, and 1915 lbs/ft. for the UX1400.

The 50/50 – CG/DM blend showed lower Pr than the Monterey Sand overall. For the normal stresses of 4 and 8 psi the 50/50 blend was about 0.6 to 0.8 times the Pr's of the sand; for the 6 psi normal stress the 50/50 blend was about 0.95 times that of the sand. For the confining pressure of 4 psi, the Pr of the blend with the UX1700 was about 2.6 times that of the UX1400 (1,594 and 616 lbs/ft respectively); this difference decreased as the confining pressure increased. For 6 psi normal stress, the Pr of the UX1700 and UX1400 were 2,325 and 1,265 lbs/ft respectively giving a 1.8 times increase in Pr from the UX1400 to the UX1700. For 8 psi normal stress, the Pr of the UX1700 and UX1400 were 2,550 and 1,709 lbs/ft respectively giving a 1.4 times increase in Pr from the UX1400 to the UX1700. This blend was compacted at the same relative compaction as the 80/20 – CG/DM blend at 80% of $\gamma_{d,max}$ Standard Proctor.

The 80/20 – CG/DM blend showed Pr well below the Monterey Sand. At the confining stress of 4 psi the Pr for this blend was about 0.65 times the Pr for Monterey Sand for both geogrids, this factor dropped to 0.6 at 6 psi, and to about 0.4 at 8 psi confining stress. The difference in performance based on geogrid is consistent with the other blends with increases in Pr by factors of about 2.1, 2.0, and 1.6 for confining

stresses of 4, 6, and 8 psi respectively. This blend was compacted to 100% $\gamma_{d,max}$ from Standard Proctor.

The 100% DM performed the least well of all the materials. The Pr of the 100% DM varied from 0.4 to 0.2 times that of the Monterey Sand. The difference between the UX1400 and the UX1700 geogrids is less severe for the DM than for the other materials with only about a 1.3 times increase in Pr from the UX1400 to the UX1700.

From inspection of the results presented above, the following preliminary observations can be drawn immediately:

- Crushed Glass exhibits a greater resistance to pullout than dredged material. The difference in Pullout Resistance ranges from 3 to 4 times for the UX1400 at 4 and 6 psi respectively and 5.7 to 7 times for the UX 1700 at 4 and 6 psi respectively. Among the various blends, the Pullout Resistance increases with increasing proportion of crushed glass.
- The 100% CG and the 80/20 – CG/DM blend have a greater Pullout Resistance than the Monterey Sand at normal pressures of 4 psi and 6 psi. These materials show promise as candidates for use as a backfill material. The 50/50 – CG/DM blend was slightly less resistant to pullout than the Monterey Sand so the suitability as a backfill material for this blend (as with all materials) would rely more on the design requirements of the backfill. The rest of the blends displayed Pullout Resistance too far below Monterey Sand.

- Pullout Resistance increases with increasing confining stress. The geogrid is harder to pull out from the soil when subjected to greater normal forces. This effect is more pronounced as the percentage of crushed glass increases. For the 100% DM especially, there is very little increase in Pullout Resistance with increased effective normal stress.
- The UX1700 geogrid shows a much greater Pullout Resistance than the UX1400 as expected due to the difference in stiffness between the two, with the UX1700 being the stiffer geogrid. Given that the geogrids have similar geometry, with the thickness being the main difference between these geogrids, an interpretation of the Pullout Resistance in terms of various geometric properties of the geogrid and the fill material is modelled in Chapter 4.5.

The 100% CG and the 80/20-CG/DM blend show greater pullout resistance than the other blends. By inspection these blends are more granular in nature while the 50/50 CG-DM blend is about equal parts granular and equal parts fine material or clay. The remaining blends were very clayey by nature. The as tested water contents of the finer blends were indeed higher than the optimum and higher than the granular blends, which might have influenced the impact of particle size and overall interaction during pullout. The differences in relative compaction of the various materials may also have played a role though the degree of impact may be minimal.

In a series of direct shear interface tests, Seed and Boulanger (1991) measured the strengths of two materials that were under a wide range of water contents and dry densities; one material was composed of 98% fines and had LL = 82 and PI = 48; the second material had 60-70% fines and LL = 27 and PI = 19; these materials are somewhat similar to the 100% DM (97% fines, LL = 81 and PI = 28) and the 80/20 – CG/DM blend (75% fines, LL = 80, and PI = 29), respectively. The tests were conducted in the as compacted state and with a smooth HDPE liner. Their results are presented in Figure 4.3 and Figure 4.4. The results indicated a lack of strength loss for a decrease in compaction effort at a given water content. As the water content increased above the optimum level the interface shear strengths were noticeably lower. This indicates that the difference in compaction efforts between the CG-DM blends might not have a significant effect on the pullout test results.

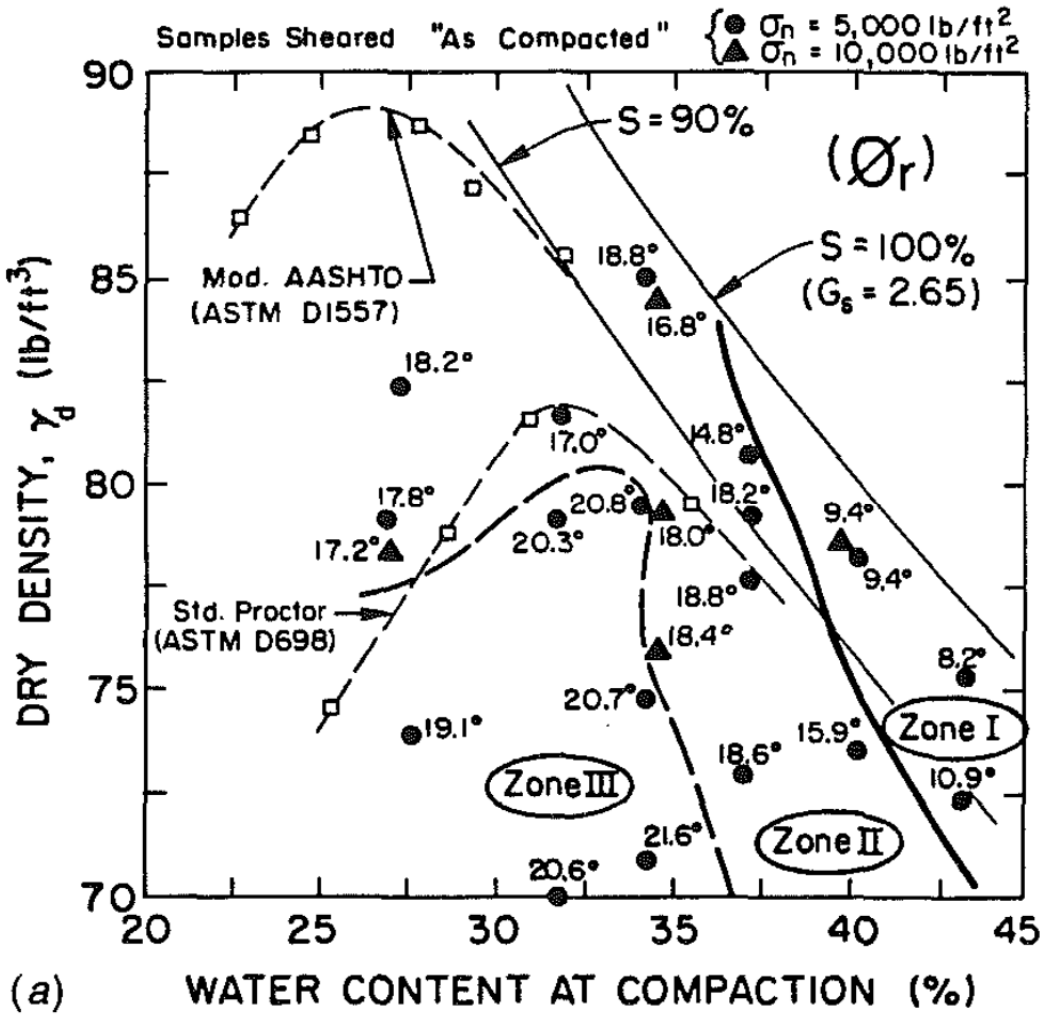

Figure 4.3: Smooth HDPE-compacted clay liner interface for material with 98% fines, LL = 82, PI = 48. Seed and Boulanger (1991).

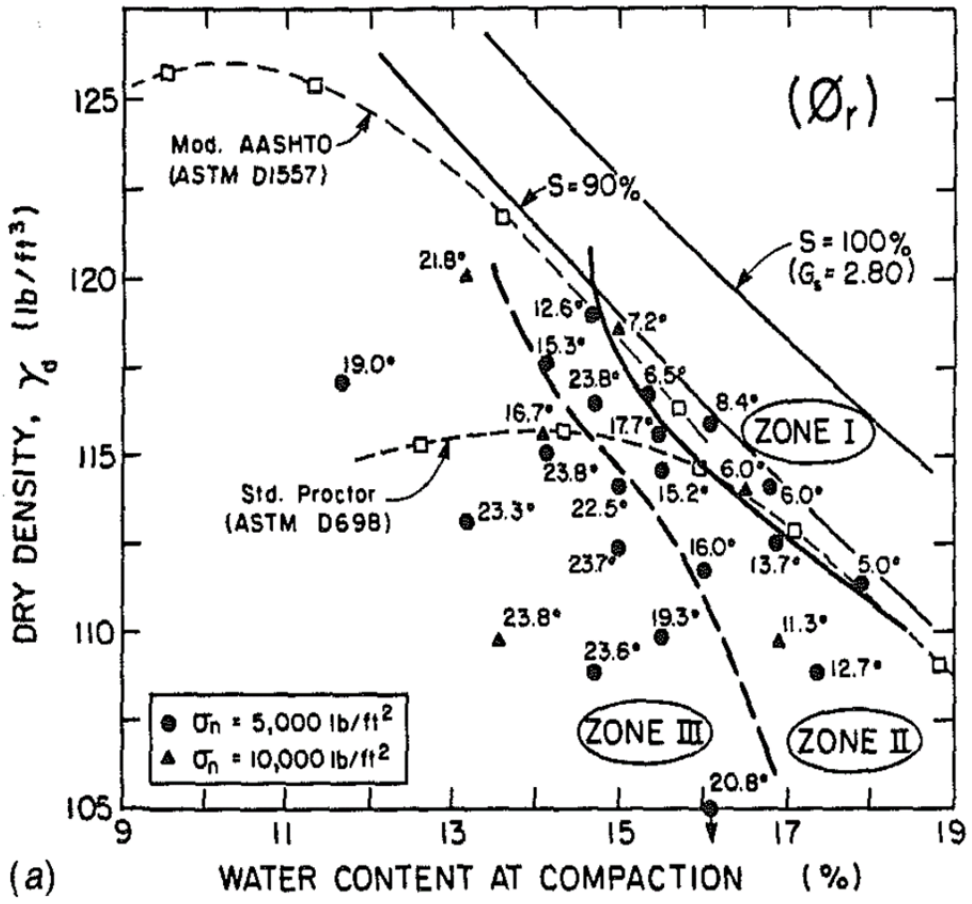

Figure 4.4: Smooth HDPE-compacted clay liner interface for material with 60-70% fines, LL = 27, PI = 19 from Seed and Boulanger (1991).

While the different compaction efforts may have some effect on the pullout results, the Pullout Resistance of each material is typically in the expected range, where the blend with the higher percentage of CG would be expected to outperform blends with lower percentages of CG. This trend is consistent with that of a similar series of pullout tests on Steel Slag Fines (SSF) blended with another Dredged Material from Maryland.

These tests were a different branch of the testing program analyzed in this report, thus the geogrids, pullout box, and tests procedures were the same, additionally the same proportions were used; 100% SSF, 100% DM, 80/20, 50/50 and 20/80 SSF-DM. The as compacted unit weights, water contents, shear strength, and particle sizes are presented in Table 4.5 (Hanumasagar, 2013); the full material properties as determined in laboratory tests by Malsavage (2012) are found in Appendix A. This shows the similarities in particle size distribution to the CG-DM blends; however, the as compacted unit weight and friction angles are higher for the SSF-DM blends than for the CG-DM blends.

Table 4.5: As compacted material properties for SSF, DM, and SSF-DM blends as reported by Hanumasagar (2013).

				Particle size		
Media Tested	γ_d (lb/ft^3)	ω (%)	ϕ (°)	Gravel (%)	Sand (%)	Fines (%)
100% SSF	121	9	45.7	35.6	61.1	3.4
80/20 SSF-DM	107	15	38.6	15.5	63	21.7
50/50 SSF-DM	93	26	45	10.3	41.4	48.3
20/80 SSF-DM	83	31	32.4	1.1	15.5	83.4
100% DM	68	41	27.3	0	1.2	98.8

The results from the pullout tests of the SSF-DM blends are presented in Figure 4.5 (Hanumasagar, 2013). The Pullout Resistance for these blends increases with the proportion of SSF such that the blend with the higher percentage of SSF has the highest Pullout Resistance for a given geogrid and normal pressure.

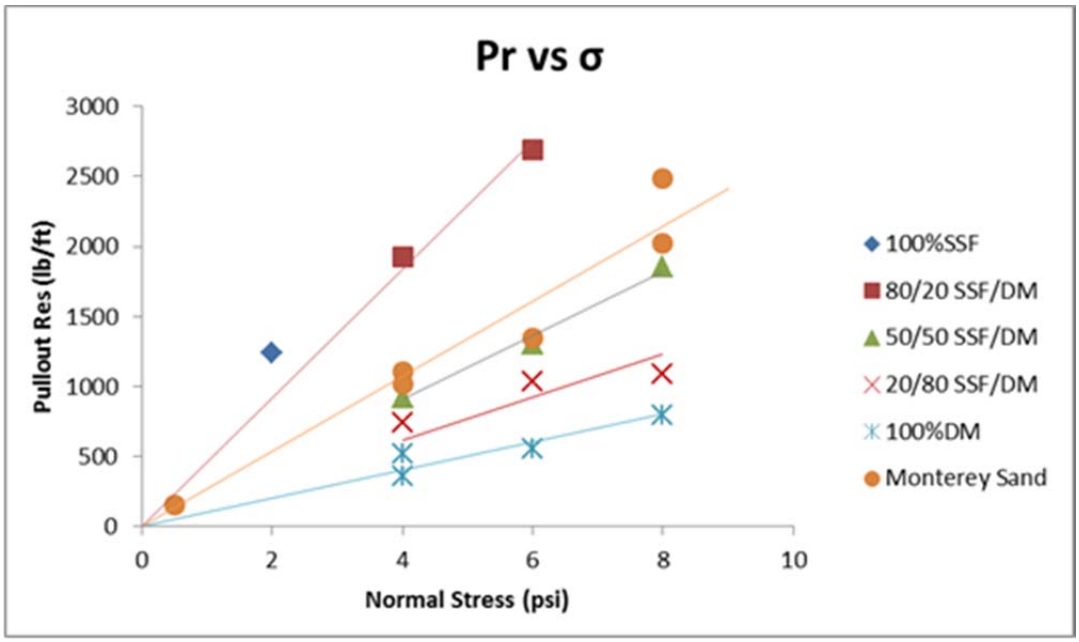

(a) UX1400

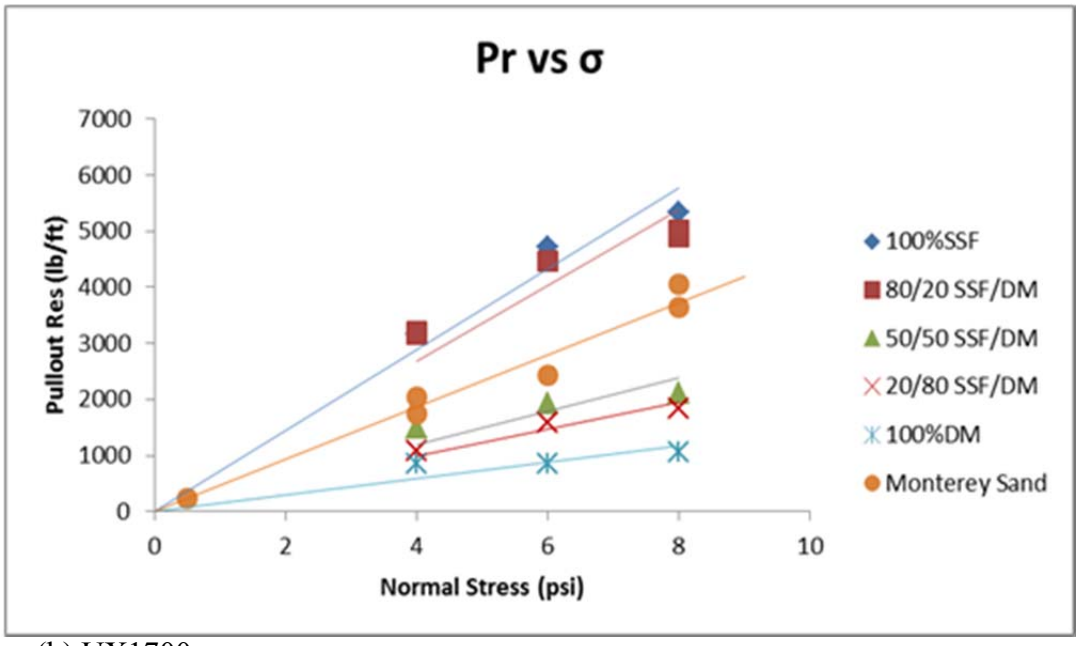

(b) UX1700

Figure 4.5: Pullout Resistance of SSF, DM, and SSF-DM blends for (a) UX1400 and (b) UX1700 (Hanumasagar, 2013).

The results of the research conducted by Hanumasagar (2013) and Seed and Boulanger (1991) support that for the CG-DM blends, the results of the pullout tests are not significantly skewed by the differences in relative compaction between the different blends.

Three-Dimensional plots of the Pullout Resistance are provided in Figure 4.6. These 3-D plots clearly show the combined effect that increasing percentage of CG and increasing normal stress has to increase the Pullout Resistance.

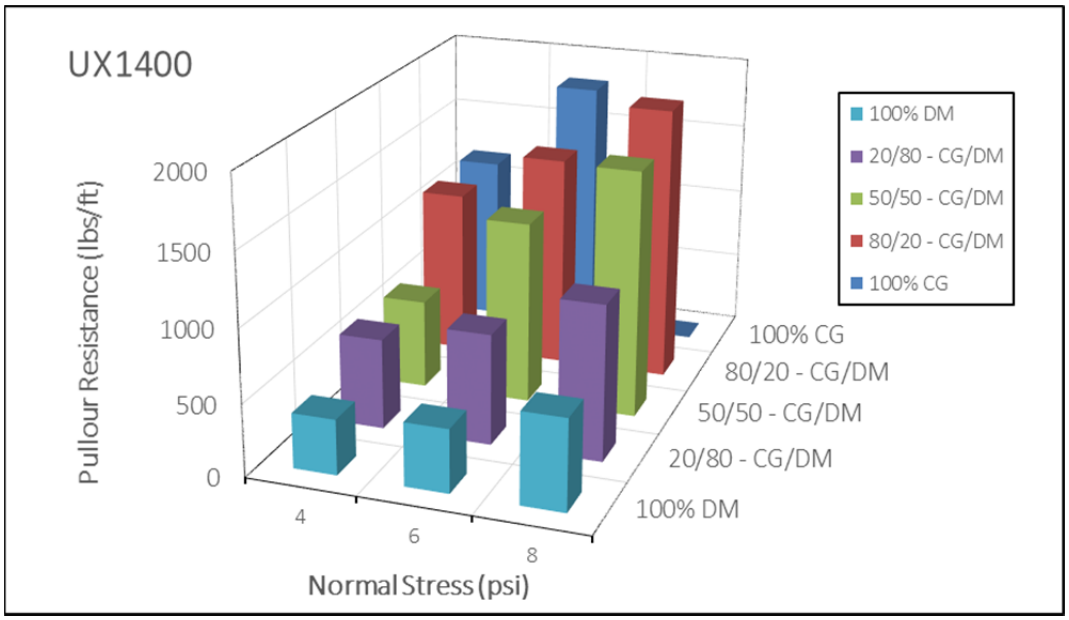

(a) UX1400

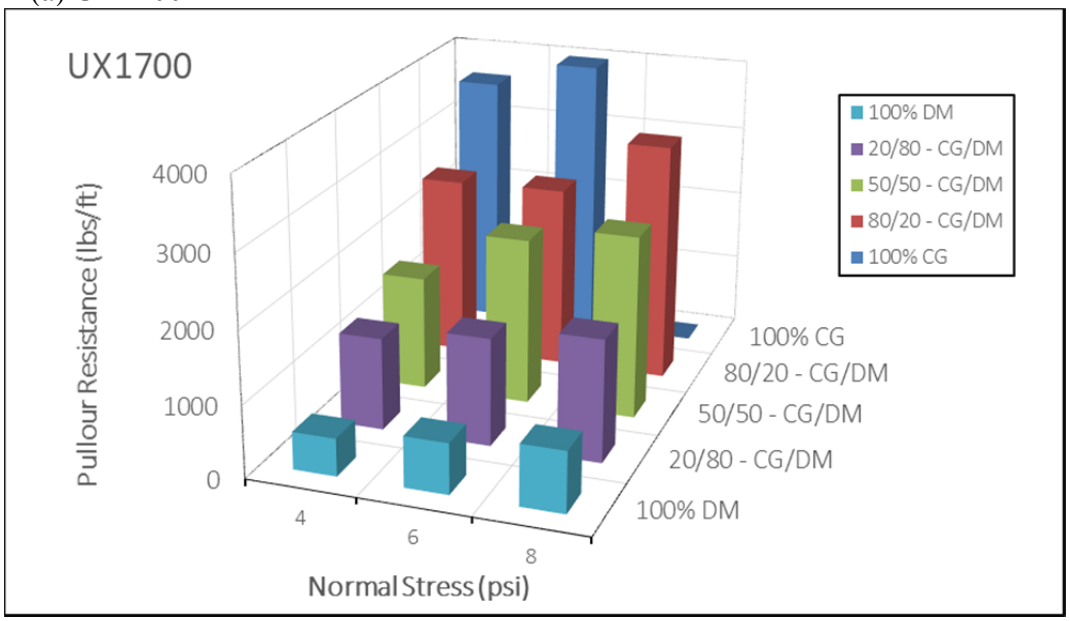

(b) UX1700

Figure 4.6: 3-D representation of Pullout Resistance of CG, DM, and CG/DM blends at different confining stresses for geogrids (a) UX1400 and (b) UX1700.

4.3 Force Displacement Curves

Force versus Displacement curves for all pullout tests are presented in Appendix B. These plots present the development mobilization of the pullout resistance with displacement. For extensible geosynthetics, these plots provide the development of the pullout resistance at various points along the geogrid. A typical force vs. displacement curve from a test on a 1 ft. wide BX1100 geogrid in Monterey Sand at a normal pressure of 3 psi is presented in Figure 4.7. In this figure LVDT A is attached to the geogrid near the sleeve opening at the front of the box, LVDT B is attached to the middle of the geogrid, and LVDT C is attached to the rear of the geogrid.

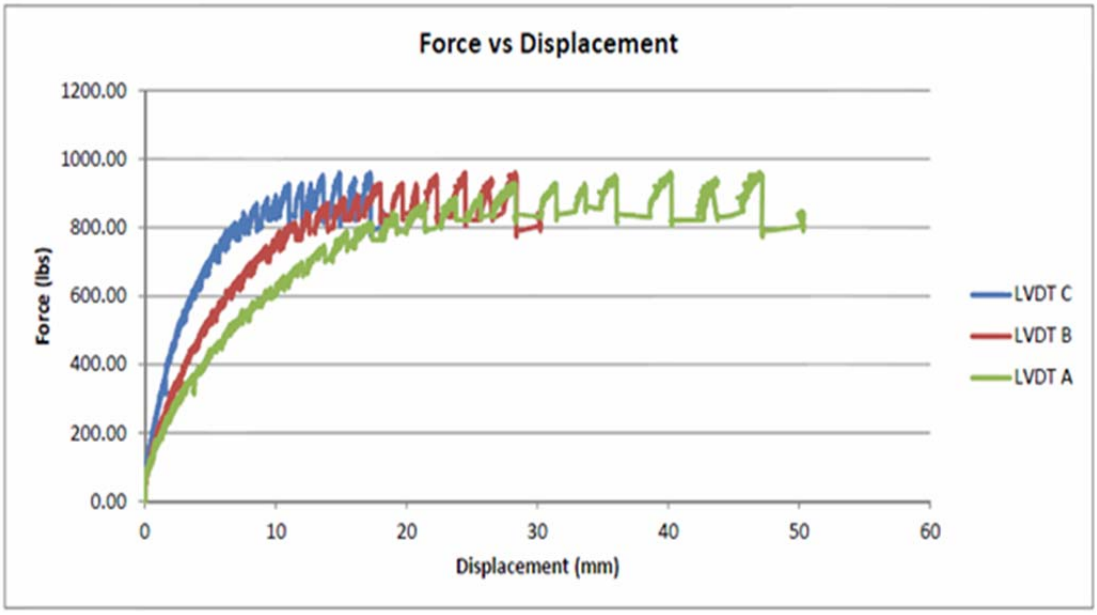

Figure 4.7; Typical force vs. displacement trend in a pullout test.

The plot in Figure 4.7 shows the Pullout Resistance at about 950 lbs/ft. Each LVDT has a different initial slope due to the extensibility of the geogrid showing the mobilization of pullout resistance at the different points on the geogrid. An inextensible geogrid would essentially displace uniformly across the length of the geogrid thus causing all the LVDTs to have the same starting point and the same slope throughout. When Pullout is achieved, there is no further increase in the load. For this example, the Pullout Load increases sharply with displacement followed by a reduction in slope until the maximum load is reached.

The plots in Figure 4.8 and Figure 4.9 provide force displacement curves of a few tests to facilitate comparisons between the blends. Figure 4.8 shows the force-displacement of both geogrids for the 100% CG and 100% DM materials. The 100% CG shows a sharp initial increase of pullout load after which point an extended gradual increase in pullout load develops until the maximum load is achieved. For the 100% DM the pullout load increases sharply similar to the CG however there is relatively little increase in pullout resistance with additional displacement after this sharp initial rise; the UX1700 geogrid shows a very small gradual increase in pullout load before plateauing while the UX1400 plateaus almost instantly after the sharp initial increase in pullout resistance.

The studies discussed in Chapter 2 contributed the initial, low displacement, resistance to pullout to the interfacial friction and contributed the resistance at large

displacement to some combination of interfacial friction and bearing resistance. As the geogrids have similar geometries it is reasonable to assume that the interfacial shear component is also similar. Thus, because of the difference in thickness of the geogrids, the difference in Pullout Resistance might be due to the contribution from bearing resistance.

Figure 4.9 presents the force-displacement plots each blend for both geogrids at 6 psi normal stress. For these plots, the initial (friction based) increase in pullout resistance increases in duration as the percentage of crushed glass in the blend increases. This observation may be explained by the increase in friction angle of the blends. However, the CIU triaxial friction angles for all the materials only varies from 34-39° with the 80/20 blend having the highest friction angle. From the UU triaxial tests, which may more accurately resemble the pullout tests in this project due to immediate testing upon compaction, the friction angle of the materials varies from 20° for the 100% DM to 40° for the 100% CG. These absolute differences in the UU friction angles correlate better with the different durations of the initial gain in pullout resistance. The duration of the secondary increase in pullout load may be due to a combination of the grain size distribution, which affects the bearing resistance, and the shear strength of the materials, which affects both the interfacial shear resistance and the bearing resistance.

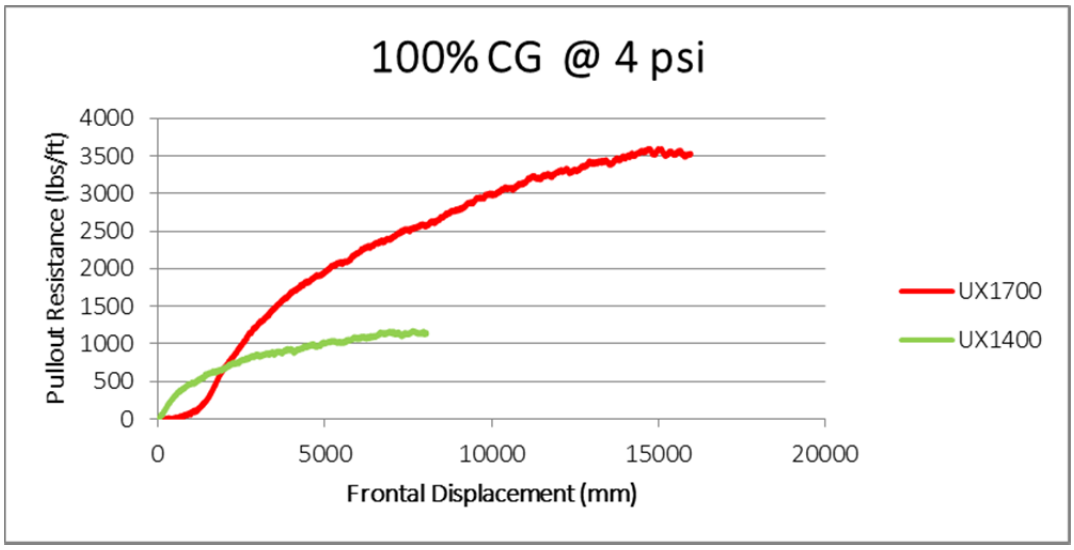

(a) 100% CG

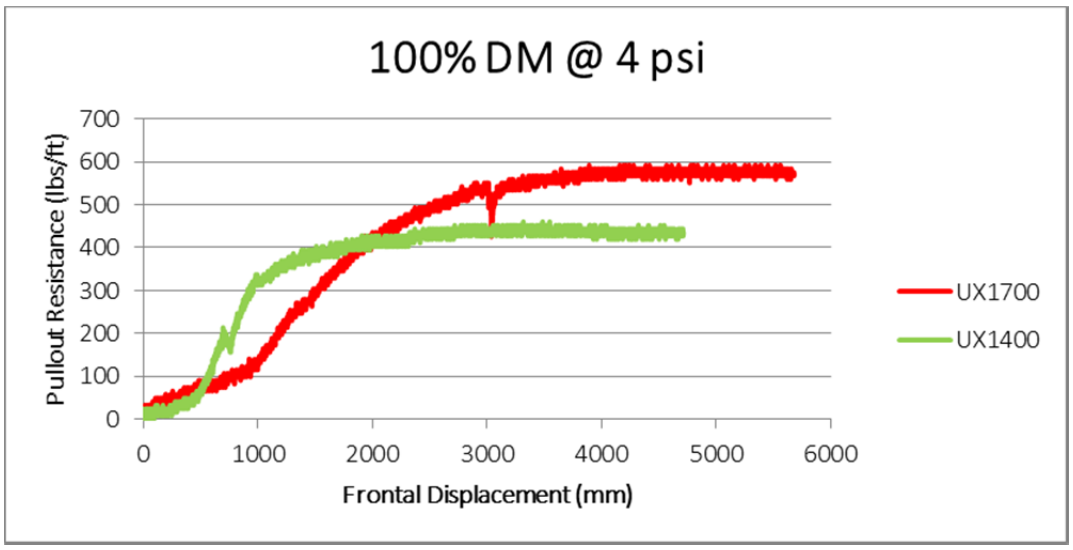

(b) 100% DM

Figure 4.8: Force-Displacement curves of both Geogrids for (a) 100% CG and (b) 100% DM.

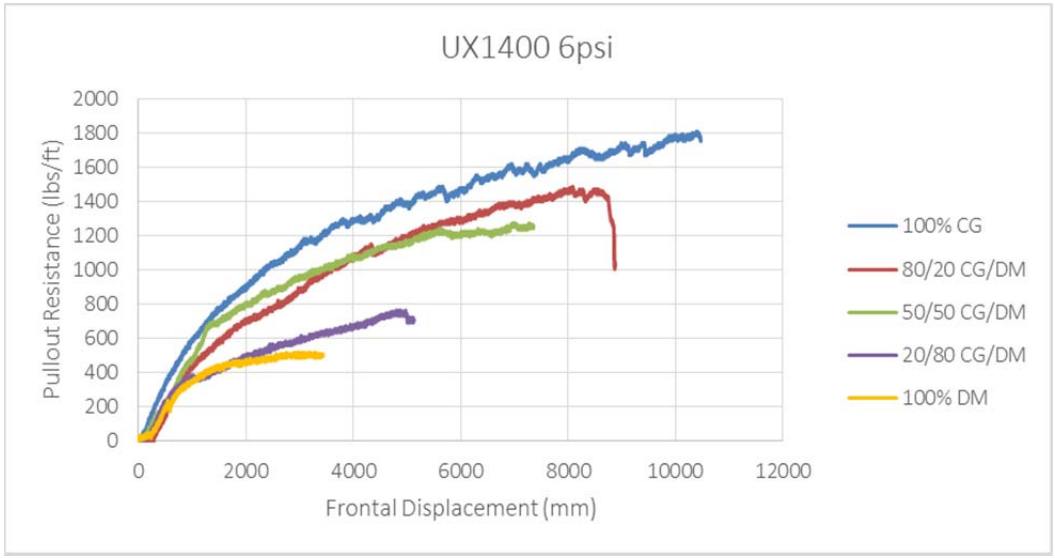

(a) UX1400

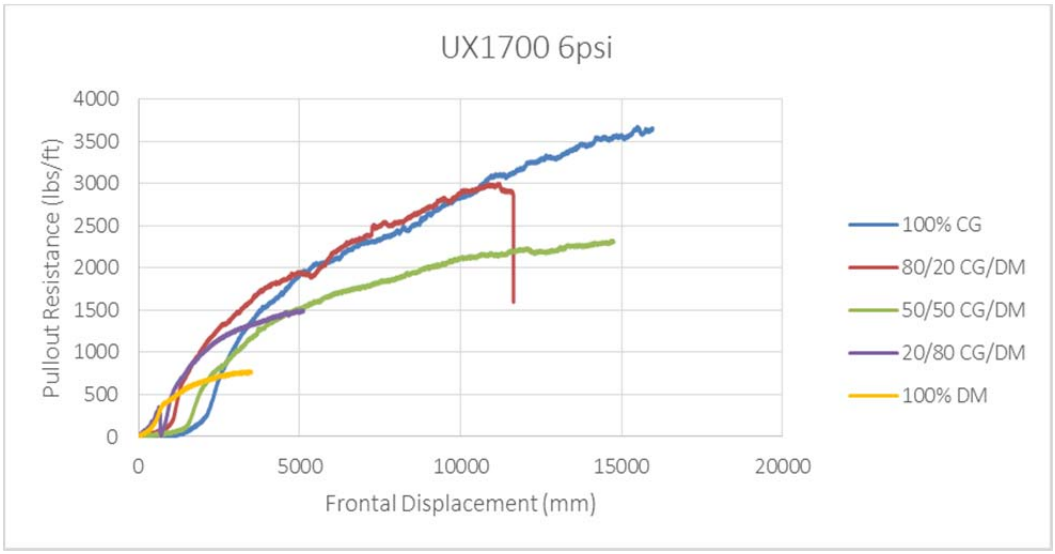

(b) UX1700

Figure 4.9: Force-Displacement curves for all materials at 6 psi for (a) UX1400 and (b) UX1700.

4.4 Coefficient of Interaction

As defined earlier in Chapter 2.2 the coefficient of interaction (CI) is a measure of the efficiency of the interaction between the soil and the geosynthetic. A common expression of the CI is:

$$ci = \frac{\tau_{s-g}}{\tau_s} = \frac{\mathrm{P_r}}{2 \times L_e \times \sigma_y \times \tan(\phi)} \tag{4.1}$$

Where P_r is the Pullout Resistance; L_e is the embedded length of the geogrid, σ_y is the normal stress on the system; and ϕ is the friction angle of the soil.

An additional, modified, expression for the CI includes the cohesion component for soils and is expressed with the following equation:

$$ci, \mathrm{mod} = \frac{\tau_{s-g}}{\tau_{s-g}} = \frac{\mathrm{P_r}}{2 \times L_e \times (\sigma_y \times \tan(\phi) + \mathrm{c})} \tag{4.2}$$

Where c is the cohesion of the fill material.

For cohesionless soils, the pullout failure envelope passes through the origin indicating zero adhesion between the fill material and the geogrid; for this case, the value for CI is the same as for ci,mod. For the materials with a cohesion component the ci,mod will be less than the CI for that material. The values of the CI and ci,mod for each test

are presented in Table 4.6 along with the parameters necessary to calculate the coefficients. Plots of the CI versus normal stress for all materials and both geogrids are presented in Figure 4.10.

The CI for the UX1400 is less than the UX1700 for a given material because the pullout resistance is lower for the UX1400. The Monterey Sand, which provided a reference point as the control media, had CI values centered around 0.4 for the UX1400 and 0.75 for the UX1700. Since this material was cohesionless, the values for CI were equal to the values for $c_{i,mod}$.

The 100% DM is the only material with significant cohesion (260 psf). The addition of even 20% CG significantly reduces the cohesion to 30 psf. The 50/50 blend does have a higher cohesion of 45 psf however the impact of the cohesion for the materials with any percentage of CG is negligible. The maximum difference between CI and $c_{i,mod}$ for a material with CG is 10% compared to a maximum difference of 40% for the 100% DM. Given this observation, the remaining discussion considers the unmodified coefficient of interaction.

For the majority of the materials, the CI decreases with increasing normal stress. However, when tested with the UX1400 geogrid, the 50/50 blend had increasing values of CI with increasing normal stress. For both geogrids, the CI for Monterey Sand was highest at a normal stress of 8 psi.

For the 100% CG tested with the UX1400 geogrid at 4 psi normal stress, the CI was 0.44 which barely exceeds the CI for Monterey Sand however this was the only point was available due to the rupture of the geogrid at 6 psi which was discussed earlier. At 4 psi normal stress with the UX1700, the CI far exceeded the Monterey Sand with a CI of 1.4; at 6 psi the CI was 0.8.

The CI of the 80/20 – CG/DM blend was nearly identical to the CI for Monterey Sand at normal stresses of 4 and 6 psi for both geogrids. However, the CI of the 80/20 blend dropped below the Monterey Sand at 8 psi normal stress. For the UX1400 the CI varied between 0.42 and 0.35; for the UX1700 the CI varied between 0.92 and 0.62.

The remaining blends performed worse than the Monterey Sand for all test conditions. For the UX1400, the *ci*'s of the 50/50 and 20/80 CG/DM blends, and 100% DM centered around 0.3, 0.25, and 0.15 respectively and showed little variation at different normal stresses. For the UX1700, the *ci*'s of the 50/50 and 20/80 CG/DM blends, and 100% DM centered around 0.6, 0.4, and 0.2 respectively and showed little variation at different normal stresses.

Table 4.6: Coefficient of Interaction and Modified Coefficient of Interaction of Pullout Tests.

Serial No.	Date of Test	Material	Geogrid	Normal Stress (psi)	Pullout Resistance (lbs/ft)	Embedment Length, Le (ft)	Friction Angle, ϕ (°)	Cohesion, c (psf)	ci	ci, modified
1	27-Feb-12	Monterey Sand	BX1100	3	1011	1.91	39	0	0.76	0.76
2	4-Mar-12		BX1100	3	962	1.98	39	0	0.69	0.69
56	4-Jul-12	100% DM	UX1400	4	380	2.85	34	260	0.17	0.10
57	5-Jul-12		UX1400	6	435	2.82	34	260	0.13	0.09
58	6-Jul-12		UX1400	8	625	2.85	34	260	0.14	0.11
59	6-Jul-12		UX1700	4	520	2.82	34	260	0.24	0.14
60	7-Jul-12		UX1700	6	700	2.85	34	260	0.21	0.15
61	8-Jul-12		UX1700	8	840	2.82	34	260	0.19	0.14
62	10-Jul-12	20/80 CG/DM	UX1400	4	624	2.85	35	30	0.27	0.25
63	12-Jul-12		UX1400	6	764	2.82	35	30	0.22	0.21
64	12-Jul-12		UX1400	8	1068	2.85	35	30	0.23	0.22
65	13-Jul-12		UX1700	4	1285	2.92	35	30	0.55	0.51
66	13-Jul-12		UX1700	6	1495	2.89	35	30	0.43	0.41
67	14-Jul-12		UX1700	8	1693	2.82	35	30	0.37	0.36
76	23-Jul-12	80/20 CG/DM	UX1400	4	1150	2.95	39	15	0.42	0.40
77	24-Jul-12		UX1400	6	1487	2.92	39	15	0.36	0.36
78	25-Jul-12		UX1400	8	1915	2.95	39	15	0.35	0.34
79	26-Jul-12		UX1700	4	2531	2.95	39	15	0.92	0.89
81	31-Jul-12		UX1700	6	3000	2.82	39	15	0.76	0.74
82	2-Aug-12		UX1700	8	3345	3.25	39	15	0.56	0.56

Table 4.6: Coefficient of Interaction and Modified Coefficient of Interaction of Pullout Tests.

83	4-Aug-12	100% CG	UX1400	4	1175	3.08	37	0	0.44	0.44
84	4-Aug-12		UX1400	6	1808	3.15	37	0	0.44	0.44
85	5-Aug-12		UX1700	4	3599	3.08	37	0	1.34	1.34
86	5-Aug-12		UX1700	6	3977	3.44	37	0	0.89	0.89
87	9-Aug-12	50/50 CG/DM	UX1400	4	616	3.12	38	45	0.22	0.20
88	10-Aug-12		UX1400	6	1265	3.08	38	45	0.30	0.28
90	14-Aug-12		UX1400	8	1709	3.08	38	45	0.31	0.29
91	17-Aug-12		UX1700	4	1594	2.95	38	45	0.60	0.55
92	17-Aug-12		UX1700	6	2325	2.89	38	45	0.60	0.56
93	18-Aug-12		UX1700	8	2550	2.85	38	45	0.50	0.47
94	17-Jul-12	Monterey Sand	UX1700	4	2005	2.85	35	0	0.87	0.87
95	17-Jul-12		UX1700	6	2475	2.95	35	0	0.69	0.69
96	18-Jul-12		UX1400	8	2500	2.99	35	0	0.52	0.52
97	19-Jul-12		UX1400	4	950	2.99	35	0	0.39	0.39
98	19-Jul-12		UX1400	6	1323	2.99	35	0	0.37	0.37
99	20-Jul-12		UX1700	8	4025	2.95	35	0	0.84	0.84

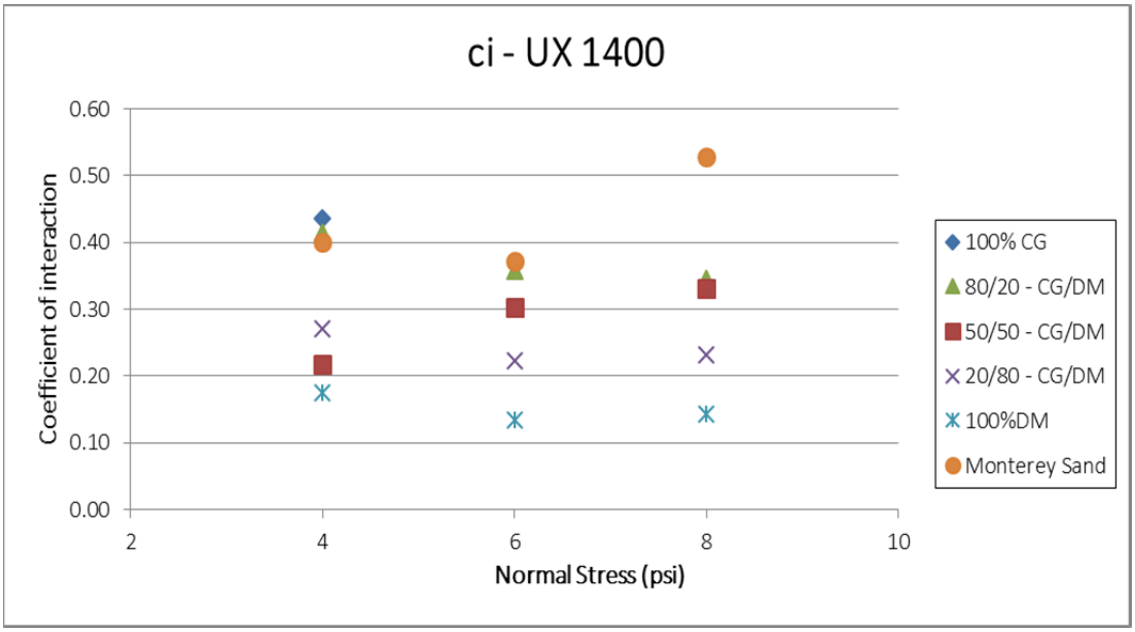

(a) UX1400

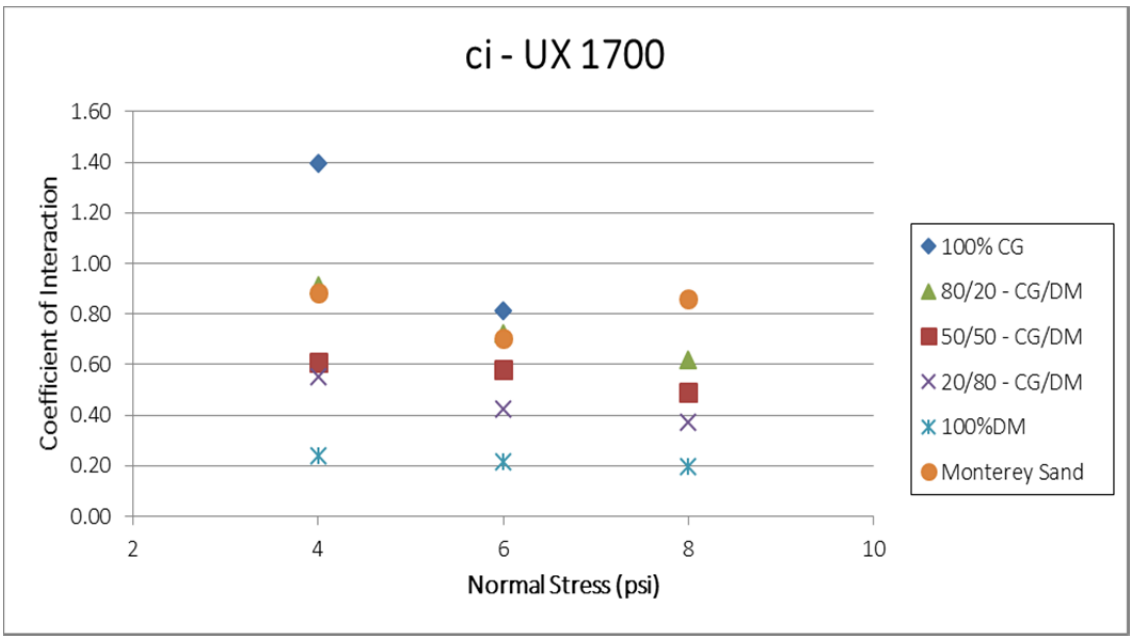

(b) UX1700

Figure 4.10: Coefficient of Interaction for all materials with geogrids (a) UX1400 and (b)

4.5 Assessment of Bearing Stress Mechanism of Pullout Tests of Geogrids

As discussed in Chapter 2.4, Palmeira studied the effect of the ratio of the thickness of the transverse rib of a geogrid (B) and the mean soil particle diameter (D_{50}) on the pullout resistance. The results from the CG – DM mixtures were investigated to determine how this concept might apply to extensible geogrids and various materials. Rather than predicting the bearing stress, this analysis seeks to identify trends in the data. For this analysis, the skin friction is assumed to be negligible and thus the bearing resistance is assumed to contribute to 100% of the pullout load; this assumption facilitates the comparison with Palmeira's results on single transverse ribs discussed in Chapter 2.4.

For the CG-DM blends, the first rib was so near the frontal opening that it was not considered in this analysis; thus only 2 transverse ribs are considered. For an analysis on specimens with multiple transverse ribs the pullout force per transverse rib was calculated using equation (4.3).

$$P_0 = \frac{P_{ult} \times W}{N_{trans}} \tag{4.3}$$

Where "P_{ult}" is the maximum Pullout Resistance, "W" is the width of the specimen, and "N_{trans}" is the number of transverse ribs on the specimen. Since each transverse rib is composed of bearing faces and joints that connect to the longitudinal

ribs, the area of the leading face that contributes to bearing resistance was calculated using equation (4.4).

$$A_{face} = W \times B - A_{long} \times N_{long} \tag{4.4}$$

Where A_{long} is the area of a longitudinal rib and N_{long} is the number of longitudinal ribs across the specimen. The bearing stress can then be calculated using equation (4.5),

$$\sigma_b = \frac{P_0}{A_{face}} \tag{4.5}$$

The normalized bearing stress can then be calculated using equation (2.5).

The results of this analysis for the blended materials and Monterey sand are presented in Figure 4.11 with the results from Palmeira's experiments for comparison. Changes in B/D_{50} are due to the different rib widths due to the data being grouped by fill material. For the materials with B/D_{50} less than 5, or 100% CG and the 80/20 – CG/DM blend, it is difficult to ascribe a trend to the data due to the limited number of tests. The 50/50 – CG/DM blend does not display any considerable change in normalized bearing stress over the range of about 20 to 50 for B/D_{50} which is consistent with Palmeira's results of little to no effect in normalized bearing stress for B/D_{50} ratios over 12. The Monterey sand shows a general decrease in normalized bearing stress for B/D_{50} ratios from about 7 to 17 which is generally consistent with Palmeira's findings.

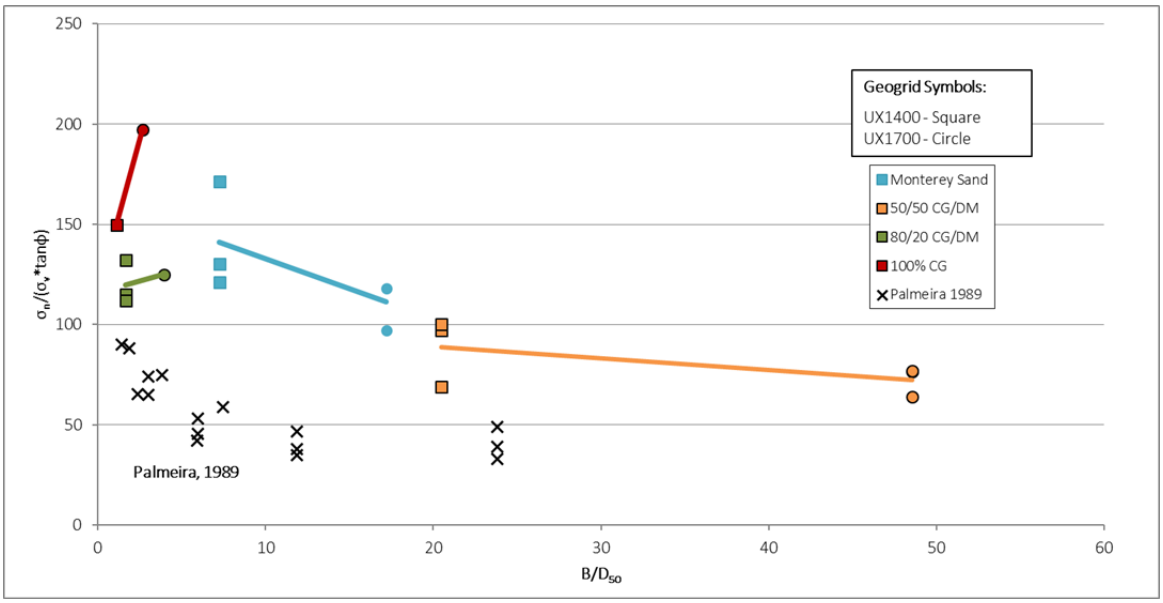

Figure 4.11: Influence of the transverse rib thickness to the mean particle diameter ratio on normalized bearing stress.

A database provided by SGI Testing Services, formerly GeoSyntec Consultants (Geosyntec) and presented in Hutcherson (2012), included pullout tests using the same UX1400 and UX1700 geogrids and various materials. The material properties and test specifications for this data set can be found in Appendix A. The B/D_{50} ratio versus normalized bearing stress of this additional database and the CG and DM blends is presented in Figure 4.12 and are grouped by a given fill material. For smaller B/D_{50} ratios, the normalized bearing stress can change considerably for a given change of the B/D_{50} ratio and as the B/D_{50} ratio gets larger, changes in this ratio for a given material have less impact on the normalized bearing stress. This figure highlights the variability of the mean particle size to rib thickness ratio between different materials.

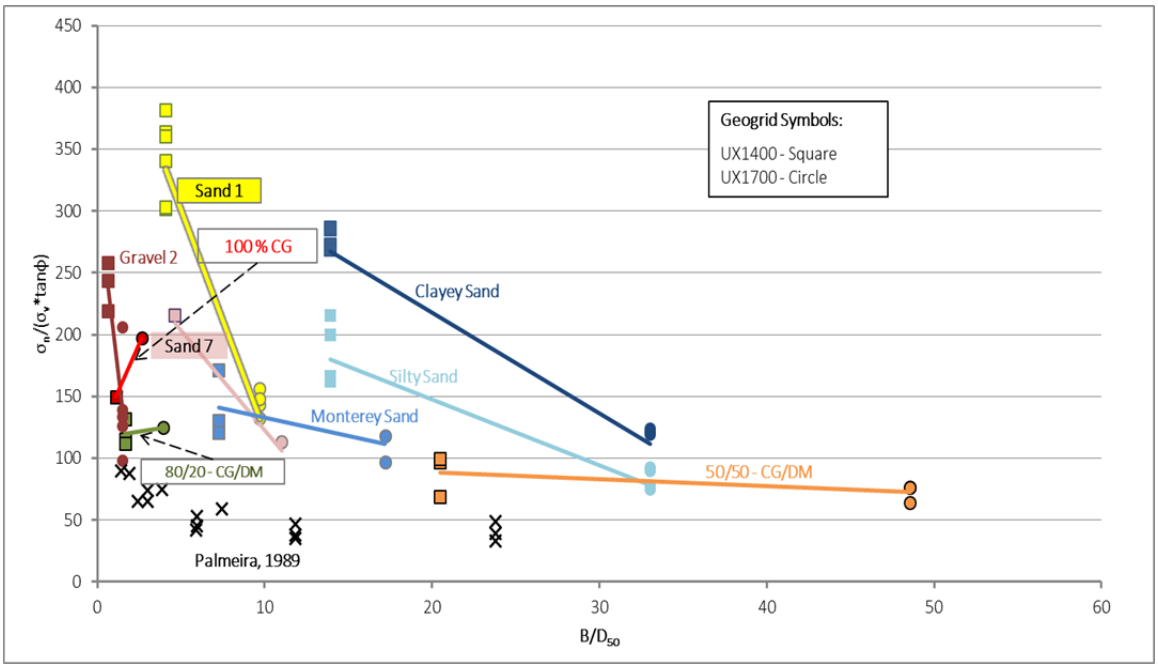

Figure 4.12: Influence of the transverse rib thickness to the mean particle diameter ratio on normalized bearing stress with the blended materials and the materials from the SGI provided database.

Figure 4.11 and Figure 4.12 show how the normalized bearing ratio changes with different transverse rib thicknesses, for a given material. Figure 4.13 shows the data grouped by geogrid such that changes in the B/D_{50} ratio are due to difference in the mean particle size of the fill material. For the UX1700 geogrid, which has a transverse rib thickness of 0.325 inches, a slight decrease in normalized bearing stress is observed with decreasing mean particle size. For the UX1400 geogrid, which has transverse rib a thickness of 0.137 inches, a general trend for a change in mean particle size is not discernible. The normalized bearing ratio is affected somewhat consistently by a change

in the mean particle size of a fill material for a geogrid with thicker transverse ribs. The normalized bearing ratio shows more variability for a change in mean particle size.

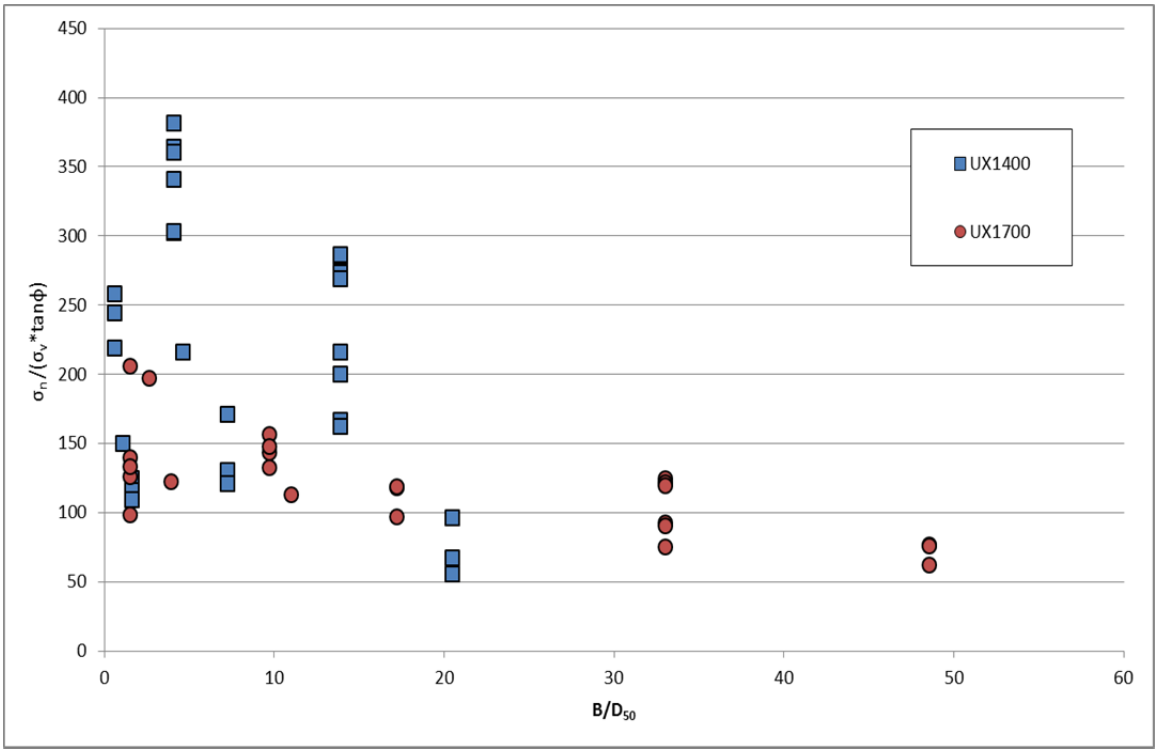

Figure 4.13: Influence of the transverse rib thickness to the mean particle diameter ratio on normalized bearing stress by geogrid.

This method of analysis is useful in comparing materials tested with varying specimen lengths and widths as the normalized bearing ratio focuses solely on the bearing resistance of a single transverse rib normalized to a unit width. With this benefit however comes the caveat that the component due to friction is attributed to the bearing capacity. As discussed in Chapter 2.4 the interface shear resistance is likely reduced

along the longitudinal ribs due to the reduced localized normal pressure at these locations the shear resistance along the transverse ribs may be increased in comparison.

One further note of comparison is that a higher normalized bearing ratio for a particular B/D_{50} ratio does not constitute a high Pullout Resistance. The normalized ratio for a given B/D_{50} essentially represents the efficiency of the interaction between the fill material and the geogrid in regards to bearing resistance at the transverse ribs.

Chapter 5: Conclusions and Recommendations

5.1 Conclusions

In this project, laboratory pullout tests were conducted using crushed glass from the city of Philadelphia's curbside collection program, fine-grained dredged material from the USACE Fort Mifflin CDF in Philadelphia, and blends of these two materials with proportions of 80/20, 50/50, and 20/80. The objective of this study was to determine the suitability of these materials and their blends for backfill of reinforced soil structures. The blends were tested in performance with two commonly used uniaxial HDPE geogrids, the UX1400 and the UX1700 manufactured by Tensar International. The pullout tests were conducted under confining pressures of 4, 6, and 8 psi to keep the anticipated pullout load less than the ultimate tensile strength of the geogrids. Moisture content and relative compaction were controlled for each individual material and the geogrid sample size and pullout rate was constant across all tests in order to facilitate direct comparison between results. Monterey No. 30 Sand was used as a control material, which served to establish repeatability and reliability of the pullout testing system and to provide a reference point for comparing the blended materials. Comparisons of the pullout resistance were drawn between all combinations of fill materials and geogrids. The findings of this research are as follows:

- The 100% CG caused damage to the geogrids. The UX1400 geogrid failed to tension below the ultimate tensile strength when tested with 100% CG at a confining pressure of 6 psi. It is likely this resulted from particles of crushed glass embedding into the geogrid reducing the effective cross-sectional area and thereby reducing the tensile capacity of the geogrid.
- The 100% CG and 80/20 – CG/DM blend are viable for backfill in reinforced soil structures based on Pullout Resistance. The 100% CG and 80/20 - CG/DM blend show a pullout resistances equal to or greater than the Monterey Sand for confining pressures of 4 and 6 psi. For the 100% CG the pullout resistance is ranges from 1.2 to 1.6 times that of the Monterey Sand and for the 80/20 – CG/DM blend the factor ranges from 1.0 to 1.2. The rest of the blends showed lower pullout resistance than the Monterey Sand. The addition of 20% DM to the CG media did reduce the pullout resistance yet it was still moderately higher than the Monterey Sand.
- For the granular materials tested, the efficiency of a geogrid in relation to the thickness of its transverse ribs decreases as the confining stress increases. For the materials with 20% CG or greater, the pullout resistance with the UX1700 was at least twice the pullout resistance with the UX1400 for a normal stress of 4 psi. For each material, this ratio decreased as the confining stress increased.

- The granular particles from the crushed glass have greater difficulty in rearranging when interacting with the thicker geogrid (UX1700) than with the thinner geogrid (UX1400). Greater difficulty for the particles to rearrange results in higher interaction between the soil and the geogrid and thereby higher Pullout Resistance.
- For the dredged material, the improvement in pullout resistance for the UX1700 versus the UX1400 was not significant. Nor did this difference between geogrids change by increasing the confining stress. This indicates that pullout tests with clayey materials are less dependent on the thickness of the geogrid transverse members and on the confining stress than coarse-grained materials. This finding may be due to the ability of the fine-grained particles to more easily rearrange under stress. Additionally, the 10% dredged material may have been tested in undrained conditions due to the rate of displacement and the wet of optimum moisture content.
- The main difference between the results with the UX1700 and the UX1400 is due to the bearing resistance at the transverse ribs. The UX1400 and UX1700 geogrids have the same texture and surface geometry; additionally, all tested samples were of similar dimensions leading to the assumption that the frictional component of the tests was approximately the same for both geogrids. The transverse rib of the UX1700 is three times thicker than that of the UX1400.

- The coefficient of interaction (CI) allows a quantitative comparison of the performance of different combinations of fill materials and geogrids. The CI of the 100% CG and the 80/20 – CG/DM blend was typically greater than or comparable to the CI of Monterey Sand. The 100% CG had the highest values of CI for any of the materials and for both geogrids. The CG/DM blends containing 50% CG and less showed increasingly poor interaction as the percentage of CG decreased. The 100% DM displayed the lowest CI signifying very poor soil-geogrid interaction. The CI is a good metric for comparing the performance of various soil-geogrid combinations.
- The normalized bearing ratio for a given B/D_{50} represents the efficiency of interaction between a fill material and geogrid in regards to bearing resistance at the transverse ribs. A higher normalized bearing ratio for a particular B/D_{50} ratio does not constitute a high Pullout Resistance.
- The normalized bearing ratio should not be used to determine or predict the pullout resistance of a geogrid but it may help in selecting a geogrid for a given fill material.

Overall, the blend with 80% crushed glass and 20% dredged material was found to be a very suitable backfill material when reinforced with a geogrid as the pullout resistances were comparable to those of Monterey Sand. The 100% crushed glass was stronger than the blend of 80% crushed glass and 20% dredged material. However,

despite the glass being crushed to sizes safe for handling purposes, the glass particles tended to become embedded into the geogrids especially at high confining pressures. This solution has the benefit of opening an avenue for the disposal of dredged material. It is uncertain whether a contribution of just 20% dredged material for a mixture with crushed glass is economically viable.

A mixture of 50% crushed glass and 50% dredged material may be suitable for use as backfill depending on the design requirements of a site. Additionally, an intermediate blend, such as 65% crushed glass and 35% dredged material, might satisfy the strength required for a particular design.

The dredged material proved to interact very poorly with the geogrid reinforcements. The addition of crushed glass is important to increase the level of interaction with a geogrid reinforcement.

Crushed glass availability is relatively independent of location as many US cities have a glass recycling program however the practical use of dredged material is limited by the distance required for transportation to inland sites.

5.2 Recommendations for Further Studies

Dredged material showed poor performance in pullout of geogrids. The blending of DM with industrial byproducts such as crushed glass to obtain a well-performing backfill material is a viable and favorable alternative. This solution is a practical method

of using materials otherwise defined as waste. This project aimed to characterize the pullout interaction of different proportions of CG and DM in order to qualify certain mixes as viable for use in industry. Based on the experiences researching and conducting tests on these materials the following recommendations are provided for better understanding the pullout behavior of CG-DM blends.

- The granular blends would be tested to higher displacements, on the order of 500 mm, to study large-strain behavior of the pullout force-displacement curves and to get true measures pullout resistance for these materials.
- Earth pressure cells and pore pressure transducers could be installed in the material to obtain the total stress and effective pore pressure that develops in the pullout box.
- A larger pullout box could be used to accommodate a larger geogrid specimen and might provide better insight into the interference between transverse ribs.
- In addition to dredged materials, the identification of other industrial byproduct sources of a fine-grained material would be highly beneficial in the adoption of use of crushed glass in backfill applications. The crushed glass alone is too abrasive and degrades extensible reinforcements.
- The identification of projects near the coast that could employ dredged material in some capacity would be very beneficial.

- Due to the embedment of crushed glass particles into the geogrid, further investigation of the damage to a geogrid for a given percentage of CG or CG/DM blend would be beneficial to prevent unexpected tensile failures.
- Stability analyses of the various materials and blends would be beneficial in recognizing projects for which these materials may be used.

Appendix A: Material Summaries

Appendix A is a collection of various material summaries discussed in this thesis including but not limited to chemical summaries, physical properties of materials, test results of CG-DM blends and materials from other sources.

Table 5.1: Summary of physical and engineering of crushed glass from two different sources (Wartman et al., 2004).

		Supplier I		Supplier II	
Test/Index	Test standard	As-received	Postcompaction	As-received	Postcompaction
Water content (%)	*ASTM D2216-98*	2.36	—	4.22	—
[range]		[2.03–2.60]		[3.49–5.32]	
Debris content (%)	Gravimetric	0.34	—	1.82	—
[range]		[0.0–0.75]		[0.62–3.41]	
Specific gravity (G_s)	*ASTM C127-88*	2.48	—	2.49	—
Minimum density (g/cm^3)	*ASTM D4254-00*	1.15	—	1.27	—
[range]		[1.14–1.16]		[1.23–1.30]	
Maximum density (g/cm^3)	*ASTM D4253-00*	1.79	—	1.74	—
[range]		[1.77–1.80]		[1.72–1.75]	
Median grain size D_{50} (mm)	—	2.24	1.6	3	2.5
[range]		[1.85–2.62]		[2.70–3.30]	
Coefficient of uniformity, C_u	—	6.2	6.5	7.2	7.8
[range]		[4.3–10.0]		[5.4–7.0]	
Sand content (.075–4.75 mm) (%)	—	91.3	87	70	76
[range]		[89.5–93.0]		[66.5–74.0]	
Fines content (<0.075 mm) (%)	—	3.2	6.2	1.2	2.2
[range]		[0.5–5.0]		[0.2–2.0]	
USCS classification	*ASTM D2487-98*	SW	SW	SW	SW-SM
AASHTO classification	*AASHTO M43-88*	No. 10	No. 10	No. 10	No. 10
LA abrasion (wt. %)	*ASTM C131-96*	24%	—	25%	—
Sodium sulfate soundness (wt. %)	*ASTM C88-99*	6.38%	—	7.1%	—
Hydraulic conductivity[a] (cm/s)	*ASTM D2434-68*	1.61×10^{-4}	—	6.45×10^{-4}	—
[range]		$[1.36\times10^{-4}–1.85\times10^{-4}]$		$[6.42\times10^{-4}–6.64\times10^{-4}]$	
Modified Proctor	*ASTM D1557-00*				
$\gamma_{d,max}$ (kN/m^3)		18.3	—	17.5	—
w_{opt} (%)		9.7	—	11.2	—
Standard Proctor	*ASTM D698-00*				
$\gamma_{d,max}$ (kN/m^3)		16.8	—	16.6	—
w_{opt} (%)		12.8	—	13.6	—
Direct shear	*ASTM D3080-98*				
Internal friction (deg)					
σ_n (kPa)					
0–60		61–63°	—	59–62°	—
60–120		58–61°	—	55–59°	—
120–200		63–68°	—	47–55°	—
Consolidated drained triaxial[a] internal friction (deg)	USACOE	48°	—	47°	—

[a]Specimens were compacted to a dry density equal to 90% (±1%) of their modified Proctor $\gamma_{d,max}$.

Table 5.2: Physical properties and soil classifications of DM, SSF, and DM-SSF blends (Malasavage, 2012)

		Specific gravity	Water content	Loss on ignition	Particle size			Plasticity indices[b]			USCS	AASHTO
		D854 (2002)	D2974 (2000b)	D2974 (2000b)	D422 (1998)			D4318 (2005)				
Media tested[a]		(—)	(%)	(%)	(% gravel)	(% sand)	(% fines)	LL	PL	PI	D2487	D3284
Dredged material (DM)		2.58	122.8	11.76	0.0	1.2	98.8	140	38	102	OH	A-7-6
Blends	80/20 DM-SSF	2.87	106.6	10.10	1.1	15.5	83.4	132	49	83	OH	A-7-6
	60/40 DM-SSF	2.92	76.3	6.87	9.1	29.2	61.7	134	45	89	OH	A-7-6
	50/50 DM-SSF	3.06	67.5	6.80	10.3	41.4	48.3	108	41	67	SM	A-7-6
	40/60 DM-SSF	3.10	59.5	7.89	14.3	43.0	42.7	96	38	58	SM	A-7-6
	20/80 DM-SSF	3.28	32.9	5.94	15.5	62.7	21.7	74	37	37	SM	A-2-7
Steel slag fines (SSF)		3.45	6.95	4.36	35.6	61.1	3.4	NP	NP	NP	SW	A-3

Note: ASTM designations shown where relevant.
[a]Blend nomenclature shows DM content first, dry weight % basis.
[b]LL = liquid limit; PL = plastic limit; PI = plasticity index.

Table 5.3: Strength, hydraulic conductivity, and consolodation parameters of SSF, DM, and SSF-DM blends (Malasavage, 2012).

		CIŪ triaxial		Hydraulic conductivity	1D consolidation				
		D4767 (2004a)		D5084 (2003)	D2435 (2004b)				
Media tested[a]		c' [kPa (psf)]	ϕ' (°)	k (cm/s)	c_v @400 kPa (cm^2/s)	c_v @800 kPa (cm^2/s)	P_c [kPa (psf)]	C_c (—)	C_r (–)
Dredged material (DM)		41(856)	27.3	1.06×10^{-8}	0.24	0.25	144 (3,000)	0.28	0.04
Blends	80/20 DM-SSF	48(1,003)	32.4	1.54×10^{-8}	0.29	0.24	129 (2,700)	0.28	0.04
	60/40 DM-SSF	70(1,462)	39.9	1.48×10^{-7}	0.3	0.26	125 (2,600)	0.21	0.02
	50/50 DM-SSF	48(1,003)	45.0	2.88×10^{-7}	0.23	0.25	129 (2,700)	0.21	0.02
	40/60 DM-SSF	62(1,295)	43.4	1.85×10^{-7}	0.39	0.39	144 (3,000)	0.19	0.04
	20/80 DM-SSF	104(2,172)	38.6	1.23×10^{-5}	0.4	0.4	168 (3,500)	0.18	0.01
Steel slag fines (SSF)[b]		48(1,003)	45.7	6.12×10^{-3}	1.46	1.78	144 (3,000)	0.12	0.008

Note: ASTM designations shown where relevant; c' = effective cohesion; ϕ' = effective friction; c_v = coefficient of consolidation; P_c = preconsolidation pressure; C_c = compression index; C_r = recompression index.
[a]Blend nomenclature shows DM content first, dry weight % basis. All specimens compacted to 95% relative compaction of maximum dry unit density per ASTM D1557 (2000a).
[b]Hydraulic conductivity for 100% SSF media per ASTM D2434 (1968).

Table 5.4: Summary of Database from Hutcherson (2012).

Geogrid ID	Soil ID	ϕ	C	Embedded		Normal Stress (psi)	Pullout Resistance (lbs/ft)	CI	D_{50} (mm)
		(°)		Length (in)	Width (in)				
HDPE 1	Clayey Sand	33	1.15	70.0	18.0	2.0	2592	0.63	0.25
HDPE 1	Clayey Sand	33	1.15	70.0	18.0	2.0	2708	0.66	0.25
HDPE 1	Clayey Sand	33	1.15	70.0	18.0	4.0	3911	0.62	0.25
HDPE 1	Clayey Sand	33	1.15	70.0	18.0	4.0	4165	0.66	0.25
HDPE 1	Gravel 2	33	1.84	40.0	18.0	2.4	2147	0.66	5.5
HDPE 1	Gravel 2	33	1.84	70.0	18.0	2.0	2673	0.51	5.5
HDPE 1	Gravel 2	33	1.84	70.0	18.0	4.0	4453	0.60	5.5
HDPE 1	Sand 1	37	0.38	70.0	18.0	2.0	2798	0.88	0.85
HDPE 1	Sand 1	37	0.38	70.0	18.0	2.0	2668	0.84	0.85
HDPE 1	Sand 1	37	0.38	70.0	18.0	2.0	2216	0.70	0.85
HDPE 1	Sand 1	37	0.38	70.0	18.0	4.0	4755	0.83	0.85
HDPE 1	Sand 1	37	0.38	70.0	18.0	4.0	4495	0.79	0.85
HDPE 1	Sand 1	37	0.38	70.0	18.0	4.0	3995	0.70	0.85
HDPE 1	Sand 7	43	0.63	38.0	18.0	2.4	1600	0.61	0.75
HDPE 1	Silty Sand	34	1.11	70.0	18.0	2.0	1914	0.46	0.25
HDPE 1	Silty Sand	34	1.11	70.0	18.0	2.0	1591	0.38	0.25
HDPE 1	Silty Sand	34	1.11	70.0	18.0	4.0	3197	0.50	0.25
HDPE 1	Silty Sand	34	1.11	70.0	18.0	4.0	2400	0.38	0.25
HDPE 1	Unknown 3	39	1.67	70.0	18.0	2.5	2427	0.39	0

Table 5.5: Summary of Database from Hutcherson (2012) continued.

Geogrid ID	Soil ID	ϕ (°)	C	Embedded		Normal Stress (psi)	Pullout Resistance (lbs/ft)	CI	D_{50} (mm)
				Length (in)	Width (in)				
HDPE 4	Clayey Sand	33	1.15	70.0	18.0	2.0	2621	0.64	0.25
HDPE 4	Clayey Sand	33	1.15	70.0	18.0	2.0	2693	0.66	0.25
HDPE 4	Clayey Sand	33	1.15	70.0	18.0	8.0	6813	0.64	0.25
HDPE 4	Clayey Sand	33	1.15	70.0	18.0	8.0	6697	0.63	0.25
HDPE 4	Gravel 2	33	1.84	40.0	18.0	7.4	8066	1.26	5.5
HDPE 4	Gravel 2	33	1.84	70.0	18.0	2.0	2733	0.52	5.5
HDPE 4	Gravel 2	33	1.84	70.0	18.0	4.0	4954	0.66	5.5
HDPE 4	Gravel 2	33	1.84	70.0	18.0	8.0	8679	0.73	5.5
HDPE 4	Gravel 2	33	1.84	70.0	18.0	8.0	8314	0.70	5.5
HDPE 4	Sand 1	37	0.38	70.0	18.0	2.0	2614	0.82	0.85
HDPE 4	Sand 1	37	0.38	70.0	18.0	4.0	4303	0.75	0.85
HDPE 4	Sand 1	37	0.38	70.0	18.0	8.0	8379	0.78	0.85
HDPE 4	Sand 1	37	0.38	70.0	18.0	8.0	7523	0.70	0.85
HDPE 4	Sand 2	34	0.00	49.0	18.0	15.0	9533	0.80	0
HDPE 4	Sand 7	43	0.63	38.0	18.0	7.4	5027	0.73	0.75
HDPE 4	Silty Sand	34	1.11	70.0	18.0	2.0	2013	0.49	0.25
HDPE 4	Silty Sand	34	1.11	70.0	18.0	4.0	2527	0.39	0.25
HDPE 4	Silty Sand	34	1.11	70.0	18.0	8.0	5200	0.48	0.25

Appendix B:Pullout Test Results

Appendix B is a collection of the Pullout test results on the Monterey Sand and all the CG-DM blends in the order corresponding to the test Serial No. that is presented in Table 4.3. Each page contains a report on the test of the blend at a given normal pressure with a specified geogrid. The report broadly includes information pertaining to pullout box, geogrid details, material details and normal stress. Geogrid details include the identity of the geogrid being tested and sample dimensions used for the test. The material properties section includes information on the name, water content, relative compaction, and strength properties of the material being tested.

Results presented are the maximum pullout resistance, displacements of the LVDT's and comments salient to the test. A plot of the pullout force against displacement at various locations of the LVDT's on the geogrid is shown for each test at the bottom.

Geogrid Details	Manufacture	Product	Ultimate Tensile Strength
	Tensar	UX1700	12000 lb/ft
Specimen Information(ft)	Width	Embedment Length (Le)	
	1	2.97	

Material Properties	
Material Name	50/50 CG
Friction Angle (φ')	38
Moisture Content (%)	20.17
Y'd,max (pcf)	75.2
Target Compaction	100%
Weight of each Lift	181
No. of Lifts	4

Test Details	
Normal Stress σ' (psi)	Rate of Pullout (in/min)
6	0.04

Maximum Displacements	
LVDT	Disp (mm)
A	128.961
B	66.097
C	135.015

RESULTS

Maximum Load (lb)	2325.96	
Pullout Resisatnce (lb/ft)	2325.96	
Coefficient of Interaction, ci	$\frac{Pr}{2(Le)\,(c + \sigma' \tan(\varphi'))}$	0.580

Average EPC reading (psi)	3.532

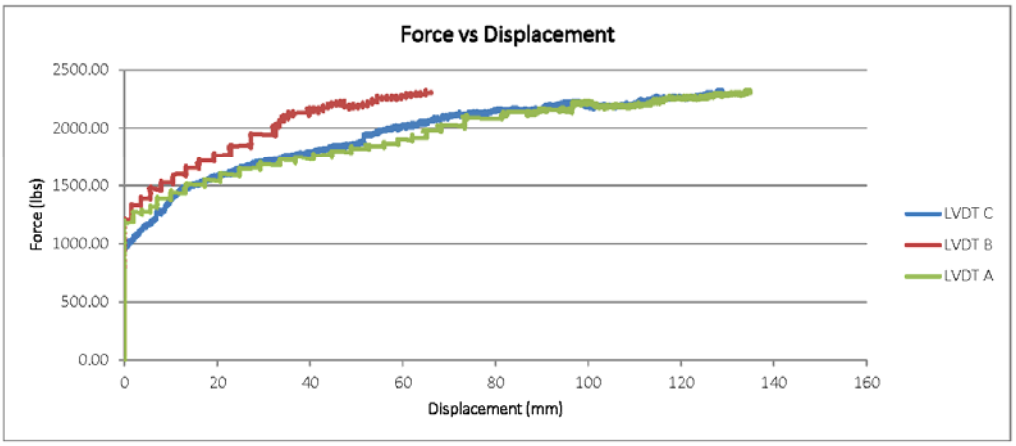

Comments:
Test Duration: 4:30pm-8:50pm
LDVTs in the back moved in steps
Pistons close to maxing out

Large Pullout Test

Test details :		
	Test Name	UX1700-50/50 CG/DM-8psi
	Date	8/19/2012
	Member	Alan

Box Dimensions (inch)	Length	Width	Depth	Area (in2)	Height from base to sleeve
	60	24	11	1440	5

Geogrid Details	Manufacture	Product	Ultimate Tensile Strength
	Tensar	UX1700	12000 lb/ft

Specimen Information(ft)	Width	Embedment Length (Le)
	1	2.871

Material Properties	
Material Name	50/50 CG
Friction Angle (φ')	38
Moisture Content (%)	20.17
Y'd,max (pcf)	75.2
Target Compaction	100%
Weight of each Lift	181
No. of Lifts	4

Test Details	
Normal Stress σ' (psi)	Rate of Pullout (in/min)
8	0.04

Maximum Displacements	
LVDT	Disp (mm)
A	64.974
B	78.839
C	83.617

RESULTS

Maximum Load (lb)	2547.87	
Pullout Resisatnce (lb/ft)	2547.87	
Coefficient of Interaction, ci	$\frac{Pr}{2(Le)(c + \sigma' \tan(\varphi'))}$	0.493

Average EPC reading (psi)	15.793

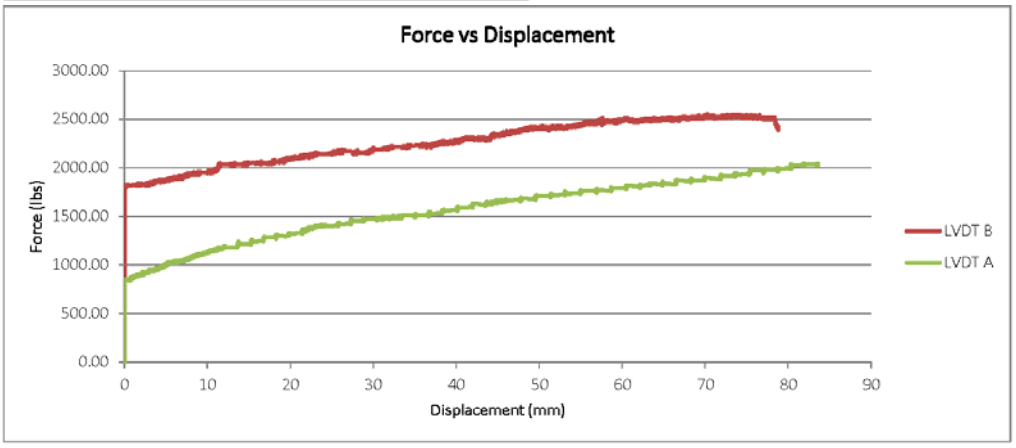

Comments:
Test Duration: 9:00am-1:00pm
LVDT C not working
Pistons Maxed Out

Large Pullout Test

Test details :		
	Test Name	UX1700-Mont Sand)-4psi
	Date	7/17/2012
	Member	-

Box Dimensions (inch)	Length	Width	Depth	Area (in2)	Height from base to sleeve
	60	24	11	1440	5

Geogrid Details	Manufacture	Product	Ultimate Tensile Strength
	Tensar	UX1700	12000 lb/ft

Specimen Information(ft)	Width	Embedment Length (Le)
	1	2.871

Material Properties	
Material Name	Mont sand
Friction Angle (φ')	35
Moisture Content (%)	1.5%
Yd,max (pcf)	99.3
Target Compaction	100%
Weight of each Lift	201
No. of Lifts	4

Test Details	
Normal Stress σ' (psi)	Rate of Pullout (in/min)
4	0.04

Maximum Displacements	
LVDT	Disp (mm)
A	33.008
B	14.240
C	50.066

RESULTS

Maximum Load (lb)	2046.51	
Pullout Resisatnce (lb/ft)	2046.51	
Coefficient of Interaction, ci	$\frac{Pr}{2(Le)(c + \sigma' \tan(\varphi'))}$	0.884

Average EPC reading (psi)	2.599

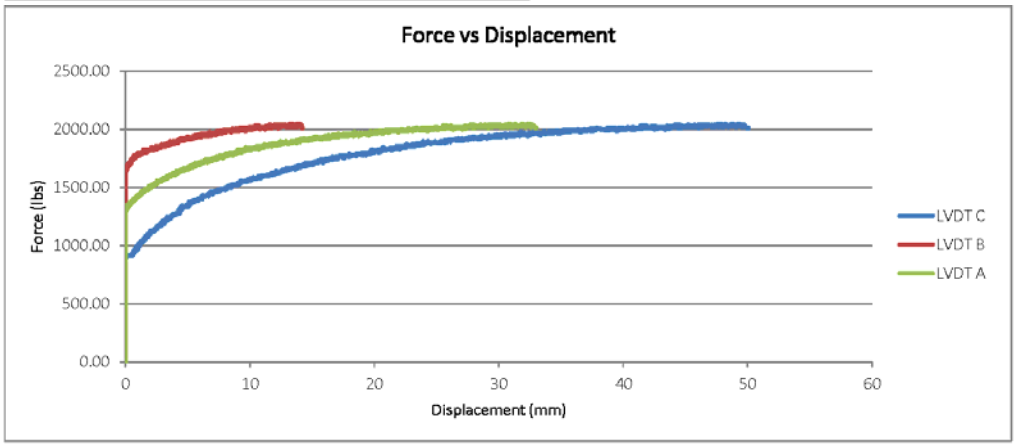

Comments:

Large Pullout Test

Test details :		
	Test Name	UX1700-Mont Sand)-4psi
	Date	7/17/2012
	Member	-

Box Dimensions (inch)	Length	Width	Depth	Area (in2)	Height from base to sleeve
	60	24	11	1440	5

Geogrid Details	Manufacture	Product	Ultimate Tensile Strength
	Tensar	UX1700	12000 lb/ft

Specimen Information(ft)	Width	Embedment Length (Le)
	1	3

Material Properties	
Material Name	Mont sand
Friction Angle (φ')	35
Moisture Content (%)	1.5%
Yd,max (pcf)	99.3
Target Compaction	100%
Weight of each Lift	201
No. of Lifts	4

Test Details	
Normal Stress σ' (psi)	Rate of Pullout (in/min)
6	0.04

Maximum Displacements	
LVDT	Disp (mm)
A	105.928
B	91.595
C	174.001

RESULTS

Maximum Load (lb)	2523.21	
Pullout Resisatnce (lb/ft)	2523.21	
Coefficient of Interaction, ci	$\frac{Pr}{2(Le)\,(c + \sigma' \tan(\varphi'))}$	0.695

Average EPC reading (psi)	3.784

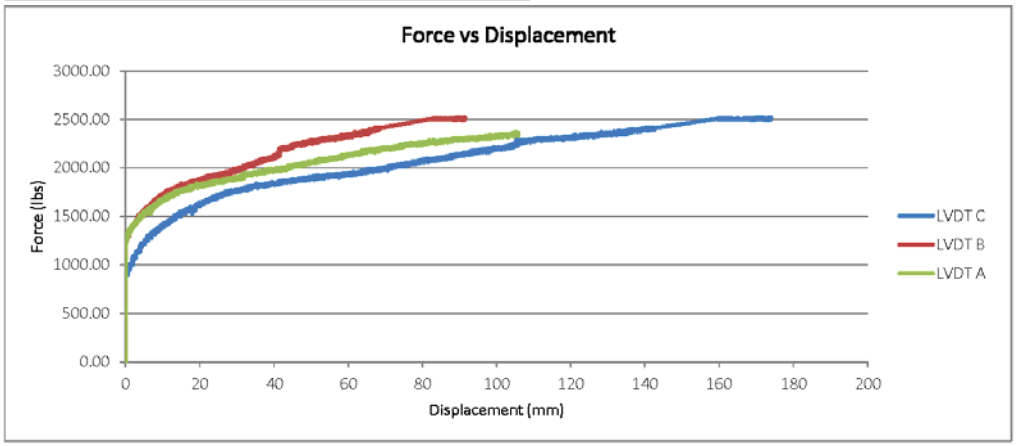

Comments:

Large Pullout Test

Test details :		
	Test Name	UX1400-Mont Sand)-8psi
	Date	7/18/2012
	Member	-

Box Dimensions (inch)	Length	Width	Depth	Area (in2)	Height from base to sleeve
	60	24	11	1440	5

Geogrid Details	Manufacture	Product	Ultimate Tensile Strength
	Tensar	UX1400	4800 lb/ft

Specimen Information(ft)	Width	Embedment Length (Le)
	1	3

Material Properties	
Material Name	Mont sand
Friction Angle (φ')	35
Moisture Content (%)	1.5%
Yd,max (pcf)	99.3
Target Compaction	100%
Weight of each Lift	201
No. of Lifts	4

Test Details	
Normal Stress σ' (psi)	Rate of Pullout (in/min)
8	0.04

Maximum Displacements	
LVDT	Disp (mm)
A	136.590
B	62.306
C	154.035

RESULTS

Maximum Load (lb)	2572.52	
Pullout Resisatnce (lb/ft)	2572.52	
Coefficient of Interaction, ci	$\frac{Pr}{2(Le)(c + \sigma' \tan(\varphi'))}$	0.532

Average EPC reading (psi)	10.484

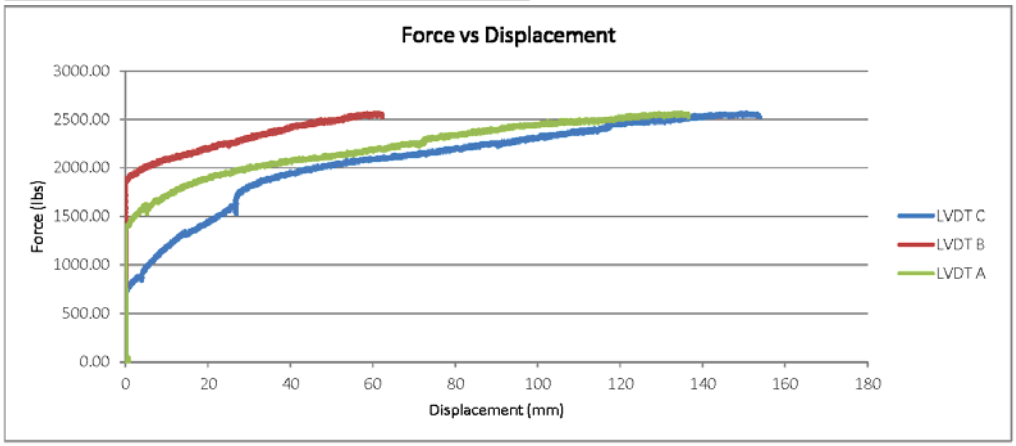

Comments:

Large Pullout Test

Test details :		
	Test Name	UX1400-Mont Sand-4psi
	Date	7/19/2012
	Member	-

Box Dimensions (inch)	Length	Width	Depth	Area (in2)	Height from base to sleeve
	60	24	11	1440	5

Geogrid Details	Manufacture	Product	Ultimate Tensile Strength
	Tensar	UX1400	4800 lb/ft

Specimen Information(ft)	Width	Embedment Length (Le)
	1	3

Material Properties	
Material Name	Mont sand
Friction Angle (φ')	35
Moisture Content (%)	1.5%
Yd,max (pcf)	99.3
Target Compaction	100%
Weight of each Lift	201
No. of Lifts	4

Test Details	
Normal Stress σ' (psi)	Rate of Pullout (in/min)
4	0.04

Maximum Displacements	
LVDT	Disp (mm)
A	29.661
B	5.136
C	43.156

RESULTS

Maximum Load (lb)	1019.15	
Pullout Resisatnce (lb/ft)	1019.15	
Coefficient of Interaction, ci	$\frac{Pr}{2(Le)(c + \sigma' \tan(\varphi'))}$	0.421

Average EPC reading (psi)	1.105

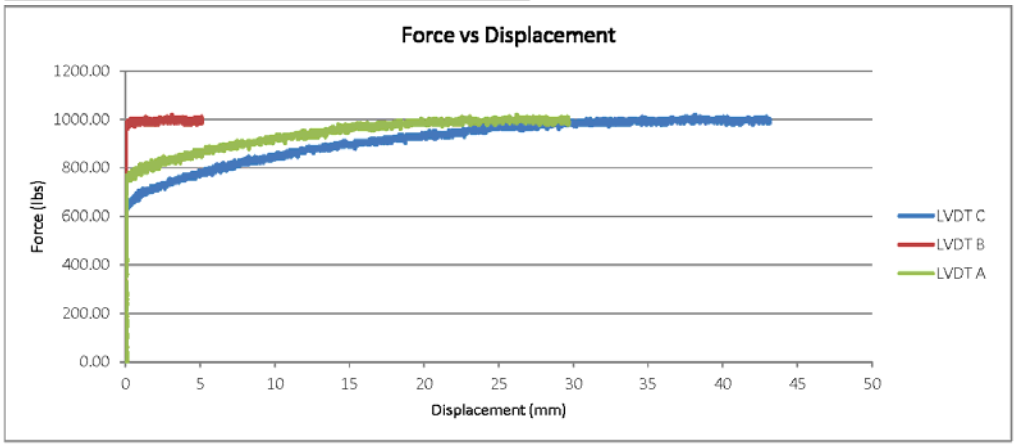

Comments:

Large Pullout Test

Test details :		
	Test Name	UX1400-Mont Sand-6psi
	Date	7/19/2012
	Member	-

Box Dimensions (inch)	Length	Width	Depth	Area (in2)	Height from base to sleeve
	60	24	11	1440	5

Geogrid Details	Manufacture	Product	Ultimate Tensile Strength
	Tensar	UX1400	4800 lb/ft

Specimen Information(ft)	Width	Embedment Length (Le)
	1	3

Material Properties	
Material Name	Mont sand
Friction Angle (φ')	35
Moisture Content (%)	1.5%
Yd,max (pcf)	99.3
Target Compaction	100%
Weight of each Lift	201
No. of Lifts	4

Test Details	
Normal Stress σ' (psi)	Rate of Pullout (in/min)
6	0.04

Maximum Displacements	
LVDT	Disp (mm)
A	148.804
B	64.991
C	177.752

RESULTS

Maximum Load (lb)	1356.12	
Pullout Resisatnce (lb/ft)	1356.12	
Coefficient of Interaction, ci	$\frac{Pr}{2(Le)(c + \sigma' \tan(\varphi'))}$	0.374

Average EPC reading (psi)	-0.453

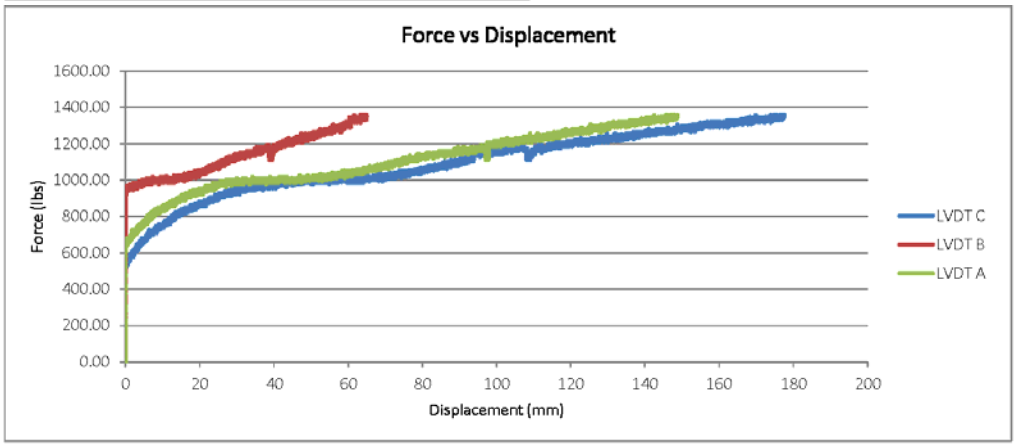

Comments:

Large Pullout Test

Test details :		
	Test Name	UX1700-Mont Sand-8psi
	Date	7/20/2012
	Member	-

Box Dimensions (inch)	Length	Width	Depth	Area (in2)	Height from base to sleeve
	60	24	11	1440	5

Geogrid Details	Manufacture	Product	Ultimate Tensile Strength
	Tensar	UX1700	12000 lb/ft

Specimen Information(ft)	Width	Embedment Length (Le)
	1	3

Material Properties	
Material Name	Mont sand
Friction Angle (φ')	35
Moisture Content (%)	1.5%
Yd,max (pcf)	99.3
Target Compaction	100%
Weight of each Lift	201
No. of Lifts	4

Test Details	
Normal Stress σ' (psi)	Rate of Pullout (in/min)
8	0.04

Maximum Displacements	
LVDT	Disp (mm)
A	69.451
B	40.148
C	105.095

RESULTS

Maximum Load (lb)	4060.15	
Pullout Resisatnce (lb/ft)	4060.15	
Coefficient of Interaction, ci	$\frac{Pr}{2(Le)\,(c + \sigma' \tan(\varphi'))}$	0.839

Average EPC reading (psi)	2.585

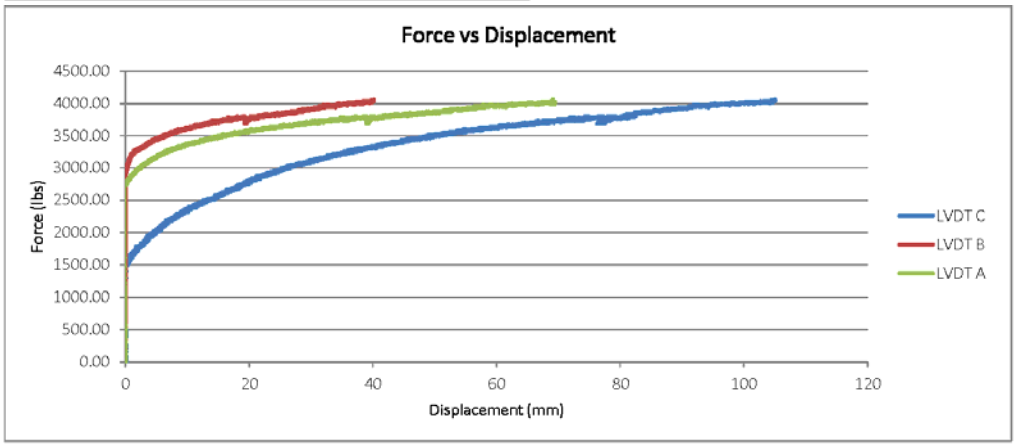

Comments:

Large Pullout Test

Test Name	BX1100-MonterySand-3psi
Date	2/27/2012

Box Dimensions		
L	60 in.	1.5 m
B	24 in.	0.6 m
H	11 in.	0.275 m

Area of Box	1440 in2
	900000 cm2

Height from bottom of box to bottom of sleeve	5 in.	0.125 m

Geogrid Specimen Details				
Product	**UX1700MSE**			
Manufacturer	Tensar			
Ultimate Tensile Strength	11990 lb/ft			
Width	1	ft	0.3	m
Embedment Length Le	1.9	ft	0.58	m

Material Properties	
Material Name	**Monterey Sand**
Friction Angle (φ')	35
Moisture Content (%)	1.5
$\gamma_{d,max}$ (pcf)	99.3
Target Compaction	100%
Weight of each Lift	133.6 lbs
No. of Lifts	6

Test Details	
Normal Stress σ' (psi)	**3**
Rate of Pullout	1 mm/min
	0.04 in/min

Results

Max. Displacements	
LVDT	Disp (mm)
A	25.305
B	57.100
C	4.670

Coefficient of Interaction ci	$\frac{P}{2(Le) \times \tan(\varphi') \times \sigma'}$

Maximum Load	1010.93 lb
Pullout Resistance P	1010.93 lb/ft

ci	**0.879**

Average EPC reading (psi)	3.725

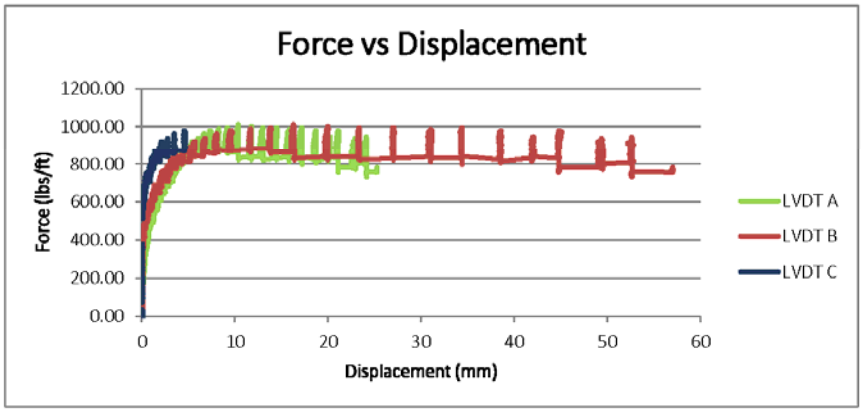

Large Pullout Test

Test Name	BX1100-Mont. Sand - 2.8psi
Date	3/4/2012

Box Dimensions		
L	60 in.	1.5 m
B	24 in.	0.6 m
H	11 in.	0.275 m

Area of Box	
	1440 in2
	900000 cm2

Height from bottom of box to bottom of sleeve	5 in.	0.125 m

Geogrid Specimen Details	
Product	**UX1700MSE**
Manufacturer	Tensar
Ultimate Tensile Strength	12000lb/ft

Width	1	ft	0.45	m
Embedment Length Le	1.97	ft	0.6	m

Material Properties	
Material Name	**Monterey Sand**
Friction Angle (φ')	35
Moisture Content (%)	1.5
$\gamma_{d,max}$ (pcf)	99.3
Target Compaction	100%
Weight of each Lift	133.6 lbs
No. of Lifts	6

Test Details	
Normal Stress σ' (psi)	**2.8**
Rate of Pullout	1 mm/min
	0.04 in/min

Results

Max. Displacements	
LVDT	Disp (mm)
A	18.207
B	30.322
C	50.368

Coefficient of Interaction ci	$\frac{P}{2(Le) \times \tan(\varphi') \times \sigma'}$

Maximum Load	953.40 lb
Pullout Resistance P	953.40 lb/ft

ci	**0.857**

Average EPC reading (psi)	63.275

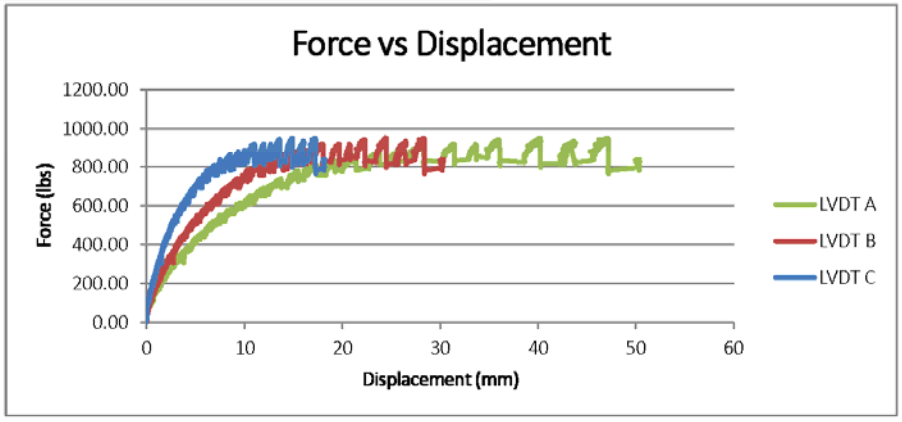

Large Pullout Test

Test details :		
	Test Name	UX1400-100%DM (phil)-4psi
	Date	7/4/2012
	Member	Kemp

Box Dimensions (inch)	Length	Width	Depth	Area (in2)	Height from base to sleeve
	60	24	11	1440	5

Geogrid Details	Manufacture	Product	Ultimate Tensile Strength
	Tensar	UX1400	12000 lb/ft

Specimen Information(ft)	Width	Embedment Length (Le)
	1	2.871

Material Properties	
Material Name	100%DM (Phil)
Friction Angle (φ')	33
Moisture Content (%)	50%
Yd,max (pcf)	75
Target Compaction	0.8
Weight of each Lift	180
No. of Lifts	4

Test Details	
Normal Stress σ' (psi)	Rate of Pullout (in/min)
4	0.04

Maximum Displacements	
LVDT	Disp (mm)
A	45.942
B	18.887
C	1.909

RESULTS

Maximum Load (lb)	460.26	
Pullout Resisatnce (lb/ft)	460.26	
Coefficient of Interaction, ci	$\frac{Pr}{2(Le)(c + \sigma' \tan(\varphi'))}$	0.214

Average EPC reading (psi)	117.481

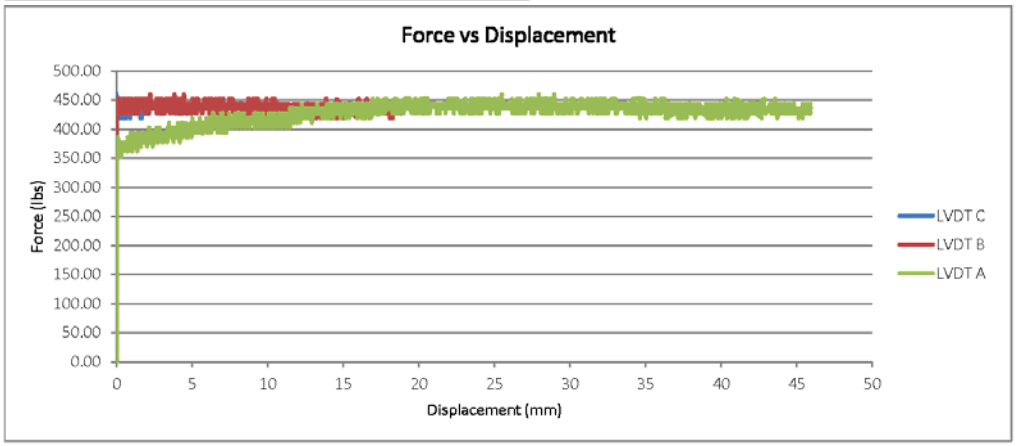

Comments:

Large Pullout Test

Test details :		
	Test Name	UX1400-100%DM (phil)-6psi
	Date	7/5/2012
	Member	Kemp

Box Dimensions (inch)	Length	Width	Depth	Area (in2)	Height from base to sleeve
	60	24	11	1440	5

Geogrid Details	Manufacture	Product	Ultimate Tensile Strength
	Tensar	UX1400	12000 lb/ft

Specimen Information(ft)	Width	Embedment Length (Le)
	1	2.838

Material Properties	
Material Name	100%DM (Phil)
Friction Angle (φ')	33
Moisture Content (%)	50%
Yd,max (pcf)	75
Target Compaction	0.8
Weight of each Lift	180
No. of Lifts	4

Test Details	
Normal Stress σ' (psi)	Rate of Pullout (in/min)
6	0.04

Maximum Displacements	
LVDT	Disp (mm)
A	27.050
B	9.509
C	19.364

RESULTS

Maximum Load (lb)	517.79	
Pullout Resisatnce (lb/ft)	517.79	
Coefficient of Interaction, ci	$\frac{Pr}{2(Le)(c + \sigma' \tan(\varphi'))}$	0.163

Average EPC reading (psi)	111.883

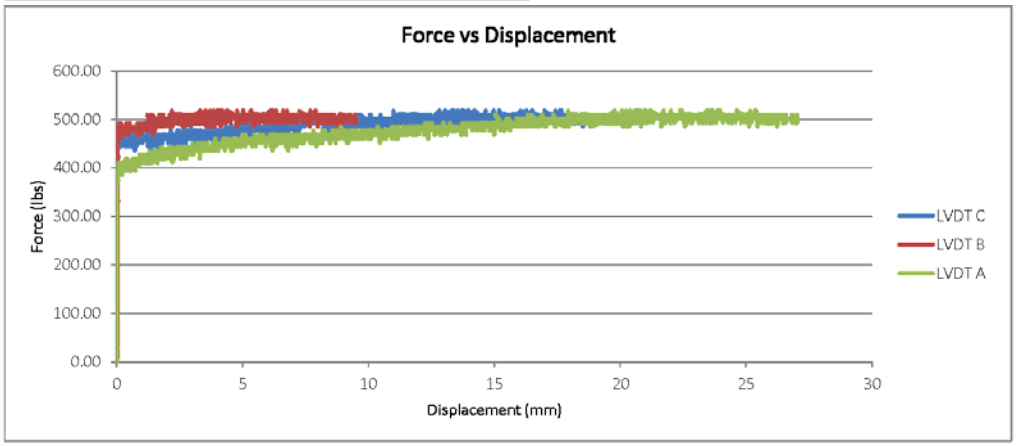

Comments:

Large Pullout Test

Test details :		
	Test Name	UX1400-100%DM (phil)-8psi
	Date	7/6/2012
	Member	Kemp

Box Dimensions (inch)	Length	Width	Depth	Area (in2)	Height from base to sleeve
	60	24	11	1440	5

Geogrid Details	Manufacture	Product	Ultimate Tensile Strength
	Tensar	UX1400	12000 lb/ft

Specimen Information(ft)	Width	Embedment Length (Le)
	1	2.871

Material Properties	
Material Name	100%DM (Phil)
Friction Angle (φ')	33
Moisture Content (%)	50%
Yd,max (pcf)	75
Target Compaction	0.8
Weight of each Lift	180
No. of Lifts	4

Test Details	
Normal Stress σ' (psi)	Rate of Pullout (in/min)
8	0.04

Maximum Displacements	
LVDT	Disp (mm)
A	35.538
B	8.959
C	8.342

RESULTS

Maximum Load (lb)	698.61	
Pullout Resisatnce (lb/ft)	698.61	
Coefficient of Interaction, ci	$\frac{Pr}{2(Le)(c + \sigma' \tan(\varphi'))}$	0.163

Average EPC reading (psi)	51.625

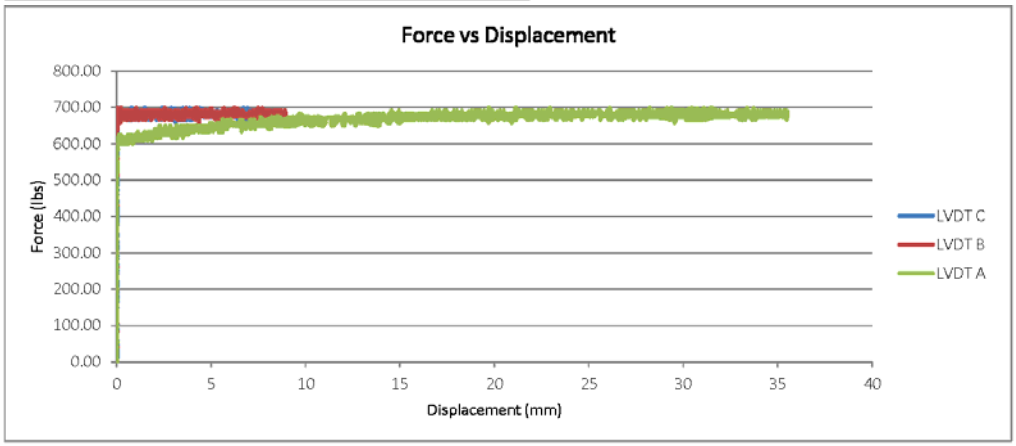

Comments:

Large Pullout Test

Test details :		
	Test Name	UX1700-100%DM (phil)-4psi
	Date	7/6/2012
	Member	Kemp

Box Dimensions (inch)	Length	Width	Depth	Area (in2)	Height from base to sleeve
	60	24	11	1440	5

Geogrid Details	Manufacture	Product	Ultimate Tensile Strength
	Tensar	UX1700	12000 lb/ft

Specimen Information(ft)	Width	Embedment Length (Le)
	1	2.838

Material Properties	
Material Name	100%DM (Phil)
Friction Angle (φ')	33
Moisture Content (%)	50%
Yd,max (pcf)	75
Target Compaction	0.8
Weight of each Lift	180
No. of Lifts	4

Test Details	
Normal Stress σ' (psi)	Rate of Pullout (in/min)
4	0.04

Maximum Displacements	
LVDT	Disp (mm)
A	36.583
B	24.213
C	1.858

RESULTS

Maximum Load (lb)	591.76	
Pullout Resisatnce (lb/ft)	591.76	
Coefficient of Interaction, ci	$\frac{Pr}{2(Le)(c + \sigma' \tan(\varphi'))}$	0.279

Average EPC reading (psi)	69.919

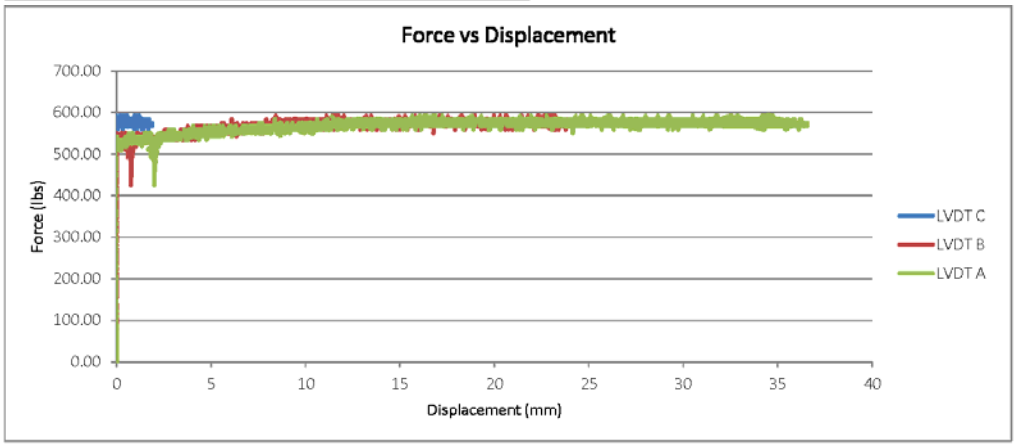

Comments:

Large Pullout Test

Test details :		
	Test Name	UX1700-100%DM (phil)-6psi
	Date	7/7/2012
	Member	Kemp

Box Dimensions (inch)	Length	Width	Depth	Area (in2)	Height from base to sleeve
	60	24	11	1440	5

Geogrid Details	Manufacture	Product	Ultimate Tensile Strength
	Tensar	UX1700	12000 lb/ft

Specimen Information(ft)	Width	Embedment Length (Le)
	1	2.871

Material Properties	
Material Name	100%DM (Phil)
Friction Angle (φ')	33
Moisture Content (%)	50%
Yd,max (pcf)	75
Target Compaction	0.8
Weight of each Lift	180
No. of Lifts	4

Test Details	
Normal Stress σ' (psi)	Rate of Pullout (in/min)
6	0.04

Maximum Displacements	
LVDT	Disp (mm)
A	22.769
B	30.906
C	42.194

RESULTS

Maximum Load (lb)	780.80	
Pullout Resisatnce (lb/ft)	780.80	
Coefficient of Interaction, ci	$\frac{Pr}{2(Le)(c + \sigma' \tan(\varphi'))}$	0.242

Average EPC reading (psi)	42.860

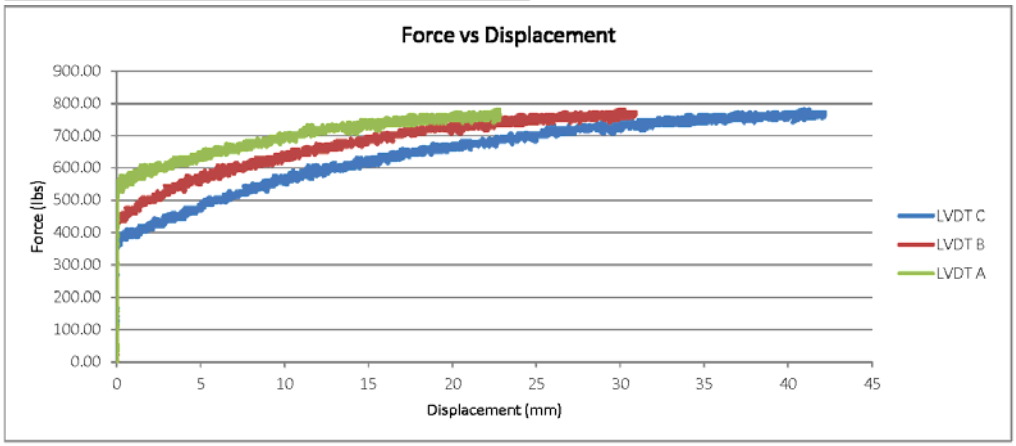

Comments:

Large Pullout Test

Test details :		
	Test Name	UX1700-100%DM (phil)-8psi
	Date	7/9/2012
	Member	Kemp

Box Dimensions (inch)	Length	Width	Depth	Area (in2)	Height from base to sleeve
	60	24	11	1440	5

Geogrid Details	Manufacture	Product	Ultimate Tensile Strength
	Tensar	UX1700	12000 lb/ft

Specimen Information(ft)	Width	Embedment Length (Le)
	1	2.838

Material Properties	
Material Name	100%DM (Phil)
Friction Angle (φ')	33
Moisture Content (%)	50%
Yd,max (pcf)	75
Target Compaction	0.8
Weight of each Lift	180
No. of Lifts	4

Test Details	
Normal Stress σ' (psi)	Rate of Pullout (in/min)
8	0.04

Maximum Displacements	
LVDT	Disp (mm)
A	47.842
B	3.401
C	43.696

RESULTS

Maximum Load (lb)	912.30	
Pullout Resisatnce (lb/ft)	912.30	
Coefficient of Interaction, ci	$\frac{Pr}{2(Le)(c + \sigma' \tan(\varphi'))}$	0.215

Average EPC reading (psi)	59.679

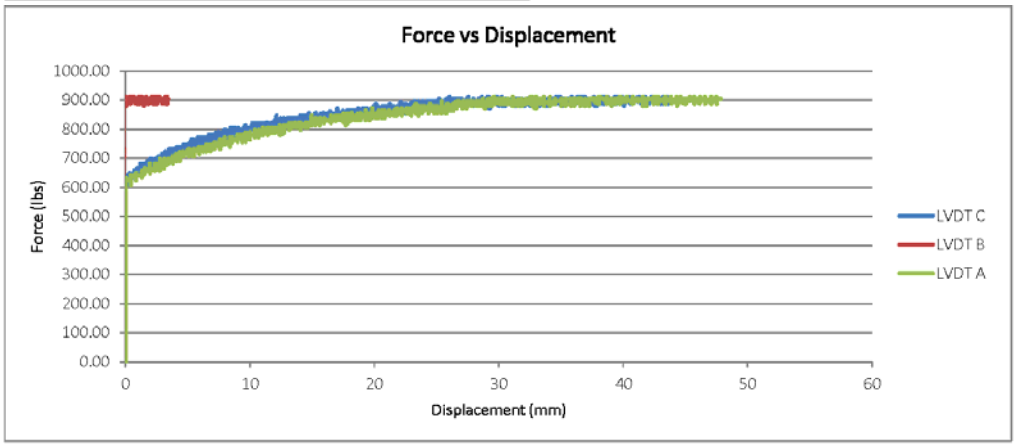

Comments:

Large Pullout Test

Test details :		
	Test Name	UX1400-20/80 CG/DM-4psi
	Date	7/11/2012
	Member	Kemp

Box Dimensions (inch)	Length	Width	Depth	Area (in2)	Height from base to sleeve
	60	24	11	1440	5

Geogrid Details	Manufacture	Product	Ultimate Tensile Strength
	Tensar	UX1400	12000 lb/ft

Specimen Information(ft)	Width	Embedment Length (Le)
	1	2.871

Material Properties	
Material Name	20/80 CG/DM
Friction Angle (φ')	35
Moisture Content (%)	33
Yd,max (pcf)	75
Target Compaction	80%
Weight of each Lift	201
No. of Lifts	4

Test Details	
Normal Stress σ' (psi)	Rate of Pullout (in/min)
4	0.04

Maximum Displacements	
LVDT	Disp (mm)
A	9.275
B	11.484
C	51.072

RESULTS

Maximum Load (lb)	624.64	
Pullout Resisatnce (lb/ft)	624.64	
Coefficient of Interaction, ci	$\frac{Pr}{2(Le)(c + \sigma' \tan(\varphi'))}$	0.270

Average EPC reading (psi)	-3.157

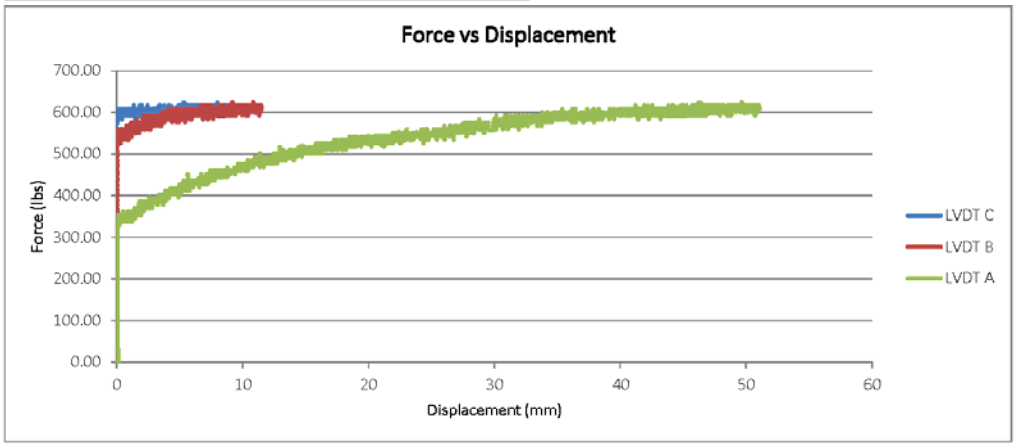

Comments:
Test Duration: 10:30am-11:50am
No EPC.

Large Pullout Test

Test details :		
	Test Name	UX1400-20/80 CG/DM-6psi
	Date	7/12/2012
	Member	Kemp

Box Dimensions (inch)	Length	Width	Depth	Area (in2)	Height from base to sleeve
	60	24	11	1440	5

Geogrid Details	Manufacture	Product	Ultimate Tensile Strength
	Tensar	UX1400	4800 lb/ft

Specimen Information(ft)	Width	Embedment Length (Le)
	1	2.838

Material Properties	
Material Name	20/80 CG/DM
Friction Angle (φ')	35
Moisture Content (%)	33
Yd,max (pcf)	75
Target Compaction	80%
Weight of each Lift	201
No. of Lifts	4

Test Details	
Normal Stress σ' (psi)	Rate of Pullout (in/min)
6	0.04

Maximum Displacements	
LVDT	Disp (mm)
A	11.873
B	9.094
C	57.237

RESULTS

Maximum Load (lb)	764.36	
Pullout Resisatnce (lb/ft)	764.36	
Coefficient of Interaction, ci	$\frac{Pr}{2(Le)(c + \sigma' \tan(\varphi'))}$	0.223

Average EPC reading (psi)	-3.253

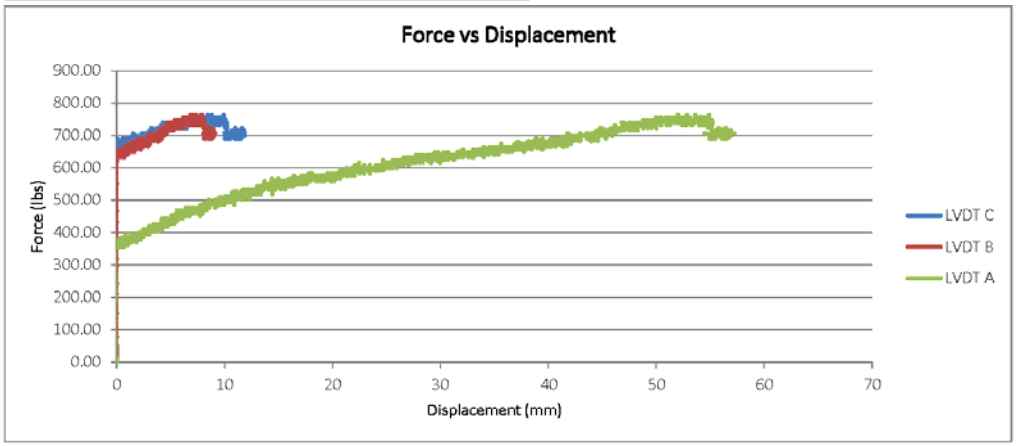

Comments:
Test Duration: 8:40am-10:15am
No EPC.

Large Pullout Test

Test details :		
	Test Name	UX1400-20/80 CG/DM-8psi
	Date	7/12/2012
	Member	Kemp

Box Dimensions (inch)	Length	Width	Depth	Area (in2)	Height from base to sleeve
	60	24	11	1440	5

Geogrid Details	Manufacture	Product	Ultimate Tensile Strength
	Tensar	UX1400	4800 lb/ft

Specimen Information(ft)	Width	Embedment Length (Le)
	1	2.871

Material Properties	
Material Name	20/80 CG/DM
Friction Angle (φ')	35
Moisture Content (%)	33
Yd,max (pcf)	75
Target Compaction	80%
Weight of each Lift	201
No. of Lifts	4

Test Details	
Normal Stress σ' (psi)	Rate of Pullout (in/min)
8	0.04

Maximum Displacements	
LVDT	Disp (mm)
A	58.413
B	26.861
C	291.409

RESULTS

Maximum Load (lb)	1068.46	
Pullout Resisatnce (lb/ft)	1068.46	
Coefficient of Interaction, ci	$\frac{Pr}{2(Le)(c + \sigma' \tan(\varphi'))}$	0.231

Average EPC reading (psi)	14.721

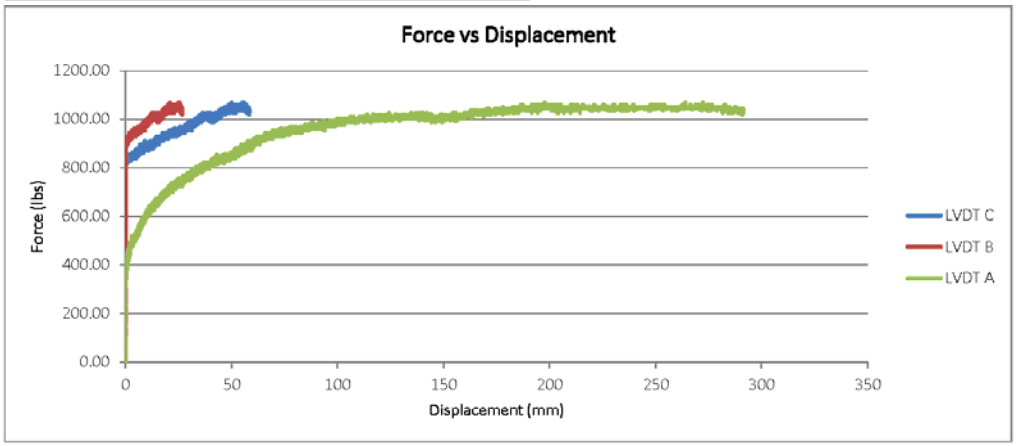

Comments:
Test Duration: 11:45-2:30
EPC reading about 15 psi

Large Pullout Test

Test details :		
	Test Name	UX1700-20/80 CG/DM-4psi
	Date	7/13/2012
	Member	Kemp

Box Dimensions (inch)	Length	Width	Depth	Area (in2)	Height from base to sleeve
	60	24	11	1440	5

Geogrid Details	Manufacture	Product	Ultimate Tensile Strength
	Tensar	UX1700	12000 lb/ft

Specimen Information(ft)	Width	Embedment Length (Le)
	1	2.871

Material Properties	
Material Name	20/80 CG/DM
Friction Angle (φ')	35
Moisture Content (%)	33
Yd,max (pcf)	75
Target Compaction	80%
Weight of each Lift	201
No. of Lifts	4

Test Details	
Normal Stress σ' (psi)	Rate of Pullout (in/min)
4	0.04

Maximum Displacements	
LVDT	Disp (mm)
A	19.962
B	2.666
C	63.223

RESULTS

Maximum Load (lb)	1282.15	
Pullout Resisatnce (lb/ft)	1282.15	
Coefficient of Interaction, ci	$\frac{Pr}{2(Le)(c + \sigma' \tan(\varphi'))}$	0.554

Average EPC reading (psi)	0.990

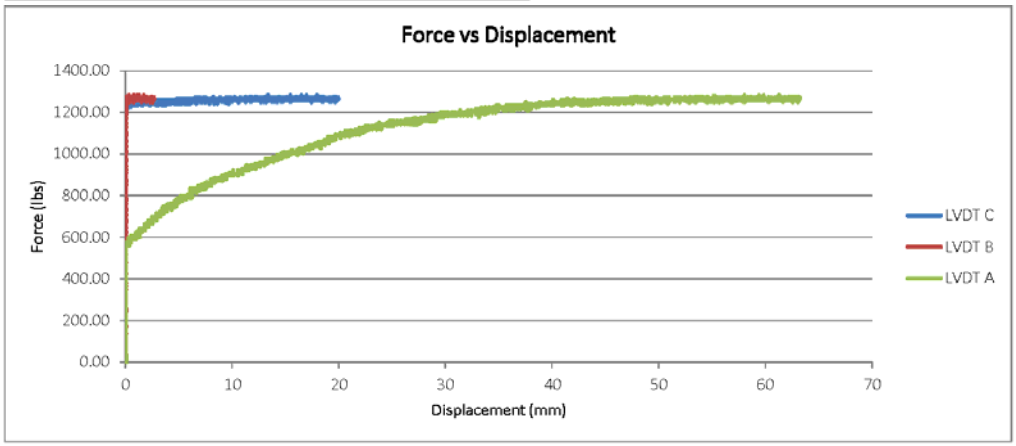

Comments:
Test Duration: 8:30am-10:05am
EPC varied from -1 psi tp +4 psi

Large Pullout Test

Test details :		
	Test Name	UX1700-20/80 CG/DM-6psi
	Date	7/13/2012
	Member	Sangy

Box Dimensions (inch)	Length	Width	Depth	Area (in2)	Height from base to sleeve
	60	24	11	1440	5

Geogrid Details	Manufacture	Product	Ultimate Tensile Strength
	Tensar	UX1700	12000 lb/ft

Specimen Information(ft)	Width	Embedment Length (Le)
	1	2.904

Material Properties	
Material Name	20/80 CG/DM
Friction Angle (φ')	35
Moisture Content (%)	33
Yd,max (pcf)	75
Target Compaction	80%
Weight of each Lift	201
No. of Lifts	4

Test Details	
Normal Stress σ' (psi)	Rate of Pullout (in/min)
6	0.04

Maximum Displacements	
LVDT	Disp (mm)
A	30.330
B	22.092
C	50.264

RESULTS

Maximum Load (lb)	1495.85	
Pullout Resisatnce (lb/ft)	1495.85	
Coefficient of Interaction, ci	$\frac{Pr}{2(Le)(c + \sigma' \tan(\varphi'))}$	0.426

Average EPC reading (psi)	-4.280

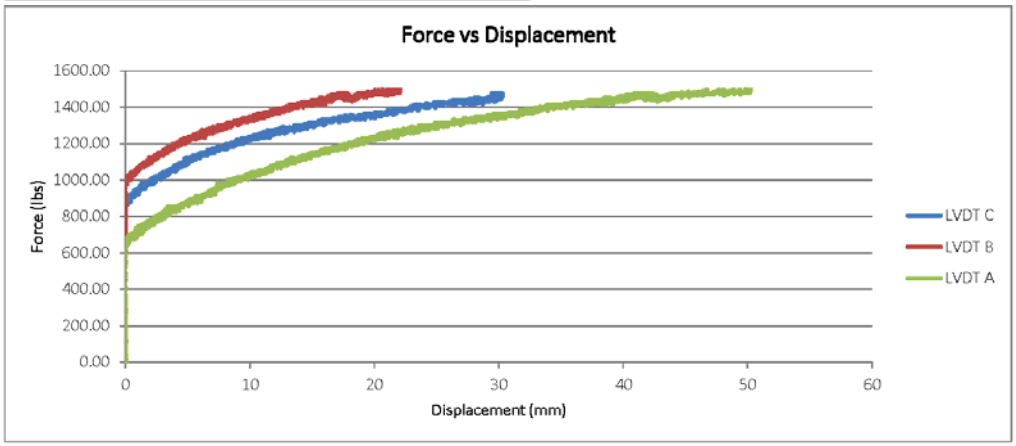

Comments:
Test Duration: 3:30pm-5:00pm

Large Pullout Test

Test details :		
	Test Name	UX1700-20/80 CG/DM-8psi
	Date	7/14/2012
	Member	Sangy

Box Dimensions (inch)	Length	Width	Depth	Area (in2)	Height from base to sleeve
	60	24	11	1440	5

Geogrid Details	Manufacture	Product	Ultimate Tensile Strength
	Tensar	UX1700	12000 lb/ft

Specimen Information(ft)	Width	Embedment Length (Le)
	1	2.838

Material Properties	
Material Name	20/80 CG/DM
Friction Angle (φ')	35
Moisture Content (%)	33
Yd,max (pcf)	75
Target Compaction	80%
Weight of each Lift	201
No. of Lifts	4

Test Details	
Normal Stress σ' (psi)	Rate of Pullout (in/min)
8	0.04

Maximum Displacements	
LVDT	Disp (mm)
A	191.683
B	24.429
C	77.536

RESULTS

Maximum Load (lb)	1693.10	
Pullout Resisatnce (lb/ft)	1693.10	
Coefficient of Interaction, ci	$\frac{Pr}{2(Le)(c + \sigma' \tan(\varphi'))}$	0.370

Average EPC reading (psi)	5.333

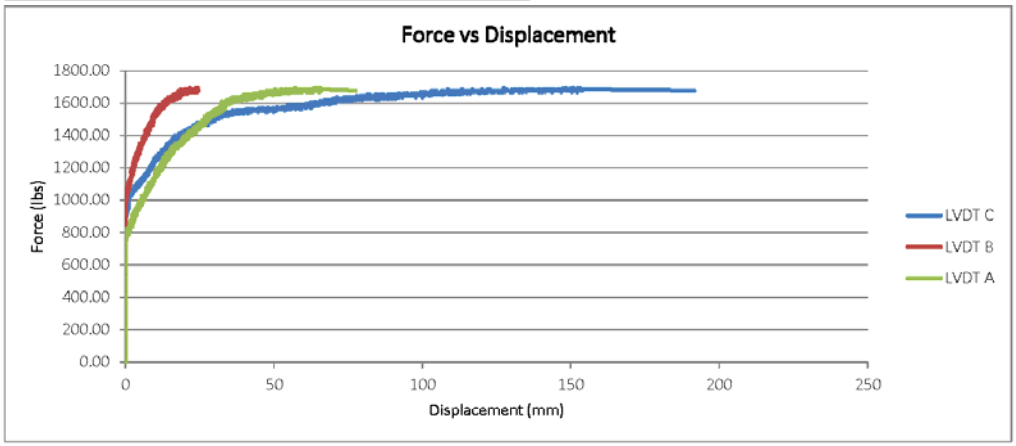

Comments:
Test Duration: 4:00pm-5:45pm

Large Pullout Test

Test details :		
	Test Name	UX1400-80/20 CG/DM-4psi
	Date	7/23/2012
	Member	Kemp

Box Dimensions (inch)	Length	Width	Depth	Area (in2)	Height from base to sleeve
	60	24	11	1440	5

Geogrid Details	Manufacture	Product	Ultimate Tensile Strength
	Tensar	UX1400	12000 lb/ft

Specimen Information(ft)	Width	Embedment Length (Le)
	1	2.97

Material Properties	
Material Name	80/20 CG
Friction Angle (φ')	39
Moisture Content (%)	14
Yd,max (pcf)	88
Target Compaction	100%
Weight of each Lift	199.5
No. of Lifts	4

Test Details	
Normal Stress σ' (psi)	Rate of Pullout (in/min)
4	0.04

Maximum Displacements	
LVDT	Disp (mm)
A	67.350
B	81.990
C	97.577

RESULTS

Maximum Load (lb)	1150.65	
Pullout Resisatnce (lb/ft)	1150.65	
Coefficient of Interaction, ci	$\frac{Pr}{2(Le)(c + \sigma' \tan(\varphi'))}$	0.415

Average EPC reading (psi)	0.913

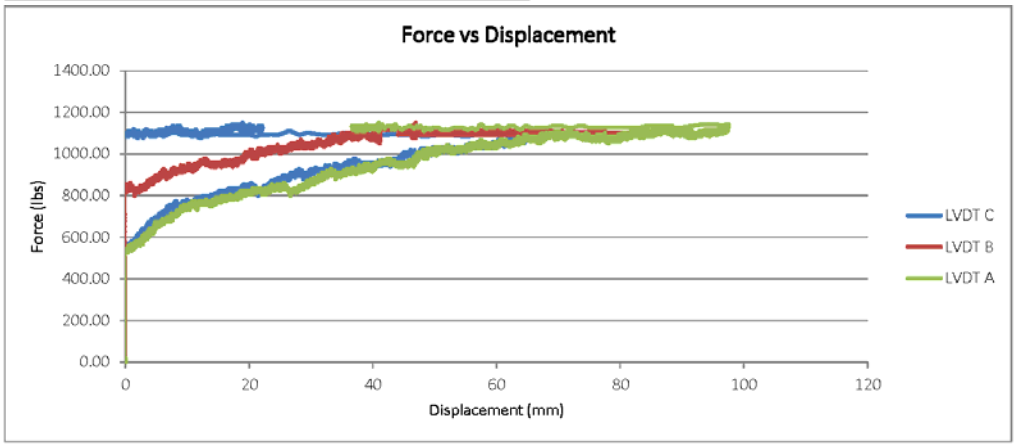

Comments:
Test Duration: 1:15pm-4:00pm
LVDT B engaged latest

Large Pullout Test

Test details :		
	Test Name	UX1400-80/20 CG/DM-6psi
	Date	7/24/2012
	Member	Sangy + Kemp

Box Dimensions (inch)	Length	Width	Depth	Area (in2)	Height from base to sleeve
	60	24	11	1440	5

Geogrid Details	Manufacture	Product	Ultimate Tensile Strength
	Tensar	UX1400	12000 lb/ft

Specimen Information(ft)	Width	Embedment Length (Le)
	1	2.97

Material Properties	
Material Name	80/20 CG
Friction Angle (φ')	39
Moisture Content (%)	14
Yd,max (pcf)	88
Target Compaction	100%
Weight of each Lift	199.5
No. of Lifts	4

Test Details	
Normal Stress σ' (psi)	Rate of Pullout (in/min)
6	0.04

Maximum Displacements	
LVDT	Disp (mm)
A	47.044
B	0.000
C	80.808

RESULTS

Maximum Load (lb)	1487.63	
Pullout Resisatnce (lb/ft)	1487.63	
Coefficient of Interaction, ci	$\frac{Pr}{2(Le)(c + \sigma' \tan(\varphi'))}$	0.358

Average EPC reading (psi)	0.986

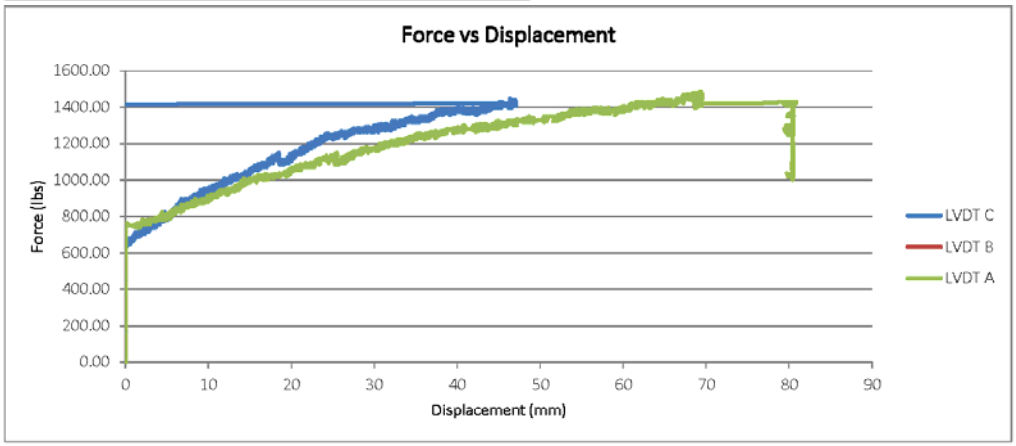

Comments:
Test Duration: 1:45pm-4pm
No 3rd LVDT
Clamp bar rotated and load cell lost contact; pullout may have occurred.

Large Pullout Test

Test details :		
	Test Name	UX1400-80/20 CG/DM-8psi
	Date	7/25/2012
	Member	Kemp

Box Dimensions (inch)	Length	Width	Depth	Area (in2)	Height from base to sleeve
	60	24	11	1440	5

Geogrid Details	Manufacture	Product	Ultimate Tensile Strength
	Tensar	UX1400	12000 lb/ft

Specimen Information(ft)	Width	Embedment Length (Le)
	1	2.97

Material Properties	
Material Name	80/20 CG
Friction Angle (φ')	39
Moisture Content (%)	14
Yd,max (pcf)	88
Target Compaction	100%
Weight of each Lift	199.5
No. of Lifts	4

Test Details	
Normal Stress σ' (psi)	Rate of Pullout (in/min)
8	0.04

Maximum Displacements	
LVDT	Disp (mm)
A	45.550
B	163.264
C	95.345

RESULTS

Maximum Load (lb)	1915.01	
Pullout Resisatnce (lb/ft)	1915.01	
Coefficient of Interaction, ci	$\frac{Pr}{2(Le)(c + \sigma' \tan(\varphi'))}$	0.346

Average EPC reading (psi)	1.590

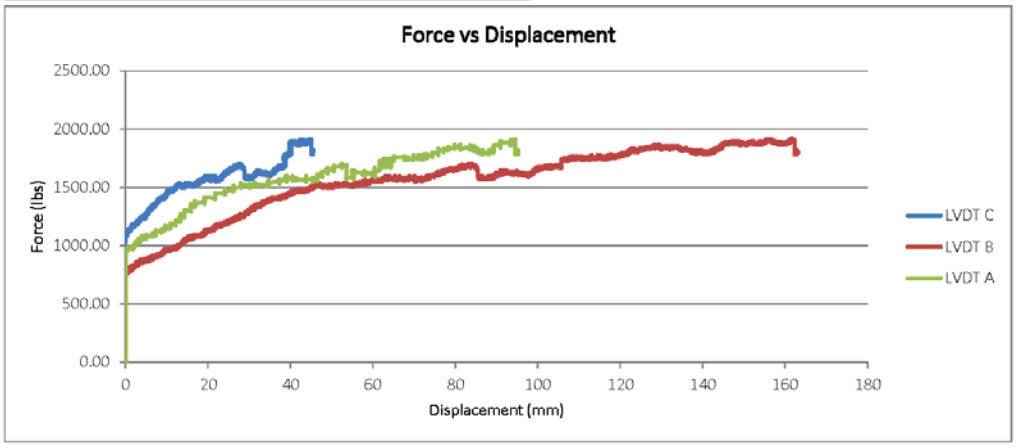

Comments:
Test Duration: 11:10am-2:30pm

Large Pullout Test

Test details :		
	Test Name	UX1700-80/20 CG/DM-4psi
	Date	7/26/2012
	Member	Kemp

Box Dimensions (inch)	Length	Width	Depth	Area (in2)	Height from base to sleeve
	60	24	11	1440	5

Geogrid Details	Manufacture	Product	Ultimate Tensile Strength
	Tensar	UX1700	12000 lb/ft

Specimen Information(ft)	Width	Embedment Length (Le)
	1	2.97

Material Properties	
Material Name	80/20 CG
Friction Angle (φ')	39
Moisture Content (%)	14
Yd,max (pcf)	88
Target Compaction	100%
Weight of each Lift	199.5
No. of Lifts	4

Test Details	
Normal Stress σ' (psi)	Rate of Pullout (in/min)
4	0.04

Maximum Displacements	
LVDT	Disp (mm)
A	328.956
B	192.553
C	329.625

RESULTS

Maximum Load (lb)	2539.65	
Pullout Resisatnce (lb/ft)	2539.65	
Coefficient of Interaction, ci	$\frac{Pr}{2(Le)(c + \sigma' \tan(\varphi'))}$	0.917

Average EPC reading (psi)	102.286

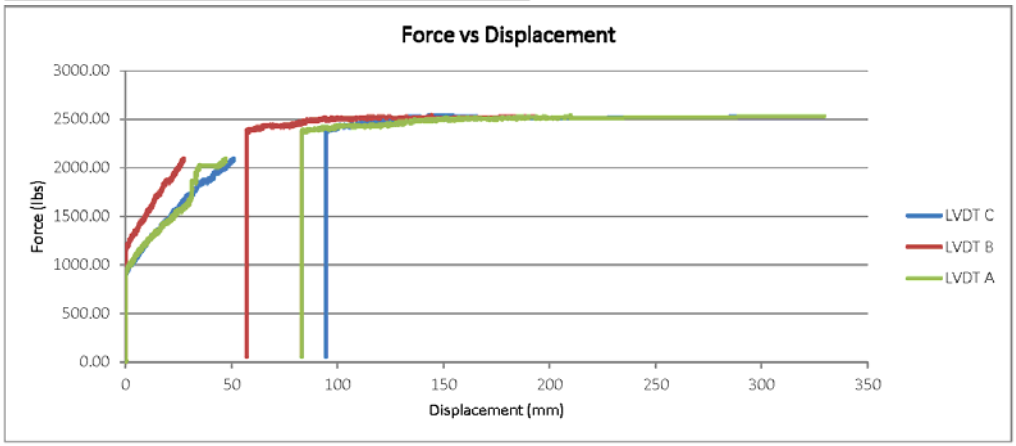

Comments:
Test Duration: 7:50pm-10:50pm
EPC not working
Didn't save for about 30 minutes; see next page for screenshot of test.

Large Pullout Test

Test details :		
	Test Name	UX1700-80/20 CG/DM-8psi
	Date	8/2/2012
	Member	Alan

Box Dimensions (inch)	Length	Width	Depth	Area (in2)	Height from base to sleeve
	60	24	11	1440	5

Geogrid Details	Manufacture	Product	Ultimate Tensile Strength
	Tensar	UX1700	12000 lb/ft

Specimen Information(ft)	Width	Embedment Length (Le)
	1	2.97

Material Properties	
Material Name	80/20 CG
Friction Angle (φ')	39
Moisture Content (%)	14
Yd,max (pcf)	88
Target Compaction	100%
Weight of each Lift	199.5
No. of Lifts	4

Test Details	
Normal Stress σ' (psi)	Rate of Pullout (in/min)
8	0.04

Maximum Displacements	
LVDT	Disp (mm)
A	134.123
B	79.226
C	124.860

RESULTS

Maximum Load (lb)	2975.25	
Pullout Resisatnce (lb/ft)	2975.25	
Coefficient of Interaction, ci	$\frac{Pr}{2(Le)(c + \sigma' \tan(\varphi'))}$	0.537

Average EPC reading (psi)	-1.470

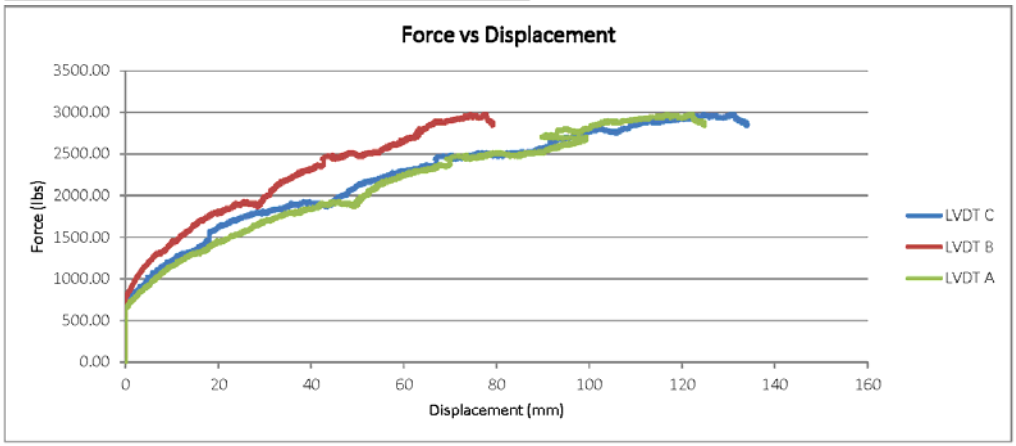

Comments:
Test Duration: 2:45pm-7:20pm
Pistons maxed
EPC not working

Large Pullout Test

Test details :		
	Test Name	UX1700-80/20 CG/DM-6psi
	Date	7/31/2012
	Member	Sangy + Fabrizio

Box Dimensions (inch)	Length	Width	Depth	Area (in2)	Height from base to sleeve
	60	24	11	1440	5

Geogrid Details	Manufacture	Product	Ultimate Tensile Strength
	Tensar	UX1700	12000 lb/ft

Specimen Information(ft)	Width	Embedment Length (Le)
	1	2.97

Material Properties	
Material Name	80/20 CG
Friction Angle (φ')	39
Moisture Content (%)	14
Yd,max (pcf)	88
Target Compaction	100%
Weight of each Lift	199.5
No. of Lifts	4

Test Details	
Normal Stress σ' (psi)	Rate of Pullout (in/min)
6	0.04

Maximum Displacements	
LVDT	Disp (mm)
A	583.210
B	79.240
C	125.024

RESULTS

Maximum Load (lb)	2999.91	
Pullout Resisatnce (lb/ft)	2999.91	
Coefficient of Interaction, ci	$\frac{Pr}{2(Le)(c + \sigma' \tan(\varphi'))}$	0.722

Average EPC reading (psi)	-1.474

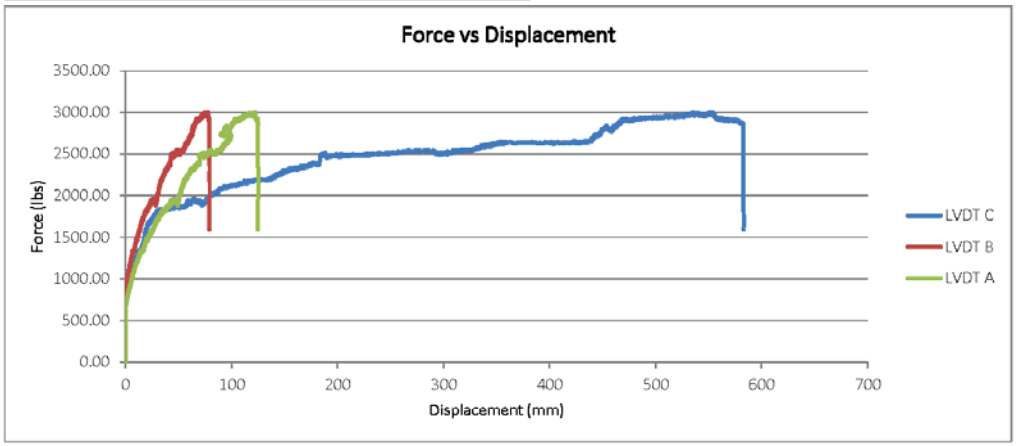

Comments:
Test Duration: 1:00pm-4:20pm
EPC not working.
Pistons Maxed

Large Pullout Test

Test details :		
	Test Name	UX1700-80/20 CG/DM-8psi
	Date	8/2/2012
	Member	Alan

Box Dimensions (inch)	Length	Width	Depth	Area (in2)	Height from base to sleeve
	60	24	11	1440	5

Geogrid Details	Manufacture	Product	Ultimate Tensile Strength
	Tensar	UX1700	12000 lb/ft

Specimen Information(ft)	Width	Embedment Length (Le)
	1	2.97

Material Properties	
Material Name	80/20 CG
Friction Angle (φ')	39
Moisture Content (%)	14
Yd,max (pcf)	88
Target Compaction	100%
Weight of each Lift	199.5
No. of Lifts	4

Test Details	
Normal Stress σ' (psi)	Rate of Pullout (in/min)
8	0.04

Maximum Displacements	
LVDT	Disp (mm)
A	603.281
B	224.063
C	674.160

RESULTS

Maximum Load (lb)	3419.07	
Pullout Resisatnce (lb/ft)	3419.07	
Coefficient of Interaction, ci	$\frac{Pr}{2(Le)(c + \sigma' \tan(\varphi'))}$	0.617

Average EPC reading (psi)	-0.335

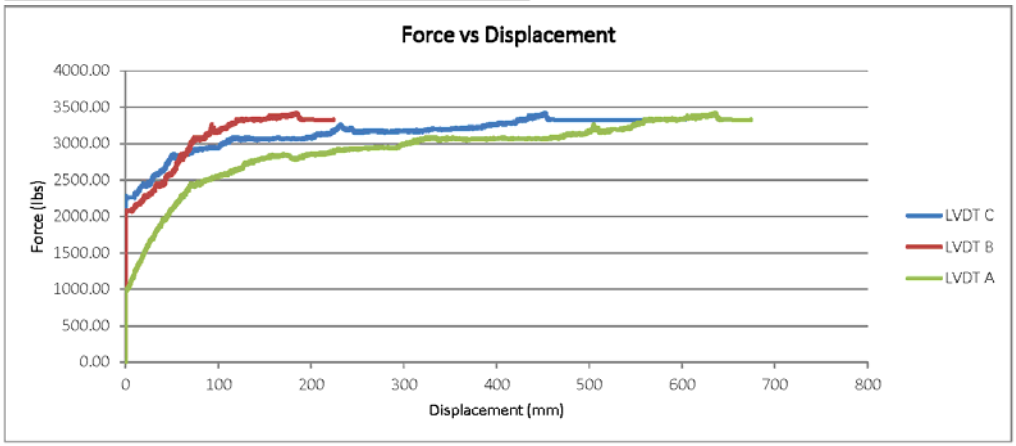

Comments:
Test Duration: 2:45pm-7:20pm
Pistons maxed
EPC not working

Large Pullout Test

Test details :		
	Test Name	UX1400-100%CG-4psi
	Date	8/4/2012
	Member	Kemp + Fabrizio

Box Dimensions (inch)	Length	Width	Depth	Area (in2)	Height from base to sleeve
	60	24	11	1440	5

Geogrid Details	Manufacture	Product	Ultimate Tensile Strength
	Tensar	UX1400	12000 lb/ft

Specimen Information(ft)	Width	Embedment Length (Le)
	1	3.102

Material Properties	
Material Name	CG
Friction Angle (φ')	37
Moisture Content (%)	0%
Yd,max (pcf)	109
Target Compaction	0.9
Weight of each Lift	211
No. of Lifts	4

Test Details	
Normal Stress σ' (psi)	Rate of Pullout (in/min)
4	0.04

Maximum Displacements	
LVDT	Disp (mm)
A	46.108
B	83.872
C	96.812

RESULTS

Maximum Load (lb)	1175.31	
Pullout Resisatnce (lb/ft)	1175.31	
Coefficient of Interaction, ci	$\frac{Pr}{2(Le)(c + \sigma' \tan(\varphi'))}$	0.436

Average EPC reading (psi)	-1.654

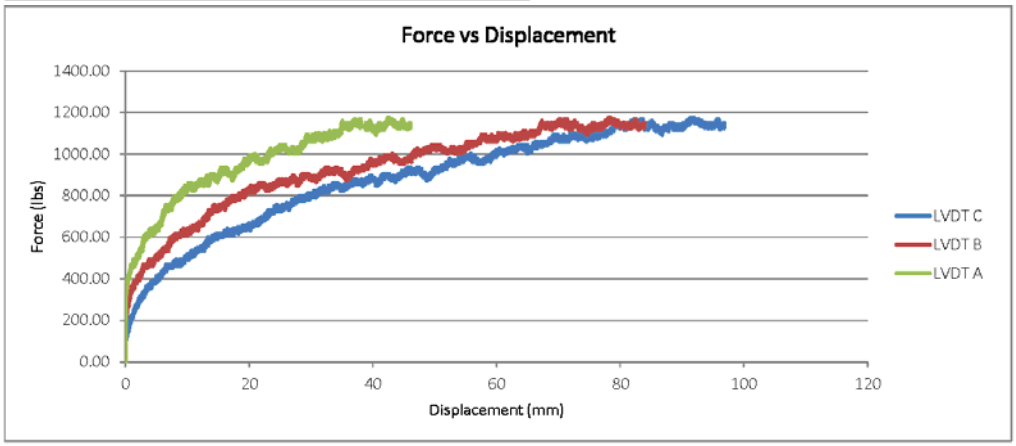

Comments:
Test Duration: 12:30pm-3:00pm
Water leaked from the bottom of the box
EPC was not working

Large Pullout Test

Test details :		
	Test Name	UX1400-100%CG-6psi
	Date	8/4/2012
	Member	Sangy + Fabrizio

Box Dimensions (inch)	Length	Width	Depth	Area (in2)	Height from base to sleeve
	60	24	11	1440	5

Geogrid Details	Manufacture	Product	Ultimate Tensile Strength
	Tensar	UX1400	12000 lb/ft

Specimen Information(ft)	Width	Embedment Length (Le)
	1	3.168

Material Properties	
Material Name	CG
Friction Angle (φ')	37
Moisture Content (%)	8%
Yd,max (pcf)	109
Target Compaction	0.9
Weight of each Lift	211
No. of Lifts	4

Test Details	
Normal Stress σ' (psi)	Rate of Pullout (in/min)
6	0.04

Maximum Displacements	
LVDT	Disp (mm)
A	56.753
B	201.383
C	174.508

RESULTS

Maximum Load (lb)	1808.16	
Pullout Resisatnce (lb/ft)	1808.16	
Coefficient of Interaction, ci	$\frac{Pr}{2(Le)(c + \sigma' \tan(\varphi'))}$	0.438

Average EPC reading (psi)	-0.004

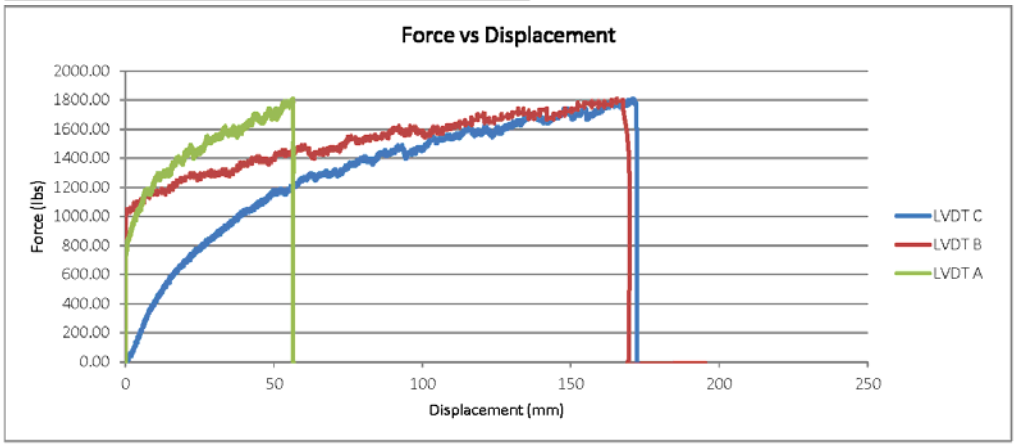

Comments:
Test Duration: 5:10pm-8:15pm
Middle LVDT moved first then front LVDT moved second and caught up/past it.
LVDT A was cut to prevent it hitting the back of the box.

Large Pullout Test

Test details :		
	Test Name	UX1700-100% CG - 4psi
	Date	8/5/2012
	Member	Kemp + Fabrizio

Box Dimensions (inch)	Length	Width	Depth	Area (in2)	Height from base to sleeve
	60	24	11	1440	5

Geogrid Details	Manufacture	Product	Ultimate Tensile Strength
	Tensar	UX1700	12000 lb/ft

Specimen Information(ft)	Width	Embedment Length (Le)
	1	2.97

Material Properties	
Material Name	100% CG
Friction Angle (φ')	37
Moisture Content (%)	8
Yd,max (pcf)	109
Target Compaction	90%
Weight of each Lift	211
No. of Lifts	4

Test Details	
Normal Stress σ' (psi)	Rate of Pullout (in/min)
4	0.04

Maximum Displacements	
LVDT	Disp (mm)
A	236.896
B	611.471
C	923.986

RESULTS

Maximum Load (lb)	3599.89	
Pullout Resisatnce (lb/ft)	3599.89	
Coefficient of Interaction, ci	$\frac{Pr}{2(Le)(c + \sigma' \tan(\varphi'))}$	1.396

Average EPC reading (psi)	-1.699

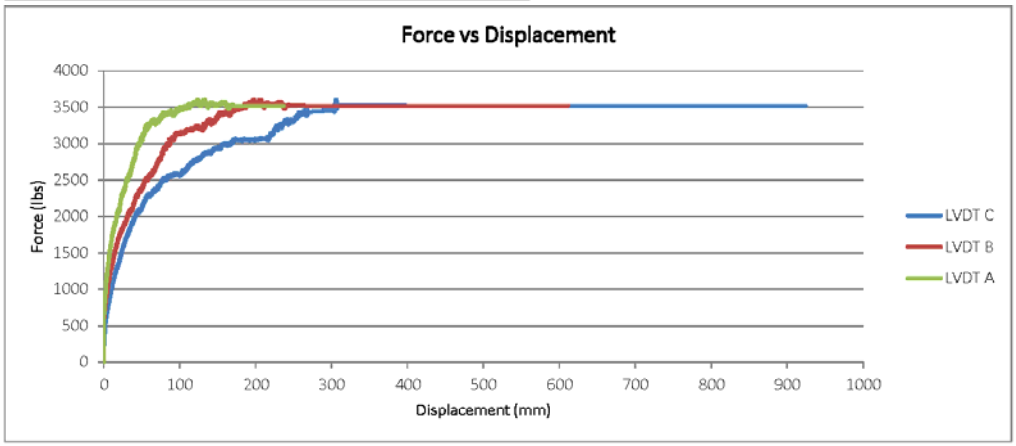

Comments:
Test Duration: 9am-1:20p: 4.3 hours
EPC not working
LVDT C was cut so it wouldn't hit the back end of the box.

Large Pullout Test

Test details :		
	Test Name	UX1700-100% CG - 6psi
	Date	8/5/2012
	Member	Sangy + Fabrizio

Box Dimensions (inch)	Length	Width	Depth	Area (in2)	Height from base to sleeve
	60	24	11	1440	5

Geogrid Details	Manufacture	Product	Ultimate Tensile Strength
	Tensar	UX1700	12000 lb/ft

Specimen Information(ft)	Width	Embedment Length (Le)
	1	3.465

Material Properties	
Material Name	100% CG
Friction Angle (φ')	37
Moisture Content (%)	8
Y'd,max (pcf)	109
Target Compaction	90%
Weight of each Lift	211
No. of Lifts	4

Test Details	
Normal Stress σ' (psi)	Rate of Pullout (in/min)
6	0.04

Maximum Displacements	
LVDT	Disp (mm)
A	57.717
B	179.891
C	308.586

RESULTS

Maximum Load (lb)	3977.96	
Pullout Resisatnce (lb/ft)	3977.96	
Coefficient of Interaction, ci	$\frac{Pr}{2(Le)(c + \sigma' \tan(\varphi'))}$	0.882

Average EPC reading (psi)	2.965

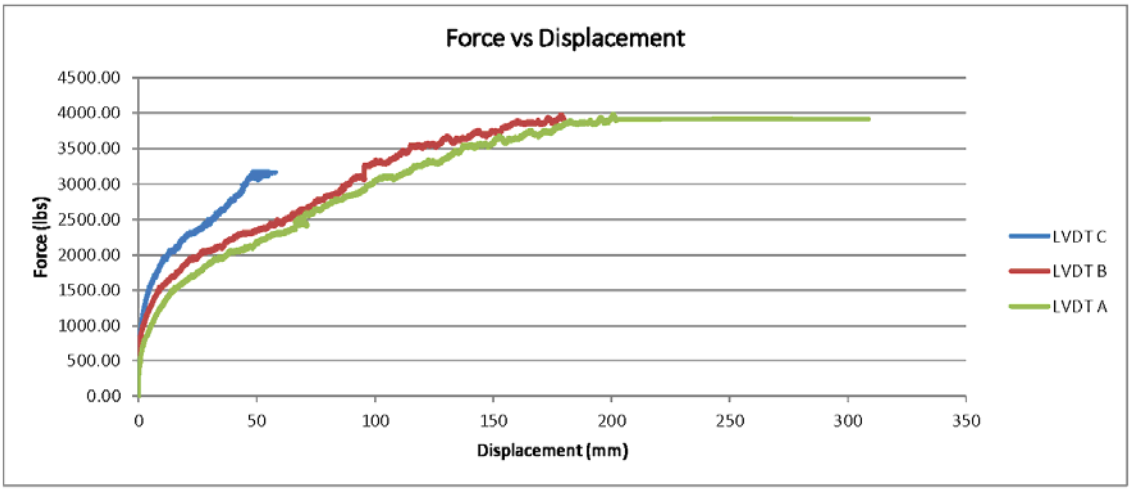

Comments: Pistons maxed out.
Test Duration: 3-8 PM, 5 hours
EPC not working properly
LVDT C ceased functioning at around 60 mm

Large Pullout Test

Test details :		
	Test Name	UX1400-50/50 CG/DM-4psi
	Date	8/9/2012
	Member	Fabrizio

Box Dimensions (inch)	Length	Width	Depth	Area (in2)	Height from base to sleeve
	60	24	11	1440	5

Geogrid Details	Manufacture	Product	Ultimate Tensile Strength
	Tensar	UX1400	4800 lb/ft

Specimen Information(ft)	Width	Embedment Length (Le)
	1	3.135

Material Properties	
Material Name	50/50 CG
Friction Angle (φ')	38
Moisture Content (%)	20.17
Yd,max (pcf)	75.2
Target Compaction	100%
Weight of each Lift	181
No. of Lifts	4

Test Details	
Normal Stress σ' (psi)	Rate of Pullout (in/min)
4	0.04

Maximum Displacements	
LVDT	Disp (mm)
A	57.788
B	100.373
C	63.417

RESULTS

Maximum Load (lb)	616.42	
Pullout Resisatnce (lb/ft)	616.42	
Coefficient of Interaction, ci	$\frac{Pr}{2(Le)(c + \sigma' \tan(\varphi'))}$	0.218

Average EPC reading (psi)	0.683

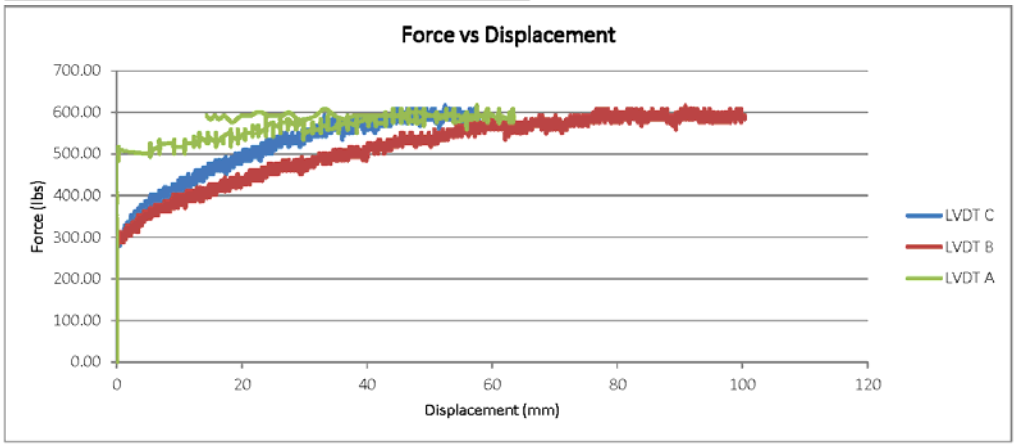

Comments:
Test Duration: 11:40am-1:53pm
EPC not working
Not plateau observed

Large Pullout Test

Test details :		
	Test Name	UX1400-50/50 CG/DM-6psi
	Date	8/10/2012
	Member	Sangy

Box Dimensions (inch)	Length	Width	Depth	Area (in2)	Height from base to sleeve
	60	24	11	1440	5

Geogrid Details	Manufacture	Product	Ultimate Tensile Strength
	Tensar	UX1400	4800 lb/ft

Specimen Information(ft)	Width	Embedment Length (Le)
	1	3.102

Material Properties	
Material Name	50/50 CG
Friction Angle (φ')	38
Moisture Content (%)	20.17
Yd,max (pcf)	75.2
Target Compaction	100%
Weight of each Lift	181
No. of Lifts	4

Test Details	
Normal Stress σ' (psi)	Rate of Pullout (in/min)
6	0.04

Maximum Displacements	
LVDT	Disp (mm)
A	38.164
B	66.376
C	51.103

RESULTS

Maximum Load (lb)	1273.93	
Pullout Resisatnce (lb/ft)	1273.93	
Coefficient of Interaction, ci	$\frac{Pr}{2(Le)(c + \sigma' \tan(\varphi'))}$	0.304

Average EPC reading (psi)	5.096

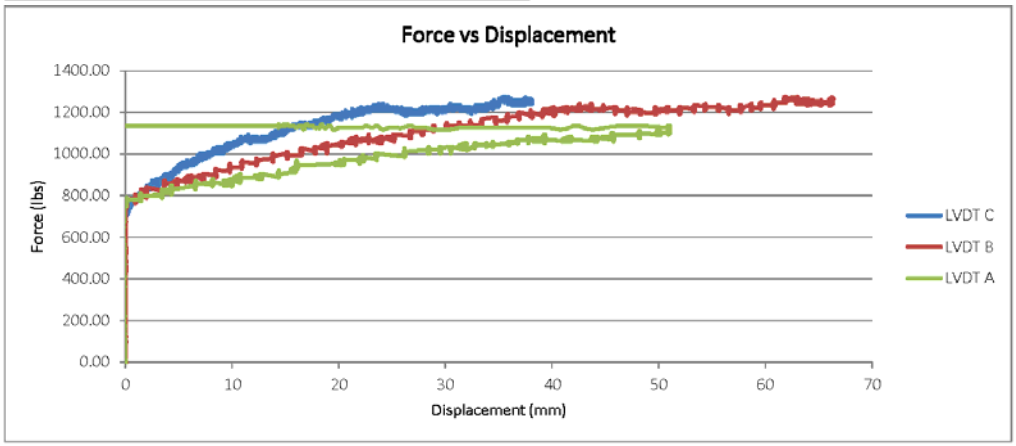

Comments:
Test Duration: 3:45pm-6:00pm

Large Pullout Test

Test details :		
	Test Name	UX1400-50/50 CG/DM-8psi
	Date	10/12/2012
	Member	Fabrizio

Box Dimensions (inch)	Length	Width	Depth	Area (in2)	Height from base to sleeve
	60	24	11	1440	5

Geogrid Details	Manufacture	Product	Ultimate Tensile Strength
	Tensar	UX1400	4800 lb/ft

Specimen Information(ft)	Width	Embedment Length (Le)
	1	2.871

Material Properties	
Material Name	50/50 CG
Friction Angle (φ')	38
Moisture Content (%)	20.17
Yd,max (pcf)	75.2
Target Compaction	100%
Weight of each Lift	181
No. of Lifts	4

Test Details	
Normal Stress σ' (psi)	Rate of Pullout (in/min)
8	0.04

Maximum Displacements	
LVDT	Disp (mm)
A	0.938
B	26.356
C	263.410

RESULTS

Maximum Load (lb)	1709.54	
Pullout Resisatnce (lb/ft)	1709.54	
Coefficient of Interaction, ci	$\frac{Pr}{2(Le)(c + \sigma' \tan(\varphi'))}$	0.331

Average EPC reading (psi)	4.530

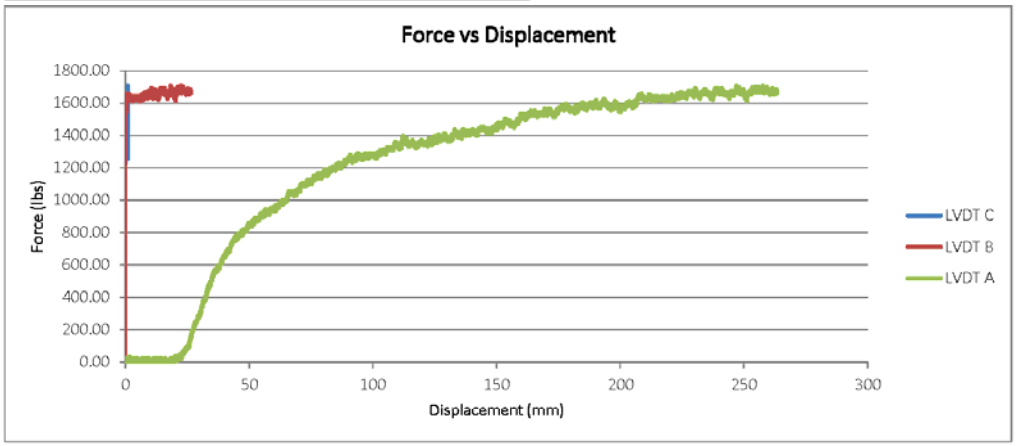

Comments:
Test Duration: 12:00-5:30pm
EPC not working
Pistons Maxed

Large Pullout Test

Test details :		
	Test Name	UX1700-50/50 CG/DM-4psi
	Date	8/17/2012
	Member	Sangy

Box Dimensions (inch)	Length	Width	Depth	Area (in2)	Height from base to sleeve
	60	24	11	1440	5

Geogrid Details	Manufacture	Product	Ultimate Tensile Strength
	Tensar	UX1700	12000 lb/ft

Specimen Information(ft)	Width	Embedment Length (Le)
	1	2.904

Material Properties	
Material Name	50/50 CG
Friction Angle (φ')	38
Moisture Content (%)	20.17
Yd,max (pcf)	75.2
Target Compaction	100%
Weight of each Lift	181
No. of Lifts	4

Test Details	
Normal Stress σ' (psi)	Rate of Pullout (in/min)
4	0.04

Maximum Displacements	
LVDT	Disp (mm)
A	120.243
B	54.652
C	51.227

RESULTS

Maximum Load (lb)	1594.47	
Pullout Resisatnce (lb/ft)	1594.47	
Coefficient of Interaction, ci	$\frac{Pr}{2(Le)(c + \sigma' \tan(\varphi'))}$	0.610

Average EPC reading (psi)	-1.359

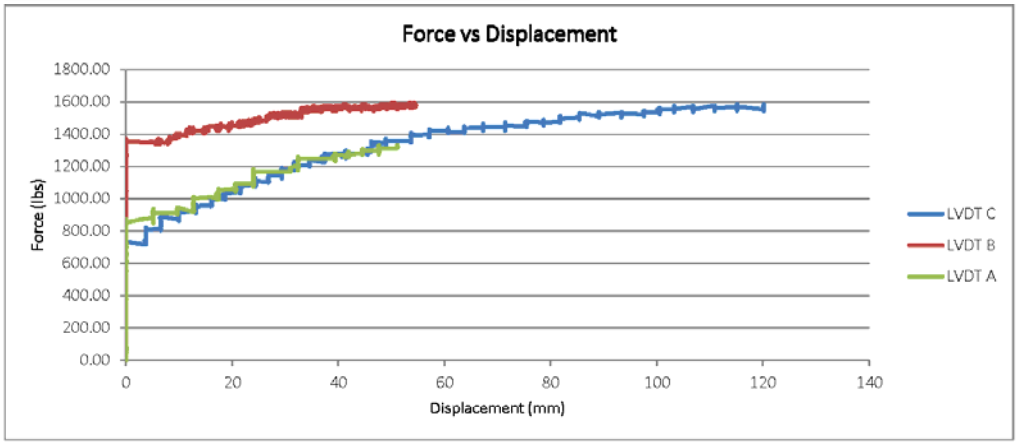

Comments:
Test Duration: 10:45am-2:30pm
LVDTs moving in steps

Geogrid Details	Manufacture	Product	Ultimate Tensile Strength
	Tensar	UX1700	12000 lb/ft
Specimen Information(ft)	Width	Embedment Length (Le)	
	1	2.97	

Material Properties	
Material Name	50/50 CG
Friction Angle (φ')	38
Moisture Content (%)	20.17
Yd,max (pcf)	75.2
Target Compaction	100%
Weight of each Lift	181
No. of Lifts	4

Test Details	
Normal Stress σ' (psi)	Rate of Pullout (in/min)
6	0.04

Maximum Displacements	
LVDT	Disp (mm)
A	128.961
B	66.097
C	135.015

RESULTS

Maximum Load (lb)	2325.96	
Pullout Resisatnce (lb/ft)	2325.96	
Coefficient of Interaction, ci	$\frac{Pr}{2(Le)(c + \sigma' \tan(\varphi'))}$	0.580

Average EPC reading (psi)	3.532

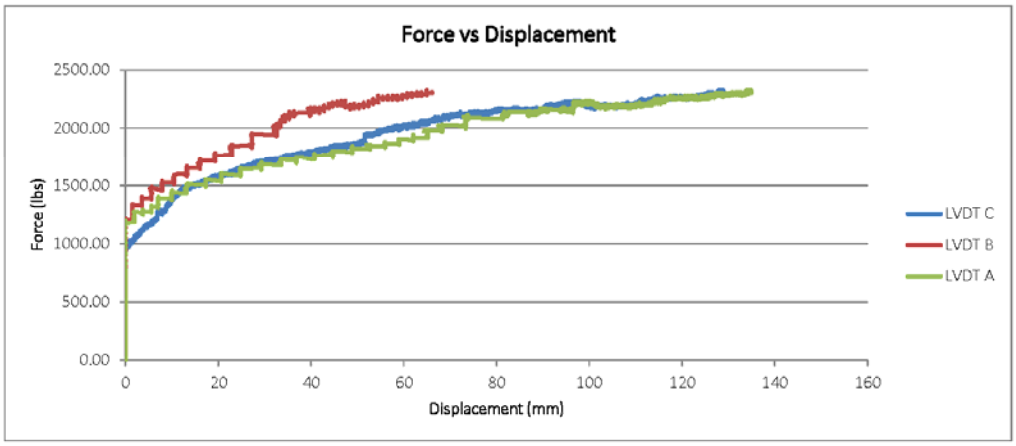

Comments:
Test Duration: 4:30pm-8:50pm
LDVTs in the back moved in steps
Pistons close to maxing out

Large Pullout Test

Test details :		
	Test Name	UX1700-50/50 CG/DM-8psi
	Date	8/19/2012
	Member	Alan

Box Dimensions (inch)	Length	Width	Depth	Area (in2)	Height from base to sleeve
	60	24	11	1440	5

Geogrid Details	Manufacture	Product	Ultimate Tensile Strength
	Tensar	UX1700	12000 lb/ft

Specimen Information(ft)	Width	Embedment Length (Le)
	1	2.871

Material Properties	
Material Name	50/50 CG
Friction Angle (φ')	38
Moisture Content (%)	20.17
Yd,max (pcf)	75.2
Target Compaction	100%
Weight of each Lift	181
No. of Lifts	4

Test Details	
Normal Stress σ' (psi)	Rate of Pullout (in/min)
8	0.04

Maximum Displacements	
LVDT	Disp (mm)
A	64.974
B	78.839
C	83.617

RESULTS

Maximum Load (lb)	2547.87	
Pullout Resisatnce (lb/ft)	2547.87	
Coefficient of Interaction, ci	$\frac{Pr}{2(Le)(c + \sigma' \tan(\varphi'))}$	0.493

Average EPC reading (psi)	15.793

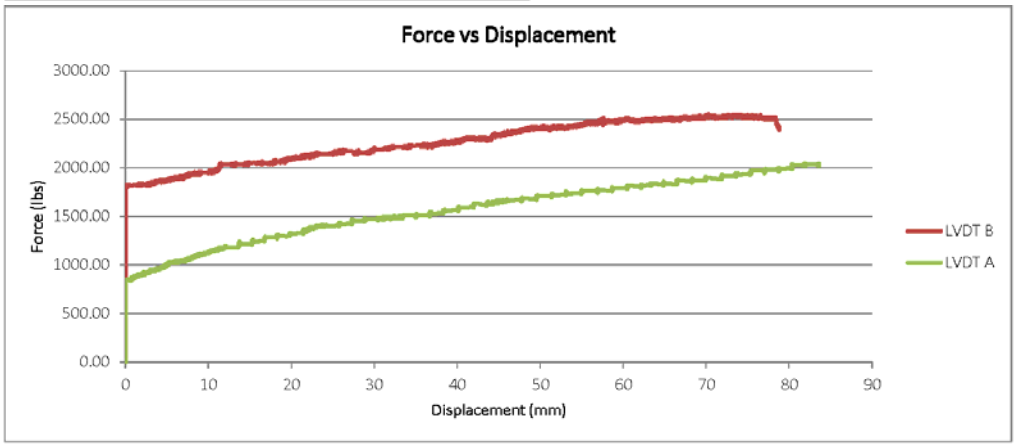

Comments:
Test Duration: 9:00am-1:00pm
LVDT C not working
Pistons Maxed Out

Large Pullout Test

Test details :		
	Test Name	UX1700-Mont Sand)-4psi
	Date	7/17/2012
	Member	-

Box Dimensions (inch)	Length	Width	Depth	Area (in2)	Height from base to sleeve
	60	24	11	1440	5

Geogrid Details	Manufacture	Product	Ultimate Tensile Strength
	Tensar	UX1700	12000 lb/ft

Specimen Information(ft)	Width	Embedment Length (Le)
	1	2.871

Material Properties	
Material Name	Mont sand
Friction Angle (φ')	35
Moisture Content (%)	1.5%
Yd,max (pcf)	99.3
Target Compaction	100%
Weight of each Lift	201
No. of Lifts	4

Test Details	
Normal Stress σ' (psi)	Rate of Pullout (in/min)
4	0.04

Maximum Displacements	
LVDT	Disp (mm)
A	33.008
B	14.240
C	50.066

RESULTS

Maximum Load (lb)	2046.51	
Pullout Resisatnce (lb/ft)	2046.51	
Coefficient of Interaction, ci	$\frac{Pr}{2(Le)(c + \sigma' \tan(\varphi'))}$	0.884

Average EPC reading (psi)	2.599

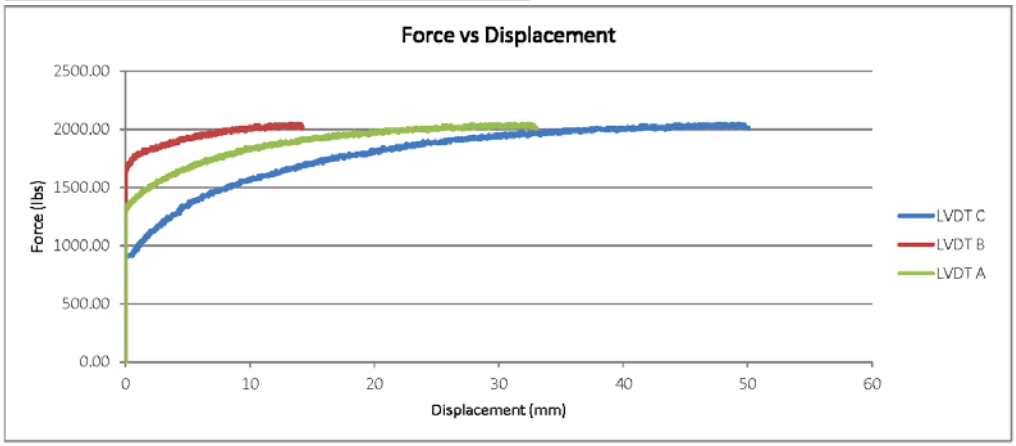

Comments:

Large Pullout Test

Test details :		
	Test Name	UX1700-Mont Sand)-4psi
	Date	7/17/2012
	Member	-

Box Dimensions (inch)	Length	Width	Depth	Area (in2)	Height from base to sleeve
	60	24	11	1440	5

Geogrid Details	Manufacture	Product	Ultimate Tensile Strength
	Tensar	UX1700	12000 lb/ft

Specimen Information(ft)	Width	Embedment Length (Le)
	1	3

Material Properties	
Material Name	Mont sand
Friction Angle (φ')	35
Moisture Content (%)	1.5%
Yd,max (pcf)	99.3
Target Compaction	100%
Weight of each Lift	201
No. of Lifts	4

Test Details	
Normal Stress σ' (psi)	Rate of Pullout (in/min)
6	0.04

Maximum Displacements	
LVDT	Disp (mm)
A	105.928
B	91.595
C	174.001

RESULTS

Maximum Load (lb)	2523.21	
Pullout Resisatnce (lb/ft)	2523.21	
Coefficient of Interaction, ci	$\frac{Pr}{2(Le)\,(c + \sigma' \tan(\varphi'))}$	0.695

Average EPC reading (psi)	3.784

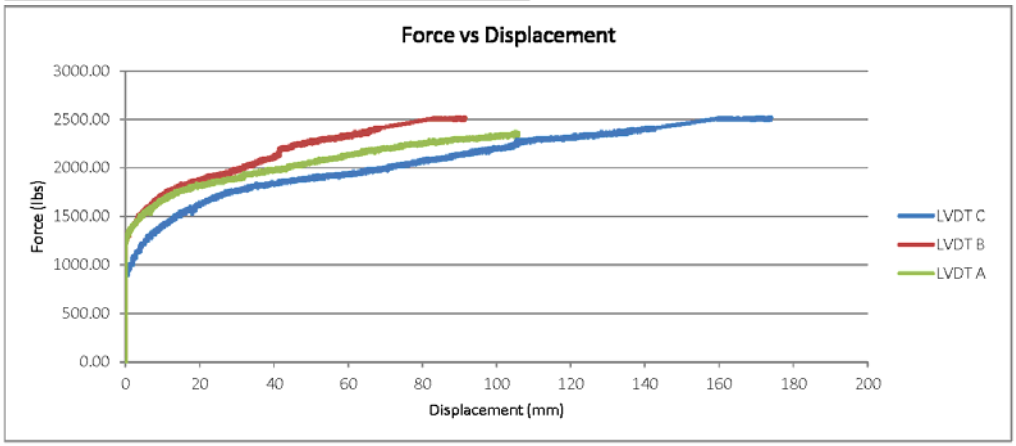

Comments:

Large Pullout Test

Test details :		
	Test Name	UX1400-Mont Sand)-8psi
	Date	7/18/2012
	Member	-

Box Dimensions (inch)	Length	Width	Depth	Area (in2)	Height from base to sleeve
	60	24	11	1440	5

Geogrid Details	Manufacture	Product	Ultimate Tensile Strength
	Tensar	UX1400	4800 lb/ft

Specimen Information(ft)	Width	Embedment Length (Le)
	1	3

Material Properties	
Material Name	Mont sand
Friction Angle (φ')	35
Moisture Content (%)	1.5%
Yd,max (pcf)	99.3
Target Compaction	100%
Weight of each Lift	201
No. of Lifts	4

Test Details	
Normal Stress σ' (psi)	Rate of Pullout (in/min)
8	0.04

Maximum Displacements	
LVDT	Disp (mm)
A	136.590
B	62.306
C	154.035

RESULTS

Maximum Load (lb)	2572.52	
Pullout Resisatnce (lb/ft)	2572.52	
Coefficient of Interaction, ci	$\frac{Pr}{2(Le)\,(c + \sigma' \tan(\varphi'))}$	0.532

Average EPC reading (psi)	10.484

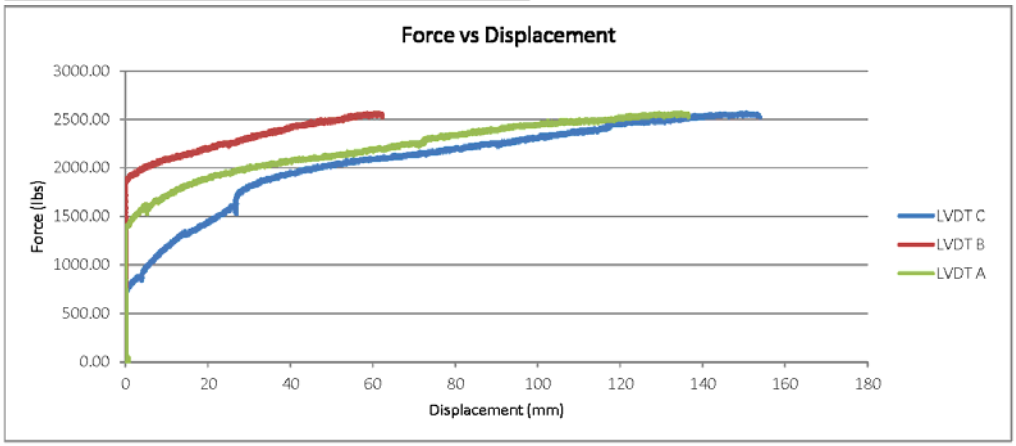

Comments:

Large Pullout Test

Test details :		
	Test Name	UX1400-Mont Sand-4psi
	Date	7/19/2012
	Member	-

Box Dimensions (inch)	Length	Width	Depth	Area (in2)	Height from base to sleeve
	60	24	11	1440	5

Geogrid Details	Manufacture	Product	Ultimate Tensile Strength
	Tensar	UX1400	4800 lb/ft

Specimen Information(ft)	Width	Embedment Length (Le)
	1	3

Material Properties	
Material Name	Mont sand
Friction Angle (φ')	35
Moisture Content (%)	1.5%
Yd,max (pcf)	99.3
Target Compaction	100%
Weight of each Lift	201
No. of Lifts	4

Test Details	
Normal Stress σ' (psi)	Rate of Pullout (in/min)
4	0.04

Maximum Displacements	
LVDT	Disp (mm)
A	29.661
B	5.136
C	43.156

RESULTS

Maximum Load (lb)	1019.15	
Pullout Resisatnce (lb/ft)	1019.15	
Coefficient of Interaction, ci	$\frac{Pr}{2(Le)(c + \sigma' \tan(\varphi'))}$	0.421

Average EPC reading (psi)	1.105

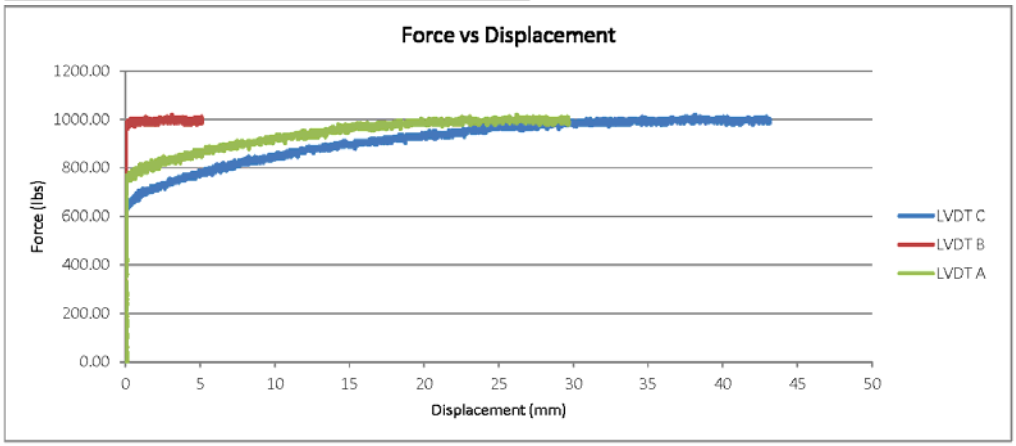

Comments:

Large Pullout Test

Test details :		
	Test Name	UX1400-Mont Sand-6psi
	Date	7/19/2012
	Member	-

Box Dimensions (inch)	Length	Width	Depth	Area (in2)	Height from base to sleeve
	60	24	11	1440	5

Geogrid Details	Manufacture	Product	Ultimate Tensile Strength
	Tensar	UX1400	4800 lb/ft

Specimen Information(ft)	Width	Embedment Length (Le)
	1	3

Material Properties	
Material Name	Mont sand
Friction Angle (φ')	35
Moisture Content (%)	1.5%
Yd,max (pcf)	99.3
Target Compaction	100%
Weight of each Lift	201
No. of Lifts	4

Test Details	
Normal Stress σ' (psi)	Rate of Pullout (in/min)
6	0.04

Maximum Displacements	
LVDT	Disp (mm)
A	148.804
B	64.991
C	177.752

RESULTS

Maximum Load (lb)	1356.12	
Pullout Resisatnce (lb/ft)	1356.12	
Coefficient of Interaction, ci	$\frac{Pr}{2(Le)(c + \sigma' \tan(\varphi'))}$	0.374

Average EPC reading (psi)	-0.453

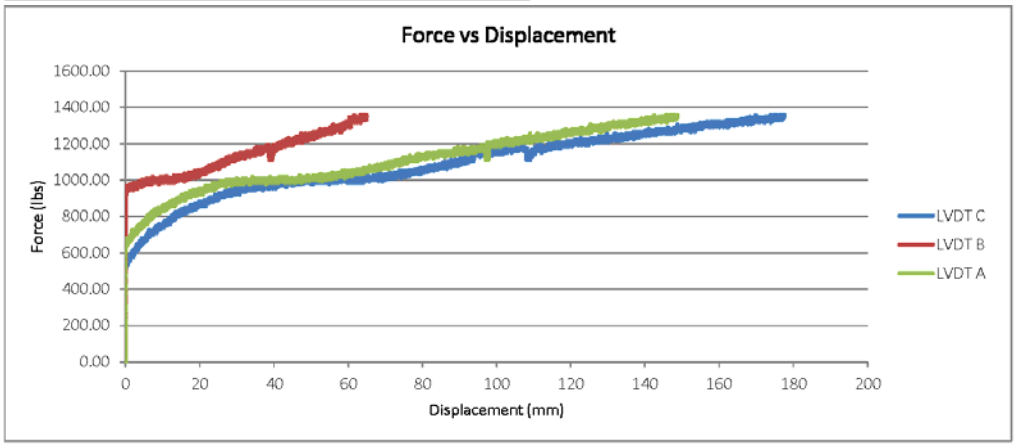

Comments:

Large Pullout Test

Test details :		
	Test Name	UX1700-Mont Sand-8psi
	Date	7/20/2012
	Member	-

Box Dimensions (inch)	Length	Width	Depth	Area (in2)	Height from base to sleeve
	60	24	11	1440	5

Geogrid Details	Manufacture	Product	Ultimate Tensile Strength
	Tensar	UX1700	12000 lb/ft

Specimen Information(ft)	Width	Embedment Length (Le)
	1	3

Material Properties	
Material Name	Mont sand
Friction Angle (φ')	35
Moisture Content (%)	1.5%
Yd,max (pcf)	99.3
Target Compaction	100%
Weight of each Lift	201
No. of Lifts	4

Test Details	
Normal Stress σ' (psi)	Rate of Pullout (in/min)
8	0.04

Maximum Displacements	
LVDT	Disp (mm)
A	69.451
B	40.148
C	105.095

RESULTS

Maximum Load (lb)	4060.15	
Pullout Resisatnce (lb/ft)	4060.15	
Coefficient of Interaction, ci	$\frac{Pr}{2(Le)(c + \sigma' \tan(\varphi'))}$	0.839

Average EPC reading (psi)	2.585

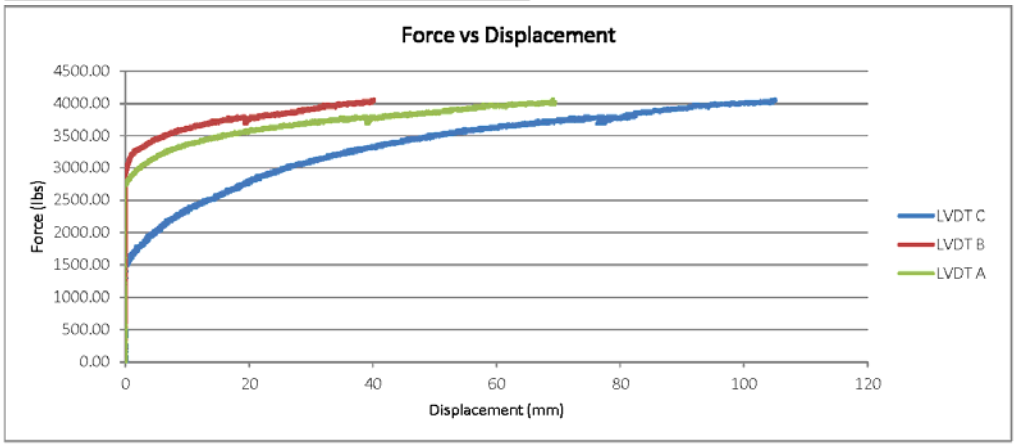

Comments:

Large Pullout Test

Test details :		
	Test Name	UX1700-50/50 CG/DM-4psi
	Date	8/17/2012
	Member	Sangy

Box Dimensions (inch)	Length	Width	Depth	Area (in2)	Height from base to sleeve
	60	24	11	1440	5

Geogrid Details	Manufacture	Product	Ultimate Tensile Strength
	Tensar	UX1700	12000 lb/ft

Specimen Information(ft)	Width	Embedment Length (Le)
	1	2.904

Material Properties	
Material Name	50/50 CG
Friction Angle (φ')	38
Moisture Content (%)	20.17
Yd,max (pcf)	75.2
Target Compaction	100%
Weight of each Lift	181
No. of Lifts	4

Test Details	
Normal Stress σ' (psi)	Rate of Pullout (in/min)
4	0.04

Maximum Displacements	
LVDT	Disp (mm)
A	120.243
B	54.652
C	51.227

RESULTS

Maximum Load (lb)	1594.47	
Pullout Resisatnce (lb/ft)	1594.47	
Coefficient of Interaction, ci	$\frac{Pr}{2(Le)(c + \sigma' \tan(\varphi'))}$	0.610

Average EPC reading (psi)	-1.359

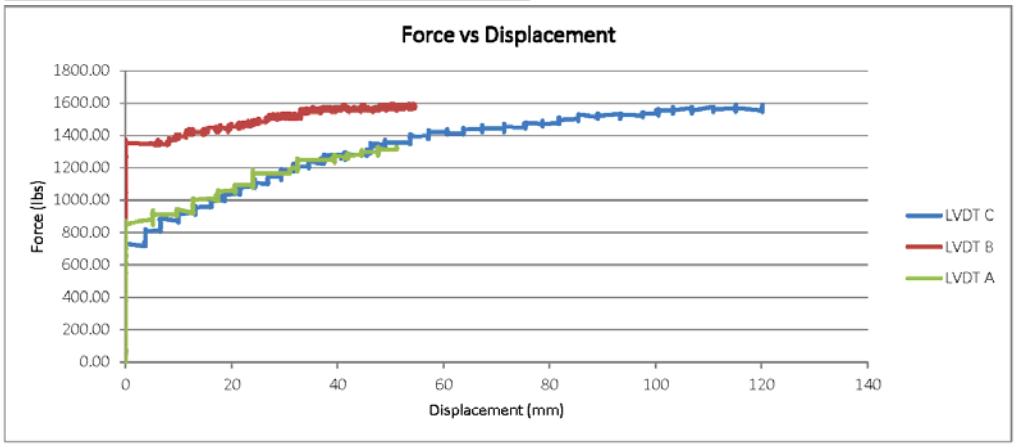

Comments:
Test Duration: 10:45am-2:30pm
LVDTs moving in steps

Bibliography

ASTM D422 (2007), “Standard Test Method for Particle-Size Analysis of Soils”, American Society for Testing and Materials, West Conshohocken, PA

ASTM D6706. (2003). “Standard Test Method for Measuring Geosynthetic Pullout Resistance in Soil”, American Society for Testing and Materials, West Conshohocken, PA.

AASHTO, NTPEP (2010), “Final Product Qualification Report for Tensar UX-MSE/UX-HS Geogrid Product Line”, NTPEP Report 8507.4.

Coduto, Donald (2001). Foundation Design. 2nd Edition. Upper Saddle River: Prentice Hall. Print.

Dias, A.C. (2003). Numerical analyses of soil-geosynthetic interaction in pull-out tests. MSc. Thesis, University of Brasilia, Brasilia, Brazil, 115 p. (in Portuguese).

Elias, V., Christopher, B.R. and Berg, R.R., (2001). “Mechanically stabilized earth walls and reinforced soil slopes design and construction guidelines”, National Highway Institute (NHI), Course No 132042, Report No FHWA-NHI-00-043, 394p.

Farrag, K., Yalcin A.B., and Juran, I., (1993). “Pull-Out Resistance of Geogrid Reinforcements”, *Geotextiles and Geomembranes*, Vol. 12, 133-159.

Grubb, Dennis, Atwood Davis, et al., (2006b). "Field Evaluation of Crushed Glass–Dredged Material Blends." *JOURNAL OF GEOTECHNICAL AND GEOENVIRONMENTAL ENGINEERING*. 132.5: 577-590.

Grubb, Dennis G., Patricia M. Gallagher, Joseph Wartman, et al., (2006a). "Laboratory Evaluation of Crushed Glass-Dredged Material Blends." *JOURNAL OF GEOTECHNICAL AND GEOENVIRONMENTAL ENGINEERING*. 132.5: 562-576. Print.

Grubb, D., Wartman, J., Malasavage, N., and Mibroda, J. (2007) Turning Mud into Suitable Fill: Amending OH, ML-MH and CH Soils with Curbside-Collected Crushed Glass (CG). Geoenvironmental Engineering: pp. 1-14.

Grubb, Dennis, Joseph Wartman, et al., (2008). "Aging of Crushed Glass-Dredged Material Blend Embankments. "*JOURNAL OF GEOTECHNICAL AND GEOENVIRONMENTAL ENGINEERING*. 134.11: 1676-1684.

Gallagher, Patricia, Murat Hamderi, et al., (2008). "Dynamic Response of Compacted CG, DM, and CG-DM Blends." *JOURNAL OF GEOTECHNICAL AND GEOENVIRONMENTAL ENGINEERING*. 135.8: 1148-1154.

Hanumasagar, Sangameshwar, (2013). "Pullout Evaluation of Steel Slag Fines and Dredged Material Blends with Geogrids." MS thesis. The University of Texas at Austin. Print.

Hutcherson, Shawn (2012). "Analysis of a Database of Uniaxial Geogrid Pullout Resistance Results." MS thesis. The University of Texas at Austin. Print.

Koerner, R.M. and Wilson-Fahmy, R.F. (1993). “Finite element modeling of soil-geogrid

interaction with application to the behavior of geogrids in a pullout loading condition." *Geotextiles and Geomembranes*, 12(5), 479-501.

Landris, T.L., (2007). Recycled glass and dredged materials. US Army Corps of Engineers, Engineer Research and Development Center, Report No. ERDC TNDOER- T8, Mississippi.

Lopes, M.J. and Lopes, M.L. (1996). "Soil-Geosynthetic Interaction -Influence of Soil Particle Size and Geosynthetic Structure", *Geosynthetics International*, Vol. 6 (4), pp. 261-282.

Lopes, M.L. and Ladeira, M. (1996). "Influence of the confinement, soil density and displacement ratio on soil-geogrid interaction", *Geotextiles and Geomembranes*, 14(10), 543-554.

Malasavage, N. E., Jagupilla, S. C., Grubb, D. G., Wazne, M., and Coon, W.P., (2012). "Geotechnical Performance of Dredged Material – Steel Slag Fines Blends: Laboratory and Field Evaluation", *J. Geotech. Geoenviron. Eng.*, 138 (8), 981-991.

Milligan, G.W.E., Earl, R.F. & Bush, D.I. (1990). "Observations of photo-elastic pullout tests on geotextiles and geogrids." *4th International Conference on Geotextiles, Geomembranes and Related Products, The Hague The Netherlands*, Vol.2, 747-751.

Mitchell, J.K. and Zornberg, J.G. (1995). "Reinforced Soil Structures with Poorly Draining

Backfills. Part II: Case Histories and Applications." *Geosynthetics International*, 2(1), 265-307.

Moraci, N., Gioffre, D., (2006). "A simple method to evaluate the pullout resistance of extruded geogrids embedded in a compacted granular soil", *Journal of geotextiles and geomembranes*, 24, 116–128.

Moraci, N., Romano, G., and Montanelli, F., (2004). "Factors affecting the interface apparent coefficient of friction in pullout conditions", *3rd European Geosynthetics Conference*, Vol. 1, Monaco, pp. 313-318.

Palmeira, E.M. & Milligan, G.W.E. (1989a.). "Scale and other factors affecting the results of pull-out tests of grids buried in sand." *Geotechnique*, 39(3), 511- 524.

Palmeira, E.M. (2004). "Bearing force mobilization in pull-out tests on geogrids." *Geotextiles and Geomembranes*, 22(6), 481-509.

Palmeira, E.M. (2008), "Soil-geosynthetic interaction: Modeling and Analysis", Mercer Lecture, presented at *4th European Conference on Geosynthetics*-EuroGeo4, Edinburgh 2008

Palmeira, E.M. (2009). "Soil–geosynthetic interaction: Modeling and analysis." *Geotextiles and Geomembranes*, 27(5), 368-390.

Reindl, John (2013). "Clean Washington Center." Best Practices Manual for Recycled Glass. Clean Washington Center.

Teixeira, S., Bueno, B., and Zornberg, J. (2007). ”Pullout Resistance of Individual Longitudinal and Transverse Geogrid Ribs.” *J. Geotech. Geoenviron. Eng.*, 133(1), 37–50.

Wilson-Fahmy, R.F., Koerner, R.M., Sansone, L.J. (1994). “Experimental Behavior of Polymeric Geogrids in Pullout”, *Journal of Geotechnical Engineering*, 120 (4), 661-677.

Wartman, Joseph, Dennis G. Drubb, and A. S. M. Nasim, (2004). "Select Engineering Characteristics of Crushed Glass." JOURNAL OF MATERIALS IN CIVIL ENGINEERING. 16.6: 526-539.